University of Crete School of Medicine

Boston University School of Medicine

Master Thesis

THE ROLE OF AMINO ACIDS 218-222 OF APOLIPOPROTEIN A-I IN THE BIOGENESIS OF HDL

Ο ΡΟΛΟΣ ΤΩΝ ΑΜΙΝΟΞΕΩΝ 218-222 ΤΗΣ ΑΠΟΛΙΠΟΠΡΩΤΕΪΝΗΣ Α-Ι ΣΤΗΝ ΒΙΟΓΕΝΝΕΣΗ ΤΗΣ HDL

by

MELISSA ASHLEY BECK

Submitted in partial fulfillment of the requirements for the degree of

Master of Science

for the graduate program *Molecular Basis of Human Disease*

2012

To my family

for their continuous support.

ACKNOWLEDGEMENTS

As I complete my master thesis I would like to first thank my family for their emotional and financial support in the pursuit of my degree. Their belief in me has motivated and encouraged me year after year. Thank you.

I would also like to thank my principal investigator in the lab here at Boston University, Dr. Vassilis Zannis for the opportunity to do the research for this project in his laboratory, and also for his guidance and support.

Thank you to Panagiotis Fotakis, for all of his help, encouragement, advice and teaching. He taught me how to work in the lab, and his instruction was very valuable to me in completing this work.

I am grateful to Mary Adamaki, for all of her support and assistance in Greece, and to Gayle Forbes for her technical assistance in the lab, and also to Andreas Kateifides for his advice and input.

Approved by:

First reader Vassilis I. Zannis

Vassilis I. Zannis, Ph.D.

Professor of Medicine and Biochemistry

Boston University Medical School

Second reader

Dimitris Kardassis, PhD

Professor of Biochemistry

University of Crete Medical School and IMBB-FORTH

Third reader

Evangelia Papakonstanti, PhD.

Assistant Professor of Biochemistry

Faculty of Medicine

University of Crete

ABSTRACT

Apolipoprotein A-I (apoA-I) is the predominant protein component of the high density lipoprotein (HDL) particle, and deficiency of apoA-I prevents the formation of HDL. ApoA-I activates the enzyme lecithin:cholesterol acyltransferase (LCAT), which is necessary for the esterification of cholesterol in HDL, a process associated with the conversion of nascent discoidal to mature spherical HDL particles. Previous studies showed that the hydrophobic amino acids in the 220-231 region of apoA-I are required for cholesterol efflux in vitro, and amino acid substitution of apoA-I within the 220-231 region diminishes the ability of the mutant protein to create mature spherical HDL particles in vivo.

Adenovirus-mediated gene transfer of WT apoA-I, mutant apoA-I[L218A/L219A/V221A/L222A], or mutant apoA-I plus LCAT in apoA-I$^{-/-}$ x apoE$^{-/-}$ double deficient mice was used to elucidate the role of hydrophobic residues in the 218-222 region of apoA-I in the biogenesis of HDL. Plasma obtained four days post gene transfer was analyzed by various assays to monitor the formation and maturation of HDL. Fast protein liquid chromatography (FPLC) analysis of plasma showed that in mice expressing the mutant protein, the HDL peak was greatly diminished as compared to the mice expressing the WT apoA-I. Density gradient ultracentrifugation showed that, compared to WT apoA-I, expression of the mutant protein was associated with low levels of apoA-I that floated mainly in the HDL3 region. Two dimensional gel electrophoresis of plasma and electromicroscopy of the HDL fraction showed that mice expressing the mutant protein generated pre-β HDL particles and a small number of discoidal HDL particles. In contrast, mice expressing WT apoA-I generated predominantly α1, α2, and α3 spherical HDL particles. Mice co-expressing the apoA-I mutant and LCAT generated a pronounced cholesterol shoulder in the VLDL/IDL/LDL region, shifted the apoA-I toward the lower densities, and promoted the formation of small sized HDL particles.

The findings suggest that substitution of the hydrophobic residues in the 218-222 region of the apoA-I by alanine disrupts the biogenesis of HDL. The disruption appears to result from diminished interactions of the mutant apoA-I with ABCA1, combined with inefficient conversion of nascent discoidal to mature spherical HDL particles. The observed phenotype generated by the apoA-I[L218A/L219A/V221A/L222A] mutant can be partially restored when the apoA-I mutant is co-expressed with LCAT.

ΠΕΡΙΛΗΨΗ

Η απολιποπρωτεϊνη A-I (αποA-I) είναι η κύρια πρωτεΐνη των σωματιδίων της λιποπρωτεΐνης υψηλής πυκνότητας (high density lipoprotein ήHDL). Η έλλειψη της αποA-I αναστέλλει την βιοσύνθεση της HDL. Η αποA-I ενεργοποιεί το ένζυμο ακυλοτρανσφεράση λεκιθίνης:χοληστερόλης (LCAT) το οποίο εστεροποιεί την ελεύθερη χοληστερόλη της HDL και οδηγεί στην μετατροπή των πρόδρομων δισκοειδών σε ώριμα σφαιρικά σωματίδια HDL.

Στην παρούσα διατριβή έγινε χρήση γονιδιακής μεταφοράς σε ποντικούς με διπλή έλλειψη σε αποA-I και αποE (apoA-I -/- x apoE -/- mice) για να προσδιοριστεί ο ρόλος των υδρόφοβων αμινοξέων στην περιοχή 218-222 της αποA-I στην βιογένεση της HDL. Πλάσμα που ελήφθη 4 ημέρες μετά την γονιδιακή μεταφορά της αγρίου τύπου αποA-I ή της μεταλλαγμένης μορφής της αποA-I [L218A/L219A/V221A/L222A] απουσία ή παρουσία της LCAT υπεβλήθη σε διάφορες αναλύσεις που προσδιορίζουν τον σχηματισμό και την ωρίμανση της HDL. Η κλασμάτωση του πλάσματος με υγρή χρωματογραφία πρωτεϊνών [FPLC] έδειξε ότι σε ποντικούς που εξέφραζαν την μεταλλαγμένη αποA-I, το κλάσμα που αντιστοιχεί στην HDL ήταν πολύ μειωμένο σε σύγκριση με ποντικούς εξέφραζαν την αγρίου τύπου αποA-I. Ο διαχωρισμός του πλάσματος με υπερφυγοκέντρηση σε διάλυμα KBr διαβαθμισμένης πυκνότητας και ηλεκτροφόρηση πολυακρυλαμιδίου-SDS των κλασμάτων έδειξε ότι σε σύγκριση με την αγρίου τύπου αποA-I , η έκφραση της μεταλλαγμένη αποA-I οδήγησε σε χαμηλά επίπεδα αποA-I που ήταν εντοπισμένα κυρίως στην περιοχή της HDL_3. Η ανάλυση του πλάσματος με ηλεκτροφόρηση δυο διαστάσεων και του κλάσματος της HDL με ηλεκτρονική μικροσκοπία έδειξε ότι οι ποντικοί που εξέφραζαν την μεταλλαγμένη αποA-I σχημάτισαν preβ1 HDL σωματίδια και μικρό αριθμό δισκοειδών HDL σωματιδίων. Σε αντίθεση, οι ποντικοί που εξέφραζαν την αγρίου τύπου αποA-I σχημάτισαν κυρίως α-HDL σωματίδια (α1, α2, and α3). Ποντικοί που εξέφραζαν την μεταλλαγμένη πρωτεΐνη μαζί με την LCAT είχαν μια περιοχή (shoulder) αυξημένης χοληστερόλης στην περιοχή των VLDL/IDL/LDL. Οι ποντικοί αυτοί παρουσίασαν μετατόπιση της αποA-I προς τις χαμηλότερες πυκνότητες και σχημάτισαν μικρού μεγέθους σφαιρικά σωματίδια HDL.

Τα ευρήματα αυτά εισηγούνται ότι η αντικατάσταση των υδρόφοβων αμινοξέων της περιοχής 218-222 της αποA-I με αλανίνη αναστέλλει το μονοπάτι της βιογένεσης της HDL. Η αναστολή αυτή φαίνεται να προκύπτει από ελαττωματική αλληλεπίδραση της μεταλλαγμένης μορφής της αποA-I με τον μεταφορέα ABCA1 σε συνδυασμό με μειωμένη μετατροπή των πρόδρομων δισκοειδών σωματιδίων σε ώριμα σφαιρικά σωματίδια HDL. Ο ελαττωματικός φαινότυπος που δημιουργείται από την αποA-I [L218A/L219A/V221A/L222A] μπορεί να διορθωθεί εν μέρει παρουσία περίσσειας LCAT.

Table of Contents

INTRODUCTION

Lipoprotein Structure and Function

Lipoproteins are biochemical macromolecules containing both lipids and proteins. Generally, lipoproteins allow the transport of lipids (hydrophobic compounds) in hydrophilic environments. The structure of a low density lipoprotein, detailed in Figure 1 below, allows for this important general function.

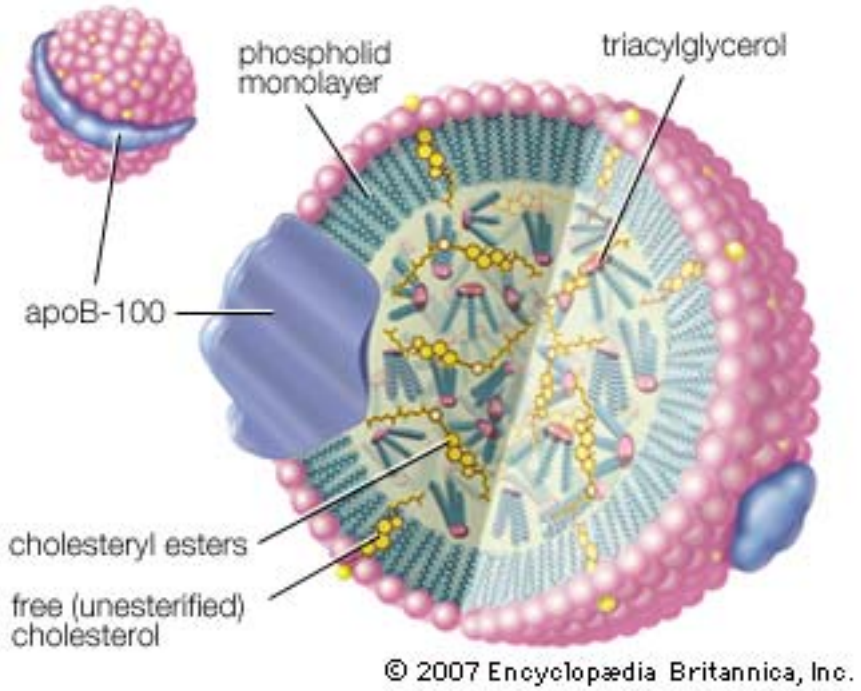

Figure 1: Structure of low density lipoprotein. Source: Encyclopedia Britannica
http://www.britannica.com/EBchecked/media/92254/Cutaway-view-of-a-low-density-lipoprotein-complex-The-LDL

Hydrophilic phospholipids and proteins make up the outer "shell" of the lipoprotein, and this allows the entire molecule to be soluble in blood, and other hydrophilic environments. The hydrophobic lipid contents (the triglycerides, cholesteryl esters, and free cholesterol) are located internally, and thus are sheilded from the hydrophilic environment.

The surface proteins, mostly apoproteins, interact with other molecules in the surrounding environment and thus contribute to cell function and cell signaling events.

Classification and Distinction of Lipoproteins

Apoproteins are classified according to their density, with high density lipoprotein (HDL) being the smallest and most dense. By definition, these HDL particles have the lowest fat to protein ratio of all the lipoproteins. HDL is commonly referred to as "good cholesterol" due to its main function of transporting cholesterol from macrophages and other tissues of the body to the liver, from where the body is rid of this cholesterol via its incorporation into bile and subsequent excretion.

Through extensive study, a correlation has been seen between high levels of LDL and low levels of HDL with an increase in one's risk of developing atherosclerosis and other cardiovascular diseases. Essentially, LDL provides cholesterol to cells, and HDL removes excess cholesterol from cells (1, 2).

HDL's Protective Effects and Properties/HDL as a Biomarker

Most generally, high-density lipoprotein is cardioprotective. There exists a long repertoire of properties of HDL that suggest its atheroprotective nature. Consider the following ever-growing body of evidence. HDL has been shown to have antibacterial, antiparasitic, antiviral, antioxidant,

antithrombotic, and antiinflammatory properties (*3-6*). HDL promotes cholesterol efflux (7, 8), promotes endothelial cell proliferation and migration (*9*), and promotes vasodilatation by stimulating the release of NO from endothelial cells (*10*). It inhibits cell apoptosis (*11*), as well as the expression of proinflammatory cytokines (*12*). HDL also inhibits the expression of adhesion molecules by endothelial cells (13, 14), and platelet aggregation and thrombosis (*15*). Additionally, HDL has been shown to prevent the oxidation of LDL (16, 17).

Murphy et al recently summarized a few mechanisms by which HDL is thought to confer its anti-atherogenic properties—HDL's ability to delay progression, or cause regression, of atherosclerosis is due to its promotion of cholesterol efflux from macrophage foam cells, which may in turn mediate emigration of macrophages from lesions during regression (*18*). The antioxidant effect of HDL is enhanced by apolipoprotein M binding to oxidized phospholipids within HDL (*19*).

Importantly, in 1989, Gordon et al showed that there is an inverse relationship between plasma levels of HDL and the risk for coronary artery disease (CAD) (*20*), and since then this correlation has been well established. However, there is evidence to suggest that this correlation is not upheld when inflammatory disease is present—for instance, in end-stage renal disease (ESRD) the correlation is completely lost (*21*). It is thought that the mechanism by which this takes place is a reduced inhibition of monocyte chemoattractant protein 1 formation in the smooth muscle of the vasculature, and also by an increased presence of the proinflammatory protein, serum amyloid A in the HDL of the ESRD patients (*22*). In support of the idea that inflammation can directly impair HDL function and reverse cholesterol transport in humans, de la l'Lera et al showed that endotoxemia-induced inflammation lead to HDL remodeling, depleting the populations of pre-β1a, small and medium HDL particles, as well as leading to a suppression of LCAT activity (*23*). This

discovery points to the idea that impaired HDL-mediated cholesterol efflux can occur in inflammatory diseases.

HDL has also been implicated in maintaining glucose homeostasis and affecting glucose metabolism, suggesting even that low levels of plasmas HDL are a risk factor for the development of type II diabetes mellitus (*24*).

Not only is the quantity of HDL in the plasma indicative of atheroprotective properties, but also the quality of the HDL particles that determines the cardioprotective properties of HDL. For instance, a clinical study of people at high risk for cardiovascular events found that simply increasing the quantity of HDL in circulation did prevent cardiovascular death from occurring (in fact, the trial was suspended due to the mortality rate) (25, 26).

Interestingly, when HDL cholesterol levels are too high, this can actually be a risk factor for cardiovascular risk, as opposed to being cardioprotective (*27*). Additionally, presence of HDL becomes a risk factor for cardiovascular events, as opposed to a protective factor, when the size of the HDL particles is too large (*27*). However, in these studies the presence of apoA-I was still associated with a decreased risk in cardiovascular events, regardless of what was happening with HDL, and also regardless of the amount of apoA-I present.

Finding the best markers for cardiovascular disease risk is not easy, and the field is constantly changing with regard its newest and most promising risk markers. It seems as though for women with a body mass index (BMI) of >30, the functional measures of HDL may be better markers for cardiovascular risk than the HDL cholesterol levels, as in these women, a decrease in cholesterol efflux via ABCA1 was associated with an increase in the nitration of apoA-I in HDL,

that leads to impaired endothelial function (impairment in endothelial function being a known biomarker of cardiovascular disease itself) (*28*).

Biogenesis of HDL

The biogenesis of HDL is known to take place in the liver. The pathway of biogenesis is complex, and requires apolipoprotein A-I (apoA-I), ATP-binding cassette A1 (ABCA1), and lecithin:cholesterol acyltransferase (LCAT) to create a structurally sound and fully functional HDL particle (*29*). Figure 2 below depicts the simplified pathway of biogenesis of HDL.

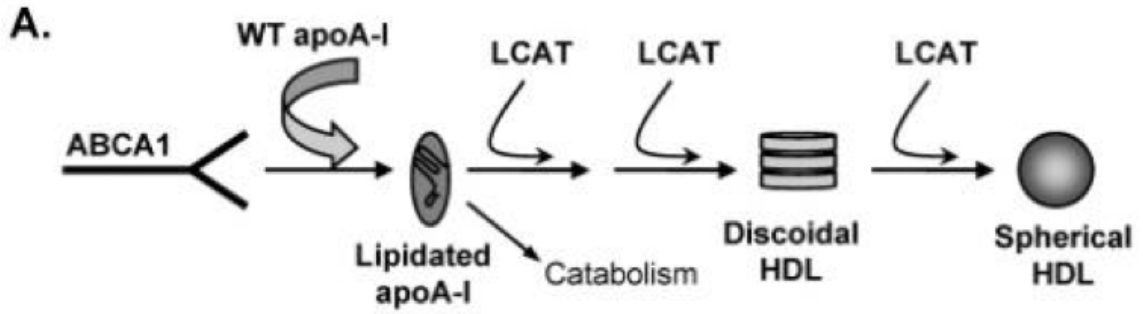

Figure 2: The simplified schematic depiction of the biogenesis of HDL. Adapted from Koukos et al 2007.

Step by step, the biogenesis involves the ABCA1-mediated transfer of cholesterol and phospholipids from the cell to extracellular lipid-poor apoA-I (or other acceptors), making it lipidated apoA-I. In a series of steps, the enzyme LCAT works on the lipidated apoA-I, converting the lipidated apoA-I to a precursor form of HDL which is discoidal in shape (*30*). Subsequntly LCAT again converts the discoidal particles to mature, spherical HDL particles. The mature

spherical HDL consists of 45-55% apolipoproteins, 26-32% phospholipids, 15-20% esterified cholesterol, 5% trigylcerides, and 3-5% cholesterol (*31*).

ApoA-I is probably the most important player in the assembly of HDL, but a mutation at any point along this pathway may affect the biogenesis, proper maturation or functionality of HDL.

Cell signaling (HDL, apoA-I)

Other protective effects on the vascular system, such as vasodilation, antiadhesion and antiinflammatory effects, are conferred by the stimulation of endothelial nitric oxide synthase (eNOS) and the production of nitric oxide, which is set in motion by the HDL-dependent activation of the Akt pathway (32, 33). In mice overexpressing apoA-I an increased phosphorylation of Akt is seen in the arterial wall (*34*), indicating that the antiatherogenic effects of HDL are conferred, at least in part, to the endothelium via the signal transduction pathway of phosphoinositide 3-kinase (PI3K)/Akt. In addition to PI3K/Akt activation of eNOS, the HDL-activated protein kinase network of Raf-1, MEK1/2 and extracellular signal-regulated kinases (ERK) 1/2 activates eNOS as well (32, 35). PI3K/Akt activation by HDL also has been shown to induce expression of a cytokine with antiinflammatory effects, transforming growth factor beta 2 (TGFβ2) (*36*). Norata et al also showed that HDL is responsible for activating even more signaling pathways that are involved in the endothelial effects of HDL, such as calcium/calmodulin kinase, protein kinase C and p38-mitogen-activated protein kinase (*37*).

HDL's antiinflammatory properties, as exhibited in human and murine endothelial cells and monocytes, take place through a variety of signaling pathways. For instance, HDL is known to repress transcription of adhesion molecules such as CD11b/CD18, VCAM-1 and ICAM-1 (*38*). It also suppresses the production of certain cytokines and chemokines, TNF-α, IL-6, IL-10, and

MCP-1 (*39*). HDL inhibits transcription factors that prevent AP-1 and NF-kB activation by suppressing IkB degredation (*40*), and also inhibits sphingosine kinase and ERK-1/2 phosphorylation (*41*). Additionally, HDL alters raft biology and depletion of membrane cholesterol in human and murine macrophages (*42*).

HDL's antiatherogenic functions can also be traced back to the expression of cyclooxygenase-2 (COX-2) and the realease of prostacyclin I-2 (PGI-2) in endothelial cells (*43*). While HDL's ability to induce COX-2 expression and PGI-2 release has been accredited to the role of HDL-integrated sphingosine-1-phosphate (S1P), new evidence suggests that human apoA-I is also able and responsible for these actions (*44*). In fact, in human umbilical vein endothelial cells (HUVECS) apoA-I even plays a key role in this process. ApoA-I –activated signaling pathways such as p38 mitogen-activated protein kinase (MAPK), extracellular receptor kinase (ERK) 1/2, and JAK2 were also found to be involved in the induction of COX-2 expression and PGI-2 release in HUVECs. In still the same study it was additionally discovered that ABCA1 is required for the apoA-I –mediated induction of COX-2 expression and PGI-2 release, indicating that apoA-I contributes to the antiatherogenic effects of HDL through ABCA1 and the activation of intracellular p38 MAPK, ERK ½, and JAK2 pathways (*44*).

The effects that HDL has on endothelial cells are very heterogeneous. HDL taken from patients with cardiopathy do not have the endothelial antiinflammatory effects seen in HDL taken from healthy subjects, and furthermore it does not have the ability to stimulate endothelial repair due to its failure to induce endothelial nitric oxide (NO) induction (*45*). It is thought that in these patients HDL activates lectin-like oxidized LDL receptor 1 (LOX-1), which triggers PKCβII activation, which inhibits eNOS-activating pathways and eNOS-dependent NO production—due to reduced HDL-associated paraoxonase (PON1) activity. This complicated pathway of activation and

subsequent loss of eNOS activation leads to the reduction in the endothelial antiinflammatory and endothelail repair-stimulating capabilities of HDL.

Last month Oh et al (*46*) described how decreased ER stress is associated with an absence in the signaling of scavenger receptors CD36 and SR-A1. The lack of this signaling was also correlated with a decrease in macrophage differentiation to type M2 (which leads to increased foam cell formation and progression of atherosclerosis). Going even further, they found that the supression of ER stress actually shifted already-differentiated M2 macrophages to a M1 phenotype, which reduced foam cell formation via increasing cholesterol efflux via HDL and apoA-1.

In rat astrocytes, the generation of HDL-like lipoproteins can be significantly enhanced when the astrocytes are treated with apoA-I—it is the interaction between phospholipase Cγ (PL-Cγ) and ABCA1 that generate the HDL-like particles, and augmented levels of apoA-I are thought to increase the signaling and interactions between PL-Cγ and ABCA1 (*47*).

3-Hydroxy-3-methylglutaryl coenzyme A (HMG-CoA) reductase inhibitors, also known as statins, help to lower LDL cholesterol in humans. Statins increase ABCA1 mRNA levels in hepatoma cell lines, and from there one can surmise how they help to lower LDL cholesterol based on much of the previous evidence and mechanisms already discussed in this thesis. Maejima et al (*48*) recently helped to uncover a more specific mechanism of action for the statin Pitavastatin, whereby it activated sterol regulatory element-binding protein (SREBP2) and increased total mRNA expression of ABCA1 as well as increased peroxisome proliferator-activated receptor α (PPARα) gene expression. The increased ABCA1 protein levels were shown to be linked to PPARα activation, which stabilized the ABCA1 protein, retarding degradation, while it enhanced the SREBP2-mediated transcription of the ABCA1 gene.

Interestingly, the environmental toxin tri-butyltin chloride (TBTC) has been shown to have the ability to modulate adipogenesis by activating the nuclear receptor retinoid X receptor (RXR)/PPARγ signaling pathway (*49*). TBTC was shown to modulate cholesterol efflux by activating liver X receptor (LXR) α/RXR signaling as well as increase ABCA1 mRNA expression thereby augmenting ABCA1 protein levels and apoA-I-mediated cholesterol efflux and HDL generation (*50*).

Developmentally, the expression of human apoA-I in embryonic stem cells (ESCs) from mice and induced pluripotent stem cells (iPSCs) from humans increases cardiac differnentiation and maturation. This pro-cardiogenic effect of apoA-I on stem cell differentiation is mediated by the BMP4-SMAD signaling pathway (*51*).

Mitochondrial inhibitory factor 1 (IF1) is known as a natural specific inhibitor of F(1)-ATPase activity (*52*). Genoux et al found that serum IF1 levels were correlated with HDL cholesterol levels, and that they were inversely correlated with triglyceride levels (*53*). The authors suggested that inhibiting F(1)-ATPase via IF1 can affect HDL levels by preventing the hepatic uptake of HDL, and may also have an effect on triglyceride metabolism (*53*) .

ApoA-I

Structure and Function

The principle apolipoprotein that I dealt with in my experiments is apolipoprotein A-I (apoA-I). Human apoA-I is derived from a 249 amino acid precursor to become a 243 amino acid plasma protein (*54*). The location of the 3kb apoA-I gene is chromosome 11q23 (*55*).

The structure of apoA-I is well suited for its defined functions. The crystal structure of the 185-243 region forms a half-circle dimer, the backbone consists of antiparallel tandem repeating proline-kinked helices, and this two-domain dimer structure based on helical repeats is consistent with apoA-I's role in the formation of discoidal HDL particles as well as suggesting an interaction with LCAT (*56*).

ApoA-I is the predominant protein of the HDL particle, and it accounts for about 70% of the apolipoprotein content of the particle (*57*). ApoA-I is synthesized in the liver and the intestines (*58*), in about a 2:1 liver to intestines ratio. This lipid-free apoA-I then mediates ABCA1-associated efflux of intracellular cholesterol, essentially receiving and keeping lipids from the cell, thus creating a nascent premature form of HDL called pre-β HDL (*6*). In fact, apoA-I deficiency prevents the formation of HDL (*57*). Conversely, overexpression of apoA-I has been shown to elevate plasma HDL concentration and attenuate progression of atherosclerosis (*59*), as apoA-I transgenic mice have elevated HDL and also a perceived protection from atherosclerosis (*60*).

Mice that overexpress apoA-I are seen to have a protection against accelerated atherosclerosis (*61*). In mice overexpressing apoA-I an increased phosphorylation of Akt is seen in the arterial wall (*34*), indicating that the antiatherogenic effects of HDL are conferred, at least in part, to the endothelium via the signal transduction pathway of phosphoinositide 3-kinase (PI3K)/Akt.

Human patients with rheumatoid arthritis have been found to have significantly higher levels of total cholesterol and trigylcerides than control subjects, as well as significantly lower levels of apoA-I (*62*).

Myeloperoxidase (MPO), found in cholesterol-laden macrophages of the human artery wall, use hydrogen peroxide to cause oxidative reactions and damage, negating the cardioprotective effects of HDL. Shao et al recently showed that the mechanism by which this happens is through apoA-I and ABCA1. ApoA-I is targeted by MPO, and specific tyrosine residues are chlorinated and nitrated, impairing its ABCA1-mediated cholesterol efflux abilities (63, 64).

ApoA-I has the ability to inhibit high-glucose-induced redox signaling in human monocyte-derived macrophages (HMDM), and the mechanism by which this is accomplished was recently elucidated. Reactive oxygen species (ROS) production, NADPH oxidase activity, p47phox translocation from the cytoplasm to the plasma membrane, and Nox2 expression were inhibited by native HDL, lipid-free apoA-I and discoidal reconstituted HDL containing phosphatidylcholine in macrophages when stimulated with high glucose (*65*). Also when stimulated with high glucose, apoA-I shows its antioxidant properties—both apoA-I and reconstituted HDL containing phosphatidylcholine were able to increase the levels of certain antioxidants, namely superoxide dismutase 1 (SOD1) and SOD2 in macrophages.

Mutations

The Zannis lab has shown previously that specific mutations in apoA-I can have dramatic effects on the biogenesis of HDL and exert their effects at different points along that pathway. They have found that apoA-I's amino acid residues 220-231 are required for lipid efflux in vitro and for HDL formation in vivo (*66*). ApoA-I(R160L)$_{Oslo}$, apoA-I(R149A), and apoA-I(151C)$_{Paris}$, when expressed in apoA-I -/- mice by adenovirus-mediated gene transfer, reduced total plasma cholesterol by between ~60-80% as well as reduced apoA-I levels, and reduced cholesteryl ester to

total cholesterol ratio (CE/TC) in mice—the resultant HDL phenotypes from mice with these mutations were aberrant (*67*). Interestingly, when these mice were treated with human lechithin:cholesterol acyltransferase (LCAT) plasma HDL levels, cholesterol levels, CE/TC ratio, and aberrant HDL phenotype were all normalized. Furthermore, abnormal phenotypes produced as a result of apoA-I mutations $(L141A)_{Pisa}$ and $(L159A)_{FIN}$ were also normalized by LCAT (*68*). The Zannis lab also reports that apoA-I(E110A/E111A) results in an increase in plasma triglyceride and plasma cholesterol levels, and physiochemical studies of this mutation reveal that apoA-I's alpha helical content is decreased as well as its stability (*69*).

Five novel mutations, A175P, F71Y, E34K, S36A, and H155MfsX46 have been recently associated with hereditary apoA-I amyloidosis, and it was shown that only these mutated proteins were deposited as amyloid fibril, whereas the wild type apoA-I protein is not (*70*).

A naturally occurring variant of apoA-I, L75P, is associated with systemic amyloidosis—Gomaraschi et al found that, in regards to HDL subpopulations and cholesterol esterification, apoA-I(L75P) is associated with a selective reduction in lipoprotein A-I particles, hypoalphalipoproteinemia, and partial defect in cholesterol esterification in carriers of this mutation in the human population (*71*). The apoA-I $(L159R)_{FIN}$ mutation is known to cause hypoalphaproteinemia, and predispose to an increased risk for atherosclerosis. A study using mice with this mutation showed that these mice developed the greatest extent of aortic cholesterol accumulation (even greater than mice lacking apoA-I altogether), suggesting that large HDL-like particles containing apoA-I(L159R) contribute to, rather than protect against, atherosclerosis most likely due to their inability to properly efflux cholesterol and their aggregation in the aorta (*72*). Hypoalphalipopriteinemia is also associated with apoA-I Zaragoza (L144R), and this mutation is

associated with enhanced HDL reverse cholesterol transport (73, 74) --suggesting that this mutation may enhance the functions of apoA-I.

Another mutation that enhances cholesterol efflux is apoA-I Milano (*75*). In animal studies, this variant of apoA-I lessened atherosclerotic lesions, and was even shown to be antiatherogenic (*76*). And in humans, apoA-I Milano was shown to be able to reverse the level of damage in atheroma plaques (*77*) and enhance incorporation of lipids into HDL particles and then accelerate catabolism of the HDL particles (*75*).

The $G26R_{IOWA}$ mutation of apoA-I leads to an increase in fibril formation, beta-strand structure, and has N-terminal protease susceptibility, and is associated with renal and hepatic accumulation (*78*). The fibrillogenic mutation of apoA-I(L178H) generates an apoA-I protein with an altered structure, decreased stability, affected protein binding profile, and ability to form helical fibrils (*79*).

Last year Haase et al were the first to describe a mutation of apoA-I (A164S) that consistently predicts an increased risk of ischemic heart disease (IHD), myocardial infarction (MI) and total mortality without low HDL cholesterol levels (*80*). This apoA-I(A164S) mutation has no effect on HDL cholesterol or apoA-I levels in the affected patients.

HDL in cholesterol efflux

As mentioned, HDL is involved in cholesterol efflux. It is this process that allows cholesterol to be removed from cells (macrophages, endothelial cells, etc) and tissues in the body and returned to the liver where it is excreted by incorporation into bile (*81*). The ability of HDL to promote cholesterol efflux is a major reason why HDL confers anti-inflammatory and antiatherosclerotic benefits (*82*). Lipid-free or lipid-poor apoA-I is also very important in this

process, since it is the acceptor of the cholesterol. This transfer of cholesterol from the cell to apoA-I is, for the most part, mediated by ABCA1. After this initial acceptance of cholesterol, apoA-I can acquire even more cholesterol and phospholipids by interactions with ABCG1 and ABCG4 (*30*). LCAT acts on the discoidal HDL particles, esterifying the unesterified cholesterols and sequestering the resulting cholesteryl esters into the center of the particle, effectively converting the disc into a sphere (*83*).

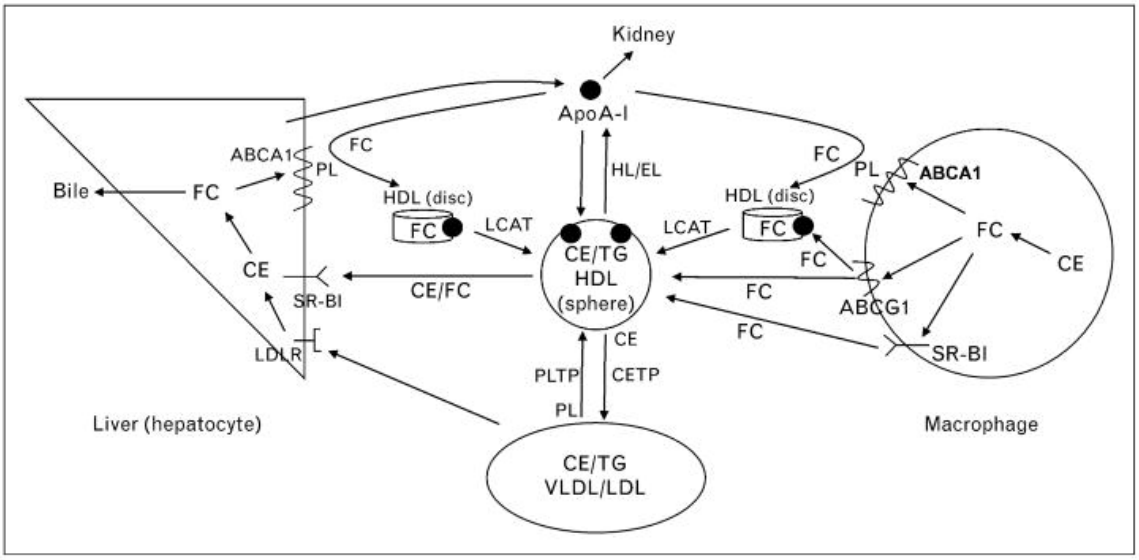

Figure 3: Rothblat et al's schematic overview of the major pathways involved in HDL-mediated macrophage cholesterol efflux and reverse transport to the liver (*84*).

ABC Transporter A1

Major Roles

The ABC transporters play a major role in the homeostasis and transport of cellular lipids, via a mechanism of action involving ATP hydrolysis to provide the energy necessary for substrate

active transport across a membrane (*85*). ABCA1 and ABCG1 are modulators of lymphocyte proliferative responses as well as regulators of macrophage expression of inflammatory chemokines and cytokines (*86*). The ABC transporter family's significant physiological contribution is further emphasized by the fact that many human defects of lipid desorption from cell membranes can be traced back to ABC transporters (*87*). ABCA1 donates lipids to apoA1 and apoE, taking them one step further along the pathway of high-density lipoprotein formation, and when an organism lacks ABCA1, functional HDL is not sufficiently formed (*88*). ABCA1 may have the ability to promote macrophage engulfment of apoptotic cells (*89*) via the translocation of phosphatidylserine (*90*), a suggested primary substrate of ABCA1 (*91*).

ABCA1 is also essential in the process of reverse cholesterol transport from macrophages to the liver. It is because of these two main functions of ABCA1—its contribution to the formation of HDL and reverse cholesterol transport—that ABCA1 is important for the protection against cardiovascular diseases. ABCA1 is considered an important therapeutic target in cardiovascular disease prevention (*92*).

Both ABCA1 and ABCG1, aside from their traditional roles in cholesterol efflux from macrophages, have been shown to influence the activation of neutrophils and monocytes, and to have some degree of control over hematopoietic stem cell proliferation, monocytosis and neutrophilia (*18*).

ABCA1 is essentially the rate-limiting step in the pathway along the formation of HDL particles. The Francis group reported that ABCA1 expression, and subsequently HDL formation, are impaired in Niemann-Pick disease type C, a lysosomal cholesterol storage disorder (*93*). They also recently found that in cholesteryl ester storage disease (CESD) certain mutations in the lipase

A, lysosomal acid, cholesterol esterase (LIPA) gene, which result in suppression of normal lysosomal acid lipase (LAL) activity, cause an impairment in ABCA1 activity and regulation and therefore an impairment in HDL particle formation as well (*94*).

ABCA1-mediated Cholesterol Efflux

There are two distinct models that are used to describe ABCA1-mediated cholesterol efflux. The first, called the molecular efflux model or the two-step transport model, starts with the transport of phospholipids from the cell (*85*). The cholesterol is transferred from caveolae to the apolipoprotein phospholipid complex, forming an intermediate complex. Additional cholesterol originating from caveolae is added to this intermediate complex, and leads to the formation of nascent HDL (*95*). According to the second model, called the membrane fusion or one-step transport model, ABCA1 drives the diffusion of phospholipids and cholesterol to apoA-I (*96*).

It has been suggested that it is only at the cell surface that ABCA1 transports cholesterol to apolipoproteins (*97*), as opposed to the previously-held view that ABCA1 transported lipids to either internalized apolipoproteins or those that are bound to the cell surface (98, 99). ABCA1 will export lipids to multiple apolipoproteins (given that they are associated with very little to no lipid at the time of transfer), such as AI, AII, E, CI, CII, CIII, and AIV (*100*).

Structure

ABCA1 is an integrated membrane protein of 2261 amino acids which exists as an oligomeric complex (*101*), with the majority of molecules forming tetramers. It is a full-sized ABC

transporter with 12 transmembrane segments (TMS). Although a somewhat unstable molecule, ABCA1 becomes stabilized when apolipoproteins are present.

The precise molecular structure of ABCA1 remains to be elucidated. It could, in all likelihood, be a channel, a pump or a flippase. Lee et al recently discovered that the extracellular levels of ATP are significantly elevated when the cells express ABCA1, and elevated extracellular ATP promoted cholesterol efflux to apoA-I (the dysfunctional ABCA1(A937V) mutant, when expressed at similar levels as WT, did not increase the extracellular concentration of ATP), (*102*).

Expression

The expression of ABCA1 is highly regulated at both the transcriptional and post-transcriptional levels. Regulation of expression can occur by secondary messengers (such as cAMP) and pleiotropic effects (by cytokines), however it is nuclear orphan receptors (such as LXR and PPARγ) that principally regulate ABCA1 expression. In mice, cyclic-AMP acts at both the transcriptional and translational level to upregulate the expression of ABCA1, however it is not clear if this occurs in humans (*103*). Since ABCA1 is considered a sterol sensitive gene, it reasonable to speculate that an inductive transcriptional effect of either a synthetic or a natural lipid could be mediated by LXR (104, 105). LXR and RXR heterodimerize, and once the heterodimer binds to the repeat response element, it promotes the expression of many genes implicated in reverse transport of cholesterol, ABCA1 being one of them (106, 107). Additionally, the PPARγ and RXR heterodimer complex promotes the expression of ABCA1, along with other genes (*108*). The downregulation of ABCA1 expression, have been implicated in SREBPs as well as IFN-γ. The LXRα signaling pathway is a functional middleman for the regulation of ABCA1 through IFN-γ

and TGF-β, with IFN-γ indirectly downregulating ABCA1 expression, and TGF-β performing as an upregulator. In summary, the general regulation of ABCA1 expression; upregulators include PPARγ/RXR, LXR/RXR, cAMP, and HDL, while downregulation is achieved by SREBPs (*108-111*).

The administration of aspirin was found to increase ABCA1 expression and also increase apoA-I-mediated cholesterol efflux (*112*).

Mutations

ABCA1 mutations contribute to Tangier Disease, an autosomal recessive disorder of lipid metabolism (113, 114) Tangier Disease is characterized by a virtual absence of circulating HDL and very low plasma levels of apoA-I. The disease is associated with an impairment of cellular efflux of cholesterol and phospholipids to lipid-poor apolipoproteins, leading to an increased risk of cardiovascular disease**.**

When mutations in the extracellular loops result in prevention of ABCA1 cross-linking to apoA-I, there is a decrease in cholesterol efflux (*115*).

A new functional variant of the ABCG1 gene, which facilitates efflux of cholesterol from macrophages to HDL particles, has been reported in the human population by Schou et al. ABCG1(Ser630Leu) can predict an increased risk of myocardial infarction (MI) and ischemic heart disease (IHD), suggesting that variations of ABCG1 can affect the risk of atherosclerosis in humans (*116*). It has long been known that ABCG1 mediates the efflux of cholesterol onto lipidated apoA-I, but the mechanism by which it does so has been unclear. Site-directed mutagenesis has recently

identified an amino acid residue that seems to be essentially for full functionality of ABCG1-mediated cholesterol efflux—the cysteine residue at 514. When a C514A mutation was generated, cholesterol efflux onto lipidated apoA-I did not occur, and when Cys514Ser and Cys514Thr (these amino acids are more conserved than alanine) mutations were introduced, there was a significant decrease, but not complete cessation of ABCG1-mediated cholesterol efflux (*117*).

Animal Studies

Knockout Mice

ABCA1 knockout studies have lead to the conclusion that ABCA1 has an anti-inflammatory function, but that this function is secondary to its cellular lipid modulatory function (118, 119). These anti-inflammatory properties are thought to extend to other lipid efflux proteins as well, such as ABCG1(*120*), indicating that such a property is not limited to ABCA1. It is not altogether uncommon for ABCA1 and ABCG1 to work in tandem, individually possessing the ability to produce the same end.

ABCA1-/- and ABCG1-/- mouse macrophages show impaired chemotactic abilities that can be restored by HDL in free cholesterol-loaded wild type macrophages. The ABCA1-/- and ABCG1-/- mouse macrophages also showed a significant increase in Rac1 signaling, and resultant impairment of macrophage migration (*121*).

Low density lipoprotein receptor (LDLr) knockout and ABCG1 knockout mice were used by Meurs et al to test the idea that ABCG1 is atheroprotective, and then determine its effect on atherosclerotic progression. They found that the effect of ABCG1 deficiency on lesion development

in the LDLr -/- mice was dependent upon the stage atherogenesis, specifically that ABCG1 is atheroprotective while the lesion is in the early stages of growth—the lesion formation was found to be retarded in ABCG1-/- x LDLr -/- mice as compared to ABCG1 +/+ x LDLr -/- mice. However, in the more advanced stages of atherosclerosis, lesion development seemed to be stimulated by ABCG1 (*122*).

Transgenic Mice

Transgenic mice expressing human ABCA1 (hABCA1) were found to have a significant increase in apoA-I-mediated cholesterol efflux from aortic endothelial cells as compared to endothelial cells from control mice. The transgenic mice also had an increase in HDL cholesterol levels both when fed a chow diet and when fed a high cholesterol, high fat diet. On the high cholesterol high fat diet, these transgenic mice also showed gene expression changes in endothelial cells that are consistent with decreased inflammation and apoptosis. The high cholesterol high fat diet-induced atherosclerosis appeared to be attenuated in the transgenic mice versus the control mice (*123*).

LCAT

Major Roles

Lecithin:cholesterol acyltransferase (LCAT) is an enzyme that is primarily synthesized by the liver, but has been found to be expressed in smaller quantities in astrocytes in the brain and also in the testes (*124*). LCAT is known for its major role in the esterification of cholesterol in lipoproteins, for its necessary involvement in HDL maturation and metabolism, and for its

important association in the first step of cholesterol efflux from macrophages and consequent enhancement of cholesterol delivery to the liver (*125*).

Activation and Mechanisms of Action

The most effective activator of LCAT is apoA-I, which allows LCAT to perform a transesterification reaction on HDL resulting in the conversion of free cholesterol to cholesteryl esters (*126*). ApoA-I specifically concentrates lipid substrates in the general vicinity of LCAT and then presents them to LCAT in a conformation conducive to binding (*127*), and the size and charge of the HDL particles influences the binding of LCAT to apoA-I (*128*). Another proposed mechanism by which apoA-I activates LCAT is by increasing exposure of palmitoyloleoylphosphatidylcholine (POPC) ester bond to LCAT, since the LCAT-POPC complex stabilizes the protein (*129*).

ApoE is also known to be an activator of LCAT, although it is not as potent apoA-I. Stimulation of LCAT by apoA-I and apoE is what causes LCAT to convert free cholesterol into cholesteryl esters in the lipoprotein core, thereby directly changing the density and shape of the particle. Carlucci et al recently focused on the alteration of LCAT during the progression of atherosclerosis (as well as apoA-I and apoE) in rabbits with extreme cholesterol efflux—they found that LCAT activity and apoA-I concentrations were decreased under these conditions, but that apoE concentrations were increased (*130*), and additionally that the HDL levels of cholesterol and cholesteryl esters increased. LCAT's enzymatic effects on cholesterol that is bound to lipoproteins containing apoA-I, such as HDL, is known as α-activity (*131*).

LCAT is thought to maintain the gradient of free cholesterol between the surface of the HDL particle and the cellular membrane, allowing for an uninterrupted flow of free cholesterol

from the cell to receiving lipoproteins (132, 133). This is also important because it prevents the cholesterol from being transferred back to the cell.

LCAT contributes to the antiatherogenic properties of HDL

The antioxidant and anti-inflammatory properties of HDL are enhanced by LCAT's ability to inhibit oxidation of LDL, further supported by the fact that HDL from LCAT compound heterozygotes and homozygotes show increased oxidation of plasma lipoproteins and reduced LCAT activity (134, 135). Based on these findings it can be theorized that impairment of LCAT function could induce atherosclerosis.

A very interesting recent study corroborates the idea that LCAT contributes to HDL's antiatherogenic/antioxidant properties—Hine et al incubated LDL with HDL, apoA-I, LCAT, and paraoxonase-1 (PON1, an HDL-associated protein that prolongs LCAT activity by preventing its inactivation) alone or in combination under oxidizing conditions (*136*). They found that all of the proteins individually had the ability to enhance the ability of HDL in inhibiting LDL oxidation, and that these effects are additive; meaning that in combination LDL was protected from being oxidized for a prolonged length of time.

With further regard to LCAT's link with HDL's antioxidant properties, Kappelle et al discovered that in patients with type II diabetes mellitus LCAT activity is increased and PON-1 activity is decreased, and that in all subjects (controls and diabetes patients) LCAT activity and the antioxidative potency of HDL were inversely correlated, and directly correlated with PON-1 activity (*137*). These data suggest that individuals with type II diabetes mellitus experience a reduced efficacy of the antioxidant properties of HDL, attributed mainly to lower HDL cholesterol, but also to the increased LCAT activity and lowered PON-1 activity and hyperglycemia.

Mouse Model Studies

Overexpression

Established LCAT mouse model studies indicate that overexpression of human LCAT affected total cholesterol levels, and the TC was increased primarily thanks to an increase in HDL-transported cholesterol esters and enhanced esterification of HDL-contained free cholesterol (*138-140*). These mice reportedly had HDL particles that were significantly increased in size and that had a high apoE content. Additionally, some but not all, of the mice were seen to have lower serum triglyceride levels.

In attempts to investigate overexpression of human LCAT on atherosclerosis pathogenesis, the Vaisman group found that, when fed a high fat/high cholesterol diet for 16 weeks, the LCAT transgenic mice exhibited higher HDL cholesterol levels, higher total cholesterol levels, higher apoA-I levels, and increased LCAT α-activity (*141*). This and other studies found that LCAT overexpression did not protect against atherosclerosis (*142-145*).

Knockouts/Deficiency

The Sakai group and the Ng group independently published results of homozygous LCAT knockout mice, in which no LCAT α-HDL activity could be detected, and of heterozygous LCAT knockout mice, in which α-HDL activity was reduced but not obliterated (146, 147). On chow diet, these knockout mice displayed reduced plasma total cholesterol and HDL cholesterol concentrations, as well as apoA-I levels. When fed an atherogenic diet the mice had almost non-existent HDL levels, but also low proatherogenic apoB-containing lipoproteins and some had high

abnormal lipoprotein X particle levels (*146-149*). Additionally, on the atherogenic diet these mice showed a smaller atherosclerotic lesion size.

LCAT knockout mice, most particularly in the LDL receptor knockout background (LCAT -/- x LDLr -/-) tend to be hypersensitive to insulin and consequently at low risk for high-fat diet-induced insulin resistance and obesity (*150*), and the LDLr -/- x LCAT +/+ mouse phenotype characterized by elevated hepatic ER stress and ER cholesterol (reduced biliary cholesterol suggests that an increased re-uptake of biliary cholesterol is to blame for this finding) was rescued by LCAT deficiency. LCAT deficiency is therefore thought to be protective against hepatic endoplasmic reticulum stress in mice induced by cholesterol (*151*).

Therapeutic Regulation of LCAT

A few ideas exist as to how to therapeutically raise levels of LCAT, for replacement purposes in LCAT deficient syndromes or for potentially reducing atherosclerosis. LCAT protein administration, viral expression of LCAT, and small molecule activators of LCAT are all strategies currently being debated for their merit (*125*). For instance, small molecule activation of LCAT via pharmacological intervention exerts effects on lipoprotein metabolism, and Chen et al believe it to be a promising approach for treating dyslipidemia and atherosclerosis based on their findings that the designated small molecule activator increased HDL cholesterol levels and decreased non-HDL cholesterol and triglyceride levels, and these effects were tracked with LCAT activity (*152*).

A new class of dual-acting hypolipidemic and antiobesity agents, indole-based fibrates, which were found to cause significant weight less in visceral fat masses of hyperlipidemic rats fed a high fat diet, interestingly are found to increase LCAT levels and receptor-mediated LDL catabolism (*153*).

There is hope that therapeutic intervention involving LCAT could help stem the consequences of LCAT deficiency syndromes in humans (metabolic disorders characterized by low HDL cholesterol levels), such as fish eye disease (FED) and familial LCAT deficiency (FLD), but the road to getting there is complex and the destination is far off, since LCAT interacts with lipoproteins in such a complex manner and since studies in FED and FLD patients seem to be contradictory and inconclusive (*125*).

SR-BI

Structure, Synthesis and Expression

Scavenger receptor class B type 1 is a membrane glycoprotein of 82 kDa expressed primarily in the liver and the steriodogenic tissue of the body, and functions as a receptor for lipoproteins (*154*). Structurally, SR-B1 has two transmembrane domains and two cytoplasmic amino and carboxy terminal domains as well a large extracellular domain (*155*). On the hepatocyte, SR-B1 is found in two locations, on the basolateral membrane and canalicular membrane where it promotes cholesterol ester uptake and efflux, respectively (*156*).

Function

While SR-B1 is a receptor for various lipoproteins, including VLDL, LDL and HDL (154, 155, 157-159), its propensity for HDL is considered one of its greatest attributes. When SR-B1 is bound to HDL via an apoprotien on the particle (ie, apoA-I), it facilitates the selective uptake of triglycerides, cholesteryl esters and phospholipids from HDL to cells (*160-165*), and also promotes the efflux of free cholesterol from cells (166). At the molecular level, cholesterol transport from

cells to HDL via SR-B1 is accomplished by a binding between the molecules and then the formation of a hydrophobic channel between them, along which the cholesterol molecules diffuse (167). Larger HDL particles are known to bind better to SR-B1, and more cholesterol ester is delivered than when compared with smaller HDL particles (168). These processes collectively drive the movement of cholesterol from the peripheral tissues of the body to the liver, where it is incorporated into bile and excreted from the body. The process contributes to the reverse cholesterol transport.

Animal Studies

Transgenics

Transgenic mice expressing SR-B1 in the liver displayed an increase in the ablilty to clear VLDL and LDL and also they had decreased apoA-I and HDL levels (169, 170). In transgenic mice overexpressing SR-B1 in the liver there was a significant decrease in the levels of plasma HDL, and there was also evidence of protection from atherosclerosis (171-173).

Deficiency

Elevated HDL cholesterol levels are associated with increased atherosclerosis in SR-B1 knockout mice (174). SR-B1 deficient mice were found to have a decrease in their ability to clear HDL cholesterol (175), and a significant two fold increase in plasma cholesterol (174).

Mice lacking SR-BI along with ABCA1 (SR-BI-/- x ABCA1 -/-), have been shown to exhibit severe hypocholesterolemia (176). While this hypocholesterolemia is thought to be mainly due to HDL loss, both HDL cholesterol and non-HDL cholesterol levels are greatly reduced in these mice (although VLDL production is increased), despite a 90% reduction of HDL cholesterol uptake

by the liver. These mice also exhibited impairment in cholesterol transport from macrophages to the liver and were associated with lung and Peyer's patches macrophage foam cell accumulation. These findings further support that ABCA1 and SR-BI are crucial players in the maintenance of cholesterol homeostasis and HDL-mediated removal of cholesterol by macrophages. Interestingly, though, no atherosclerotic lesions were found in these mice. These same investigators report however, that in LDLr KO mice reconstituted with SR-BI-/- x ABCA1 -/- bone marrow-derived cells there is atherosclerotic lesion development (177), along with enhanced macrophage foam cell formation.

In SR-BI knockout mice, abnormal platelet responsiveness has been found in two independent studies. Platelets in these mice circulate in an activated state and show an increased adherence to fibrinogen (178, 179). Thus, disruption in proper SR-B1 functionality increases the risk of thrombosis.

Recent mouse model studies have also revealed an interplay between HDL, apoA-I and SR-B1, specifically it is has been found that HDL activates eNOS through apoA-I binding to SR-B1 (180) since HDL enhanced endothelium- and NO-dependent relaxation of the aortas of wild type, but not SR-B1 null mice. The stimulation of eNOs by apoA-I's interaction of lipid-bound apoA-I with SR-B1 is accomplished specifically through Src, PI3K, and Akt activation (181).

Mutation in Humans

Up until now, no functional mutations in the gene for SR-B1 have been detected in humans, but recently a family with a functional SR-BI mutation was studied. These individuals have a missense P297S mutation, and were found to have elevated HDL cholesterol levels and a reduction

in cholesterol efflux from macrophages (a 50% reduction in SR-BI-mediated HDL-cholesteryl ester uptake by cells) (182). There was, however, no associated significant increase in atherosclerosis. It was also shown that platelets from carriers of the mutation had an impairment of function as well as increased unesterified cholesterol content. These data are significant as they mark the first evidence of impacted human physiology as a result of a functional mutation in the SR-B1 gene.

SR-B1 is now credited for participating in adrenal steriodogenesis and platelet function, in addition to its more well-established function in the cellular uptake of HDL cholesteryl esters (183). Carriers of the P297S missense mutation in the SR-B1 gene show an attenuation of adrenal steroidogenesis as evidenced by symptoms of a primary gluccocorticoid insufficiency (182). The authors extrapolate that SR-B1 is also needed to generate the appropriate amount of cholesterol required for an optimal rate of steriodogenesis.

SR-B1 has also recently been implicated in modulating platelet function. In SR-B1 P297S patients, platelet cholesterol content is elevated resulting in abnormal platelet reactivity such as increased ability to adhere to fibrinogen (182). Thus, disruption in proper SR-B1 functionality increases the risk of thrombosis.

In a separate publication validating the idea that SR-B1 mutations, while rare, are a cause of elevated HLD cholesterol in humans, investigators looked at two individuals with very high levels of HDL cholesterol and two separate mutations that segregated with high HDL cholesterol within the family members. Even though these subjects were heterozygous for these mutations, they had a 37% increase in their plasma HDL cholesterol (184).

MATERIALS AND METHODS

Experimental Procedures

Cell Culture Procedures

Changing Cell Media—Biweekly

A necessary duty of maintaining cell lines is to change the media in which the cells grow. This ensures that the cell populations are healthy and that they do not grow to be overconfluent, and it is done twice a week.

The first step is to warm the media in a water bath for 15-20 minutes. The media that one uses depends on the cell type. I use three cell types, and therefore have three different cell medias. For 911 cells, I use Mediatech's Cellgro 10-014-CV DMEM (Dulbecco's Modified Eagle Medium) with 1g/L glucose, L-glutamine & sodium pyruvate plus Cellgro 30-002-CI Penicillin Streptomycin (10,000 IU/mL penicillin and 10,000 ug/mL streptomycin) and 10% fetal calf serum added. For 293 cells I use Mediatech's Cellgro 10-045-CV L-15, 1X (Leibovitz's L-15, Modified) with L-glutamine plus Cellgro 30-002-CI Penicillin Streptomycin (10,000 IU/mL penicillin and 10,000 ug/mL streptomycin) and 10% fetal calf serum added. For HTB-13 cells I use Mediatech's Cellgro 10-045-CV L-15, 1X (Leibovitz's L-15, Modified) with L-glutamine plus Cellgro 30-002-CI Penicillin Streptomycin (10,000 IU/mL penicillin and 10,000 ug/mL streptomycin) and 10% fetal calf serum added. The 911 cells are incubated in 5% CO_2 environment, while the 293 andHTB-13 cells are kept in a CO_2–free environment.

Once the media has been adequately warmed, and the hood in the tissue culture room has been wiped down thoroughly with diluted Steris NJ138 Wescodyne and isopropanol 70%, I suction

about one inch of Wescodyne into the trap and then bring the cells into the hood. The old media is suctioned out of the 600mL Corning CellBind bottle using a 5mL Costar Stripette 4487 (with the cotton removed) attached to the trap and vacuum. I take care not to touch the sides or neck of the bottle, and especially not to touch the surface where the cells reside. About 50mL of media is suctioned out, and then 50mL of fresh media is added to the bottle using a 50mL Costar Stripette 4490 and Jencons PowerPette Pro.

Once the fresh media is added, the bottles are placed back inside their incubator, the non-CO_2 incubator for 293 and HTB-13 cells and the 5% CO_2 incubator for the 911 cells.

Recombinant Adenovirus Procedures: Infection, Amplification, Titration

Plating Triple Flasks for Viral infection of Cells

In order to plate triple flasks for the infection of cells with a virus, first the cells are split and plated to $2.5x10^6$ or $5x10^6$ in a T175 flask with 50mL of medium. Again, when using 293 cells, L-15 media is selected. One T175 flask needs to be made for every 2 triple flasks desired.

In about a week's time the flask will become confluent. One new bottle of complete medium is prepared per 5 triple flasks; this entails adding 10% fetal bovine serum and 1% Cellgro 30-002-CI Penicillin Streptomycin (10,000 IU/mL penicillin and 10,000 ug/mL streptomycin) to Mediatech's Cellgro 10-045-CV L-15, 1X (Leibovitz's L-15, Modified) with L-glutamine.

The old media contained in the T175 flasks is suctioned off using a 5mL Costar Stripette 4487 (with the cotton removed) attached to the trap and vacuum. Once this old media is removed, each flask is rinsed with 4mL of PBS. The PBS is similarly aspirated off. Next, 4mL of trypsin is added to each flask and the cells are allowed to incubate at room temperature for 5 minutes, in order

to loosen the cells from the surface of the flasks. After the 5 minutes, 6mL of the freshly-made complete medium is added to each flask, and the entire contents of each flask is then mixed by pipetting up and down a few times. Pipetting can be ceased once there are no more visible cell clumps.

Next, the contexts of about two and a half flasks are combined, aiming for a total volume of ~25mL. This 25mL is then placed into one bottle of complete media and mixed thoroughly. This is repeated until the contents of all flasks are put into complete media.

The bag of Triple flasks are now brought into the hood and opened only there. The triple flasks are then labeled with the cell type, date, initials, etc. and marked at the 100mL line. The complete media containing the cells and trypsin is then poured into the triple flasks up to the marked line at ~100mL. A little more is okay. Before capping the triple flasks, I am sure to squeeze them so as to remove as much air as possible.

The flasks are then incubated at 37°C in the "-CO^2" incubator for 4-5 days, or until the cells reach ~ 70% confluence.

Infecting the triple flasks

After the triple flasks have come to ~70% confluence, they are ready to be infected.

Initially, the stock of adenovirus is thawed on ice. It is normally stored in -80°C. If needed, fresh heat-inactivated horse serum (HIHS) and Cellgro 30-002-CI Penicillin Streptomycin (10,000 IU/mL penicillin and 10,000 ug/mL streptomycin) (P/S) is thawed as well.

While the thaw is taking place, media is prepared in quantities reflecting the following ratio of 2 full bottles for each 10 triple flasks being infected. Ten triple flasks are needed for each virus

one plans on using. First, the Leibovitz's L-15 media (Mediatech's Cellgro 10-045-CV L-15, 1X (Leibovitz's L-15, Modified) with L-glutamine) is warmed in a water bath for 15-20 minutes, and then to the 500mL bottle, 10mL (2%) HIHS is added and 5 mL (1%) P/S is added as well.

In the hood of the adenovirus room, 1 x 10^9 pfu of the thawed virus is added to the media and the mixture is swirled to ensure adequate mixing. The old media in the triple flasks from the plating is disposed of in a beaker containing 1% sodium dodecyl sulfate (SDS). To the now empty triple flasks, one bottle of complete media (500mL) is distributed between 5 triple flasks (~100mL into each), while the other bottle of complete media is distributed between the remaining 5 triple flasks (per virus). This concept is visualized below for simplicity.

Figure 4: Schematic of distribution of media—this set up is for ONE virus.

When tightening the lids on the flasks, the flasks are squeezed so that there is as little air as possible trapped in the flasks. The triple flasks are then incubated at 37°C in a "–$C0_2$" incubator until all of the cells have been infected by the virus. This usually takes between two and three days.

Once the cells are infected and most of the virus is inside the cells, they are harvested by tapping on the flasks to detach the cells from the surface. The media from 5 of the triple flasks, which now contains the cells as well, is poured into a 500mL Corning 431123 centrifuge conical tube with plug seal cap (therefore, for each virus, one needs two of these conical tubes). The conical tubes are then spun in a Beckman GS-6 centrifuge for 10 minutes at 1000 rpm and at room temperature.

After the spin, there will be a pellet containing the cells infected with the virus. The resulting supernatant is discarded into a beaker containing 1% SDS. Next, 2mL of serum-free media (L-15 with 2% HIHS but without penstrep) is added to each conical tube. The pellet in each tube is then resuspended using the media and by a motion of pipetting the entire contents of the tube up and down. The contents of both conical tubes is then transferred into a 50mL Falcon 352098 tube and stored at -80°C.

Purification of the virus

The first step in purifying a virus is a series of freeze thaws of the infected cell pellet. The pellet will be stored frozen at -80°C. This counts as the first "freezing" of the freeze/thaw cycle. It will then be thawed in a water bath of 37°C for ten minutes, then vortexed using the Fisher Vortex Genie 2 12-812. It is then refrozen in -80°C for 30 minutes. Next, it is thawed again in a 37°C water

bath for ten minutes and vortexed. It is frozen at -80°C for 30 minutes one last time, and then thawed again in a 37°C water bath for ten minutes and vortexed for the third and final time.

While the freeze/thaw cycle is taking place, I get a head start on freezing the rotor which will be used later. I put the empty rotor in the centrifuge and set it to 4°C so that it takes less time for the temperature to get down to 4°C when it is time for the infected cells to be spun.

After the final thaw has been completed, the cells are spun at 3000rpm in the Beckman GS-6 centrifuge for ten minutes at room temperature. While the cells are spinning, the tubes which will be used in the ultracentrifugation can be prepared. Two Ultra-Clear Beckman 344059 ultracentrifuge tubes are used per virus. Overlay 2mL of CsCl 0.619g/mL (density=1.379), and 4mL of CsCl 0.277g/mL (density=1.353) into a gradient for each tube. The CsCl solution with the greatest density is pippetted into the tube first, so that it is already on the bottom. Next, an equal volume (6mL) of the adenovirus supernatant is overlaid onto the top of each tube. Once the centrifuge tubes are completely prepared, they are placed in a Beckman SW 41 (O1 E 5212) rotor and spun in the Beckman L8-M Ultracentrifuge at 4°C for 90 minutes at 30,000 rpm.

During this first spin, I prepare for the next step by filling one Beckman Polyallomer Quick-Seal Centrifuge tube to about 2/3 full with ~15mL of CsCl 0.450g/mL (density=1.363). There should be one quick seal tube for each 2 ultra clear tubes—one for each virus.

After the 90 minute spin, the two tubes should appear as in Figure 5.

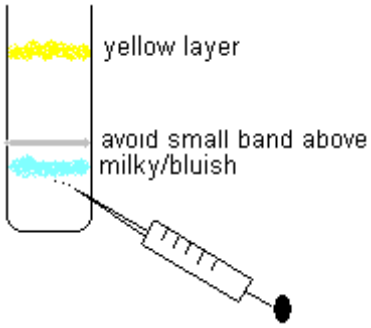

Figure 5: Viral band visualization

The blusih, milky band pictured in Figure 5 is the virus-containing band. The next step is to extract this band containing the virus. This is accomplished most easily by clamping the tube to a ring stand inside the hood with a large beaker containing 1% SDS beneath it. A 5mL Henke Sass Wolf Norm-Ject Luer Lock latex-free syringe is attached to an 18 gauge Becton Dickinson Precision Glide 18G1½ 305196 needle, and this is used to pierce the tube, with the beveled edge of the needle pointing upward. The needle is inserted about ½ an inch beneath the virus band. The needle is then angled upward so that the bevel becomes flush with the bottom surface of the virus band, and very carefully the syringe is pulled out so that the vacuum in the syringe pulls the liquid into the needle and then into the body of the syringe. Continue this until the entire virus band (and nothing else) is removed from the tube. The band is then injected from the syringe, overlaid on top of the CsCl in the quick seal tube.

The process is then repeated with the second virus band in the second tube. Once both virus bands are in the quick seal tube, it is filled up the rest of the way with CsCl 0.450g/mL (density=1.363). The tube is tapped to remove any bubbles, as I want there to be no air in the tube. As a precaution, I clean the outside of the tube with 1% SDS and then 70% alcohol to be sure it's clean before removing it from the hood.

A small metal cap is put over the opening and the tube is placed in the Beckman Tube Sealer G3 329146, under the heating element. I gently depress the heat sealing apparatus so that the bottom surface makes contact with the metal cap on the tube. Heat is transferred and the plastic begins to soften and melt. Gentle pressure is continued until the metal cap moves about 1/8 from the neck of the tube. The tube is shifted over and placed underneath the pressure applier (sans heat) and I gently push until the metal cap makes contact with the neck of the tube.

Situating the quick seal tube back inside the hood and over the beaker containing 1% SDS, the tube is squeezed and inspected to ensure that there are no leaks.

The tube is then placed into the Beckman Ti70 rotor and left to spin in the Beckman L-8 Ultracentrifuge at 4°C for 16-22 hours at 55,000 rpm.

The next day, I prepare the dialysis buffer and then keep it cool at 4°C while I wait for the spin to finish. One liter of buffer is needed for each virus. The buffer is a mixture of 10mL Tris 1M (pH=8), 20mL 0.1M $MgCl_2$, 50g sucrose, and then filled to the 1 liter mark with ddH_2O. I usually prepare the buffer in a Nalgene 1,000mL bucket.

Next, 400mL beakers with magnets in them are autoclaved—one per virus. These will be used later, but it is most efficient to let them autoclave while virus is spinning.

Once the spin is almost finished (about 10 minutes before I remove the virus), the dialysis cassettes are prepared. Slide-A-Lyzer 66380 10,000 MWCO Dialysis Cassettes are labeled and pre-rinsed in the cold dialysis buffer for one to ten minutes in the 400mL beakers that were autoclaved.

The quick seal tube containing the virus from the centrifuge and the 400mL beaker with the buffer and cassette are taken to the adenovirus room, and the tube is affixed to the ring clamp stand,

again with a larger beaker containing 1% SDS below. With another 18 gauge needle a hole is punctured in the top of the tube. Now, another 18g needle and 5mL syringe combination is used to extract the virus band once again, using the same careful method as before.

Inverting the syringe, add a volume of air that equals the volume of virus just extracted from the tube. The syringe is then inserted into the dialysis cassette at one of the corners (the corner is then marked so as to be able to identify it later), just to the point where the tip of the needle can be seen—taking care not to puncture the fragile membrane (see Figure 6.1). The air from the syringe is pushed into the cassette. This serves to separate the membranes enough so that the needle can enter more safely. The cassette and syringe are then inverted and the needle is inserted further into the cassette before the virus is injected into the cassette (see Figure 6.2). Once all of the virus has been injected, use the syringe to remove as much of the air from the cassette as possible. Remove the syringe slowly as the vacuum in the cassette is being created.

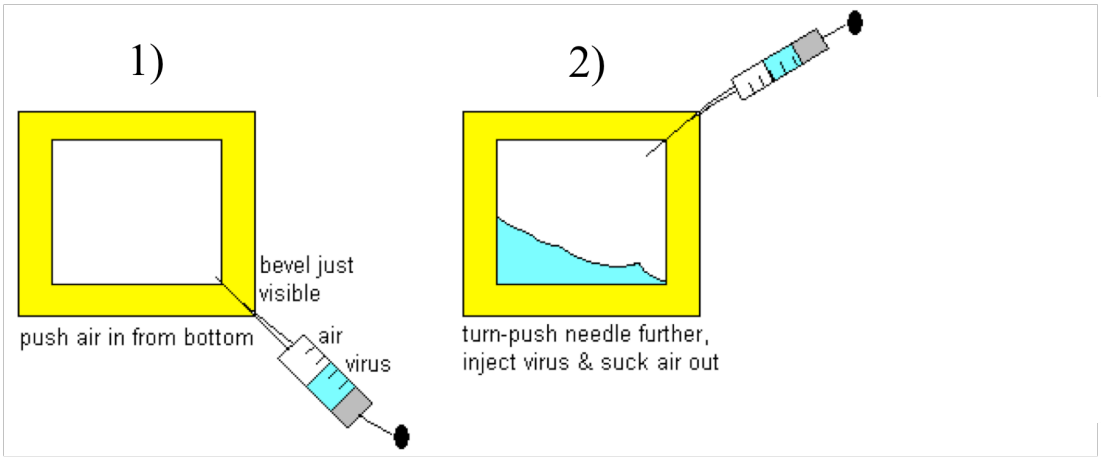

Figure 6: Orientations of cassette and syringe

Next, the dialysis cassette is placed inside a “U” shaped foam holder, and then placed into the 400mL beaker of dialysis buffer and left at 4°C for 2 hours on a magnetic spinning plate.

After two hours, the dialysis buffer is changed and it is all left to sit overnight, between 16 and 22 hours, at 4°C.

The next day the dialysis buffer is changed once again, and then left for another 2-4 hours at 4°C. While this last cycle of dialyzing at 4°C takes place, I prepare the tubes that the virus will go into. I use sterile eppendorf 1.5mL tubes, and fill them each with 50µL of the virus. For one virus, I usually get around 20 of these 50µL aliquots. It is important to keep everything on ice at this point.

After the 2-4 hours of the last dialysis, I once again get an 18g needle attached to a 5mL latex-free syringe to extract the virus. Pull back on the stopper to about 1 or 2 mL and then inject that air into the cassette (using the same hole that was used previously, it should be marked) like this:

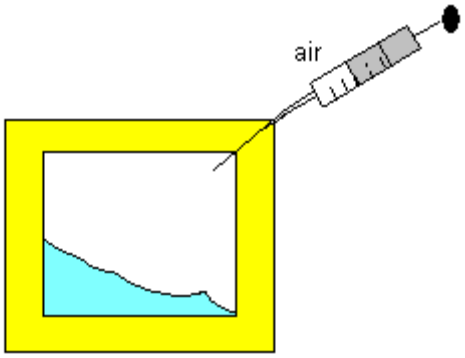

Figure 7: Injecting air into the cassette

Injecting air into the dialysis cassette so as to not puncture the membrane when extracting the dialyzed virus.

The cassette is then inverted and the dialysate containing the virus is withdrew (it should been between 1 and 2 mL).

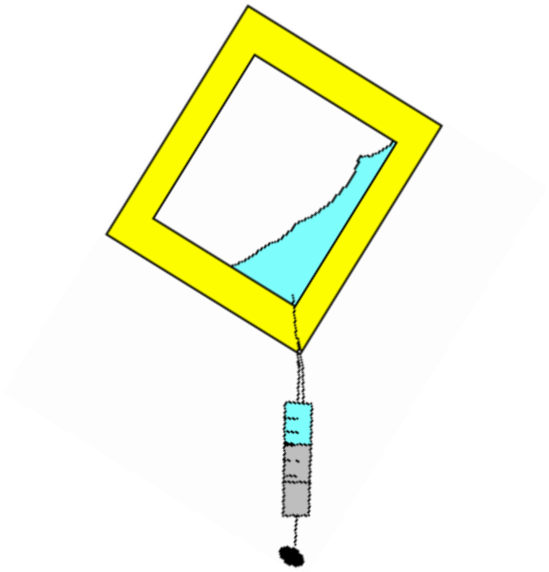

Figure 8: Withdrawal of the virus from the dialysis cassette.

All of the dialysate is placed into one of the prepared sterile 1.5mL eppendorf tubes marked for an aliquot. The dialysate is then distributed in denominations of 50µL to the other eppendorfs to create the aliquots. Store the aliquots at -80°C.

Titration of the virus

Titration of the newly-amplified virus is necessary so that those who will use the aliquots know the general concentration of the virus in plaque-forming units per any given volume.

A 6 well plate is prepared in advance to contain $2x10^6$ cells per well. The cells that I consistently use for this purpose are the 911 cells, and therefore I use the complete DMEM media (Mediatech's Cellgro 10-014-CV DMEM (Dulbecco's Modified Eagle Medium) with 1g/L

glucose, L-glutamine & sodium pyruvate plus Cellgro 30-002-CI Penicillin Streptomycin (10,000 IU/mL penicillin and 10,000 ug/mL streptomycin) and 10% fetal calf serum added). These cells are allowed to grow in the 37°C incubator containing 5% CO_2 for one to two days, or until they are about 90% confluent.

When the cells are ready, aliquots of the desired virus are placed in a bucket of ice to thaw slowly, and a water bath is set to be between 50-55°C. For each virus to be titrated, a total of 7 tubes are needed for a series of dilutions. While the viruses thaw and the water bath heats, prepare these tubes, the 1.5% agarose mixture and the medium mixture. There should be 3 eppendorfs labeled 1-3, and 4 15mL Falcons labeled 4-7. The 1.5% agarose mixture is made by combining 1.5g agarose, 4mL 1M Hepes (pH=7.4), and 96 mL ddH_20 and then autoclaving the solution to dissolve the agarose (this solution can be made ahead and then stored at 4°C). I keep my agarose solution stocked, so from the refrigerator I just place it in the microwave (for only one minute increments) until it is a liquid and then keep it at 55°C in the water bath. To make the medium mixture, calculate how much will be necessary, based on how many viruses there are to be titrated. As a general rule, 25mL of medium mixture will be plenty for one virus. To make 25mL of the medium mixture, combine 0.625mL 1M $MgCl_2$ with 1mL HIHS and 23.36mL 2x MEM. Once prepared, keep this in the 55°C water bath as well.

Once the virus has thawed, it is brought into the adenovirus room (still on ice) along with the 7 tubes and 6 well plates containing the 911 cells in order to make the series of dilutions. The dilutions are made according to the following table.

Table 1: Outline of the dilutions, and the contents of each tube.

Tube	Medium (complete DMEM)	Volume of virus (µl)	Cal. Factor
1	1 ml	20 µl (stock)	
2	1 ml	10 µl (1)	($x10^2$ / 20 µl)
3	1 ml	10 µl (2)	($x10^4$ / 20 µl)
4	1.8 ml	200 µl (3)	($x10^5$ / 20 µl)
5	1.8 ml	200 µl (4)	($x10^6$ / 20 µl)
6	5.4 ml	600 µl (5)	($x10^7$ / 20 µl)
7	5.4 ml	600 µl (6)	($x10^8$ / 20 µl)
8	1.8 ml	200 µl (omit)	($x10^9$ / 20 µl)
9	1.8 ml	200 µl (omit)	($x10^{10}$ / 20 µl)

Next, the media in each of the wells of the plates containing the cells is removed. This is accomplished via the vacuum in the hood, a double trap system with a pipette tip attached to the end of the hose.

Into the blank well, labeled "B," I put 1000µL of complete DMEM. The other wells labeled 4-7, correspond to the tube containing the diluted virus stock. The "4" well is filled with 1000µL

from the 4 tube, the "5" well with 1000μL from the 5 tube, and so on. There are three "6" wells and three "7" wells. When filling the wells, it is always advisable to begin with the least concentrated virus, and move on from there (ie. the blank is filled first, then 7, then 6, then 5, then 4). The 1000μL of virus stock is loaded into the wells very slowly and carefully in a drop-wise fashion as the cells are adhered to the bottom surface of the well and they should be as unaggitated as possible.

Once all of the wells are correctly filled, they are placed in the 37°C incubator with 5% CO_2 for 30 minutes.

The agarose solution that will overlay the infected cells is equal parts 1.5% agarose mixture and the medium mixtures, prepared earlier. It is prepared and kept in the 55°C water bath until ready for use.

After the 30 minute incubation is up, the virus-containing media is removed from the wells of the plates, and very quickly thereafter the agarose solution is slowly and carefully overlaid in the wells. Again, the blank well is filled first, then 7, then 6, etc. The "7" wells get 3mL of the agarose solution, while all of the other wells are overlaid with 2mL.

The plate is kept in the hood for about five minutes, or until the gel has solidified, and then placed into the 37°C incubator with 5% CO_2 for 9-10 days while plaque formation occurs.

On the 9^{th} or 10^{th} day, the viral titer is calculated by taking the plates to the microscope. The plates are placed upside down on the viewing surface of the microscope and the cells are first visualized under normal light. To count the plaques, the plates are viewed under a blue light only, since the infected cells will fluoresce green. The plaques are counted and recorded for the "6" wells and the "7" wells. The average plaque number for "6" is found, as it is for "7." Then these averages are each divided by 20 (the initial volume of the stock virus). The resultant number for the "6" well

is multiplied by 10^7, while the resultant number for "7" is multiplied by 10^8. This final number is the titer, in units of pfu/μL.

Testing a new virus with HTB-13 cells

In order to test the efficacy and the virulence of a virus, I typically would use HTB-13 cells. A 6 well plate is prepared, as only 4 wells are needed per virus to be tested. Since the cells are HTB-13, L-15 media plus 10% FBS and 1% P/S (Mediatech's Cellgro 10-045-CV L-15, 1X (Leibovitz's L-15, Modified) with L-glutamine plus Cellgro 30-002-CI Penicillin Streptomycin (10,000 IU/mL penicillin and 10,000 ug/mL streptomycin) and 10% fetal calf serum added) is used. There are 2mL of media in each well, and about 106 cells in each well.

The next day the media is changed, to L-15 plus 2% HIHS and 1% P/S (Mediatech's Cellgro 10-045-CV L-15, 1X (Leibovitz's L-15, Modified) with L-glutamine plus Cellgro 30-002-CI Penicillin Streptomycin (10,000 IU/mL penicillin and 10,000 ug/mL streptomycin) and 2% heat-inactivated horse serum added). Again, there are 2mL of media in each well. Next, the cells are infected with the chosen virus at various multiplicities of infection (MOI), usually 5, 10, and 20 MOI. MOI is calculated based on the titer of the virus. The fourth well is left untransfected. The plate is left overnight in a "-CO_2" 37°C incubator.

The next day the cells are washed in L-15 with 1% P/S (*no serum* should be in this media), which is then aspirated off. Each well then gets another 2mL of L-15 with 1% P/S, which is left for two hours in the "-CO_2" 37°C incubator.

After two hours, the cells are once again washed with L-15 with 1% P/S and aspirated off. Next, 1mL of L-15 with 1% P/S is put into each well and the plate is left overnight in the "-CO_2" 37°C incubator.

The next day the media is collected—the contents of each well goes into its own 1.5mL eppendorf tube, which is then dried to a concentrated form with a volume of about 500μL with Savant Speed Vac SC110 and Savant Universal Vacuum System 400.

The resultant contents of the eppendorfs contain protein, which I analyze with a standard Western blot or in a SDS-PAGE gel stained with coomasie.

Procedures on the Mice

Maintaining Mouse lines/General Care of the Mice

It is necessary to adequately care for mouse lines in order to do the research entailed in the following project. The care involves maintenance and attention daily to weekly, depending on if special care instructions or diets are in place. For general care, a census is taken once weekly to determine health status, breeding pair success, etc of all of the mice. Breeding pairs are set and monitored as needed, and pups are given three weeks with the mother to nurse, and are weaned and separated from their parents and dissimilarly sexed siblings thereafter. The mice are caged according the following rules, a maximum of 4 male mice in one cage and maximum of five female mice in one cage. They always have access to standard chow diet and water, and their cages are changed by the Husbandry Staff of BUMC frequently for sanitation purposes. The mice are presently housed at Boston University Medical Center of the Boston University Medical School on the secured 8th floor, with limited access. The floor is 'clean,' and this requires all who enter to wear barriers such as lab coats, sleeve covers, gloves, face masks, eye protection and shoe covers. Within this facility, the mice are exposed to a 12 hour light/12 hour dark cycle continuously. All experimental procedures performed for this thesis and the projects with which it was and is

associated were in line with the National Institute of Health and the guidelines set forth by the NIH protocol 14219.

Mice for the experiments used in the experiments described here within are referred to as double knockout for AI and E, since they are apoA-I $^{-/-}$ *and* apoE $^{-/-}$. The species of these mice is Mus musculus.

The original knockouts have been selectively bred, and thus the line of apoA-I $^{-/-}$ *and* apoE $^{-/-}$ has been perpetuated and remains viable for experimentation.

Obtaining blood samples from live mice

The way that I normally take blood from the mice is by performing a tail vein bleed. This usually yields about 20μL of plasma per bleed. To start, I fast the mice for four hours. The mice are transferred to new, clean cages since when there is no food available they are known to eat their own excrement. Water is, of course, still provided to them.

Once four hours have passed, the mice are individually selected from their cage and then placed into a restrainer, effecting holding their bodies still but leaving the tail loose and free. Using a very sharp razor blade, I snip the just very end of the tail off and massage the tail to encourage blood flow. The blood slowly comes out of the tail, and is collected in Microvette CB 300 K2E tubes containing EDTA dipotassium salt by Sarstedt.

Food is promptly returned to the mice, and the tubes are spun in the Eppendorf Centrifuge 5415C for 10 minutes at 3,000rpm to separate the plasma from the blood cells. The plasma is then isolated and stored at 4°C, or used/tested immediately in any given assay.

Sacrificing Mice/Obtaining blood and tissue samples for analysis

For my experiments, mice need to be sacrificed 4 days post-infection with an adenovirus. We have to sacrifice the mouse in order to see how the virus affected it and also the see the expression of said virus.

The mice are fasted for 4 hours prior to sacrificing them and blood collection, this ensures the most accurate lipid readings. After the period of fasting, one at a time the mice are put inside a jar with an isoflurane-soaked cotton ball. Isoflurane is an inhalation anesthetic, and I use Baxter brand's Aerrane for horses and dogs NDC 10019-733-60. Once the mouse has expired, the eyeball is removed and blood from the eye cavity is collected into a Sarstedt 41.1395.105 Microtube 1.3mL K3E containing 1.6mg EDTA. Usually between 0.5 and 1 mL can by obtained using this method. Immediately after the blood has been collected, the mouse is laid supine and a lateral incision is made to open the thoracic cavity and expose the organs. I quickly identify the liver and cut a small piece from one lobe and place it into a Fisherbrand Microcentrifuge Tube 2.0mL Graduated Free Standing Screw Cap Tube with Cap and O-Ring 02-682-558. This then is plunged into a vat of liquid nitrogen to undergo flashfreezing. Next, a small piece of the liver from a different lobe is cut and placed into a second microcentrifuge screw cap tube, which is also placed into the liquid nitrogen. The remaining sections of the liver are placed into yet a third microcentrifuge screw cap tube, which is then also placed into the liquid nitrogen.

Once all of the blood has been collected, the tubes are spun down in the Eppendorf 5415C centrifuge for 10 minutes at 3,000rpm, and the liver samples are stored in -80°C. The plasma is collected and stored at -4°C or -20°C, depending on how long it will be before it is used/tested.

The mouse carcasses are disposed of in a proper manner, using the hazardous waste containment on the 8th floor of the W Building at BUMC.

SDS-polyacrylamide gel electrophoresis (SDS-PAGE)

The Sodium Dodecyl Sulfate Polyacrylamide Gel Electrophoresis (SDS-PAGE) is a general electrophoresis gel that was often used in my experiments and analysis of my samples. To begin, I prep and gather all materials for making the gel itself. I use two Biorad 1.5mm glass plates for each gel, one is completely flat and the other has two raised bars on the vertical edges, so as to create a 1.5mm space for the gel when the two plates are sandwiched together. These plates are cleaned with alcohol and then sandwiched together. An aerial view of the two plates when properly placed together is seen below.

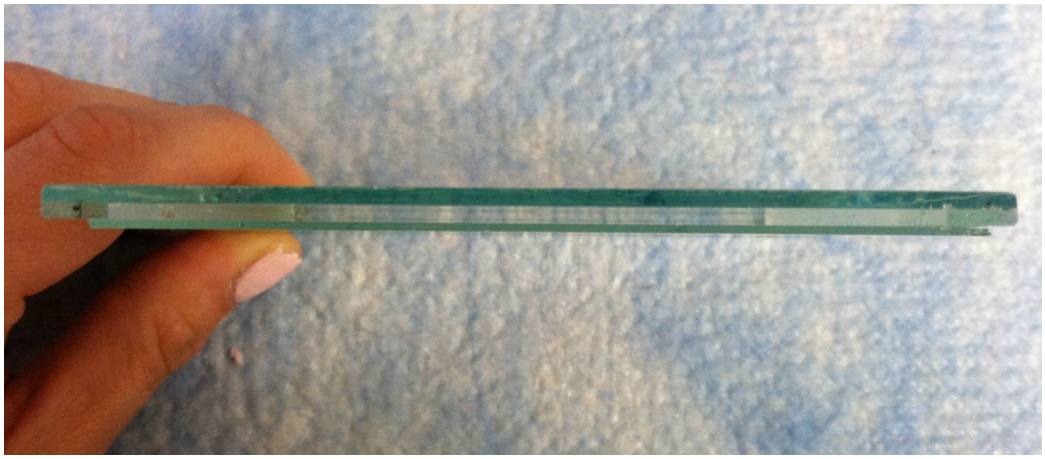

Figure 10: Proper placement of glass plates for gels.

The glasses are then secured into green Biorad clamps and I ensure that the bottom surfaces of the glass are flush with a flat surface. The glasses and clamps are positioned into a clear Biorad gel casting unit, which affixes the glasses in the correct upright position, ideal for pouring the gel.

At this point, I mix together the reagents for the gel which has two components, the running and the stacking. I use a 13% Mini Stacking Gel, containing 8.4mL of dH20, 2.55mL of 30% Acrylamide Ultra Pure ProtoGel by National Diagnostics, 3.75mL of Stacking Buffer (4X: 30g Tris, 20mL 10% SDS, pH=6.8), 150µL of 10% SDS, 25.5µL of TEMED, and 255µL of 10% APS. For the Running Gel, I also use a 13% Mini Gel recipe containing 12.26mL of dH20, 17.34mL of 30% Acrylamide Ultra Pure ProtoGel by National Diagnostics, 10mL of Running Buffer (4x: 181.7g Tris, 40mL 10% SDS, pH=8.8), 400µL of 10% SDS, 68µL of TEMED, and 266µL of 10% APS. I do not mix in the APS until immediately before I am ready to pour into the glasses, as the TEMED and APS polymerize very quickly. I pour the Running Gel in between the glass plates first, using a 5mL Costar Strippette 4487 connected to a Drummond Pipet-Aid. The glasses are filled to ~½ to ¾ of an inch from the top of the gel. This layer is then overlayed with isopropanol to ensure a smooth and flat surface. After the running gel is completely polymerized and warm to the touch (the polymerization is an exothermic reaction, so the release of heat is a proper indicator that it is taking place), the gel casting unit is turned upside down to drain off the isopropanol. Then the Stacking Gel is poured on top of the polymerized Running Gel in between the glass plates, using a style E transfer pipette. The Stacking Gel is added to point of flowing over the top of the glasses, and then a 15 well Biorad 1.5mm comb is inserted, creating the wells that sample will eventually fill. The following image depicts what the entire set up looks like up to this point.

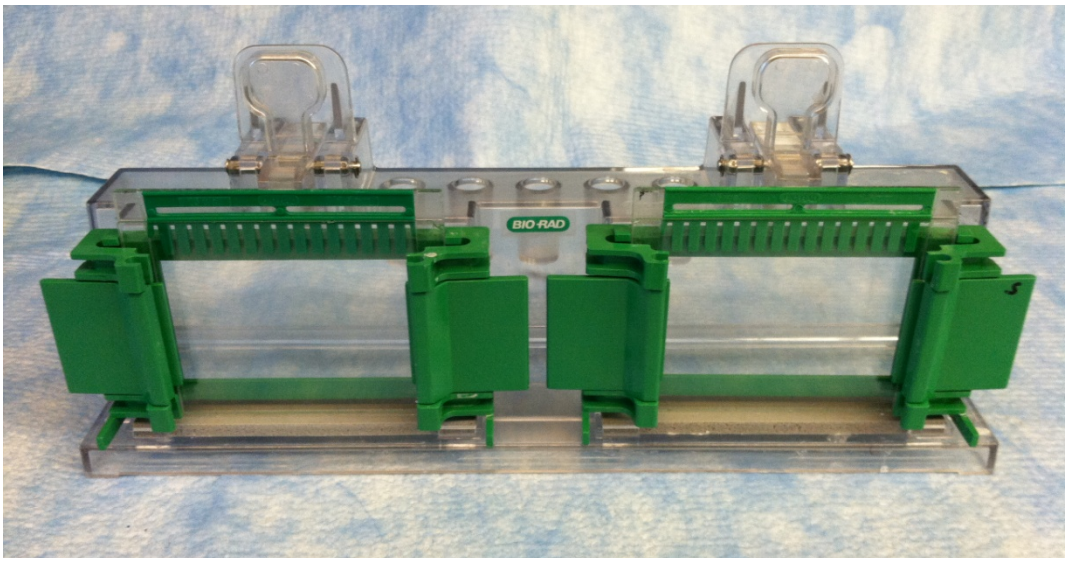

Figure 11: Glass Plates and casting gel apparatus

Once the Stacking Gel has polymerized, the gel with its glass plates and green Biorad clamps are placed into the electrode holding system, and then into the Biorad Mini-Protean II bucket. Illustrated steps are shown below.

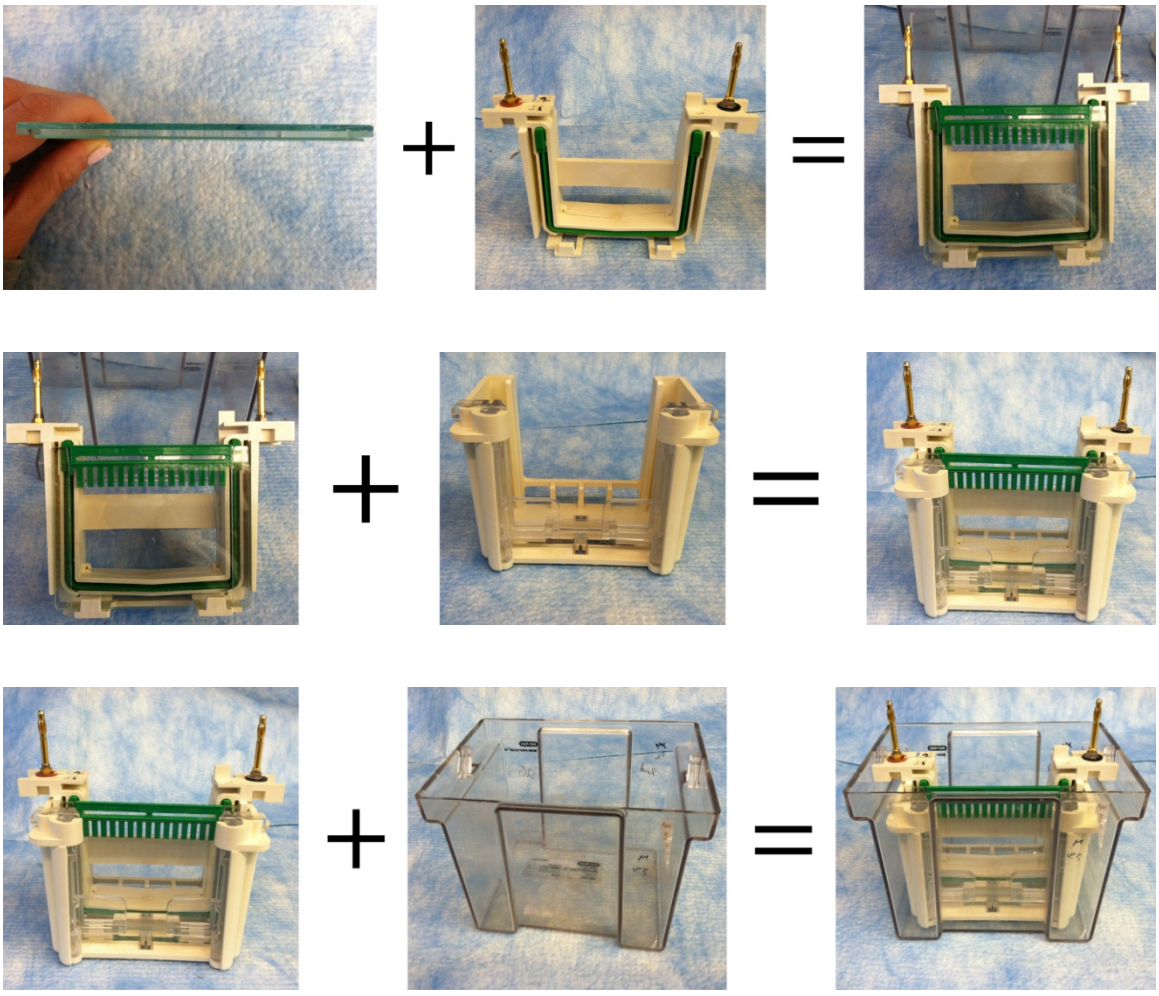

Figure 12: Steps for combining components

Once the set up is complete, the central trough is filled to overflowing, and the bottom of the bucket to ~2-3 inches, with 1X Running Buffer containing Tris, glycine, and SDS. The comb is gingerly removed from the gel at this point.

The next step is to fill the wells. The first well is always filled with 25µL a marker, I use the Prestained Protein Marker, Broad Range #P7708S from New England BioLabs. The second and third wells get filled with BSA plus 5µL 5X Loading Buffer—the second with 2µL of 1µg BSA,

and the third with 10µL of 5µg BSA. Since each well should have a total load volume of 25µL, the second well containing the 1µg BSA also contains 18µL of PBS, and similarly the third containing the 5µg BSA also contains 10µL of PBS. Beginning with the fourth well, 20µL of individual samples are loaded per well (these each contain 5µL of 5X Loading Buffer as well).

After all of the samples have been properly loaded, the bucket is capped with a green Biorad hat with red and black electrodes. The entire system is then hooked up to an E-C Apparatus Corporation EC105 voltage generator. The red electrode will connect with the red receptacle, and the black to the black.

The gel is run generally at ~105V for about an hour and a half, or until the stain travels the desired amount down the gel. It is important to turn off the voltage generator before unplugging the cords to avoid any kind of elecroshock. Next, the system is disassembled to the point of having just the gel encased by the glasses. After removing the top flat glass, I use a razor blade to remove all of the stacking gel. The remaining running gel is then carefully and slowly removed from the bottom glass plate and it is placed into a gel tray. Coomassie stain made from 2.5g of coomassie blue, 225mL methanol, 225mL H2O, and 50mL glacial acetic acid, is added to the tray as well, in order to stain the marks on the gel. The tray is then placed on a Boekel Scientific Rocker II Model 260350 and let to rock for 30 minutes to an hour.

After the hour has passed, the coomassie blue stain is discarded and the tray is now filled with enough 2D Fixative to cover the gel and a crumpled Kimwipe is placed in the corner to help absorb the dye. The fixative is made up of 300mL acetic acid, 1450mL methanol and 1450mL water. The tray is again kept in constant, gentle motion on the Boekel rocker, and the fixative is changed out every hour or so until only the bands remain stained.

Once all of the coomassie staining has been removed, the gel is re-hydrated with water, this usually takes only 10-20 minutes. After the hydration is complete, I wrap the gel in plastic wrap and scan it to the computer so as to have a color image of it on file, and then dry it out for storage. To dry the gel, I cut a piece of Whatman 3MM Chr chromatography paper 3030 917 to about 6" x 4" and wet it thoroughly. I place the gel in the middle of the paper and then put it inside the BioRad Model 583 Gel Dryer. Using the Savant Universal Vacuum System UVS400, I dry the gel for about 1.5 hours.

Density Gradient Ultracentrifugation *(and downstream analyses)*

For the isolation of lipoproteins from plasma, I used an HDL flotation assay. This takes a total of approximately four days, including a few overnight spins/dialyzations. The first thing I do for this assay is to make the 5-layer potassium bromide (KBr) gradient in Beckman #344062 Ultra-Clear Centrifuge Tubes, which are made specifically to be used with a Beckman Class G & H SW60 rotor with six 44.4 gauge tubes.

The bottom layer of the gradient consists of KBr, plasma, and PBS. The volumes of each are calculated so that the density of this layer is 1.23 and the volume is 0.4 mL. For my experiments, this meant that I used 145mg of KBr, 240 microliters of plasma, and 160microL of PBS.

The remaining layers are comprised of pre-made KBr solutions of known density. I made solutions of the following densities: 1.21, 1.063, and 1.019 using simple dilution with PBS followed by vacuum filtering.

In ascending order, I add 0.8mL of 1.21 KBr first, then on top of that I add 2mL of 1.063 KBr, and then on top of that I add 0.4mL of 1.019 KBr. For the very topmost layer in the centrifuge tubes, I add 0.4mL of PBS. The layers are visualized as shown in the illustration below. Each layer

is essentially “overlayed” over the others, very carefully in a drop-wise fashion so as to ensure the densities stay separated.

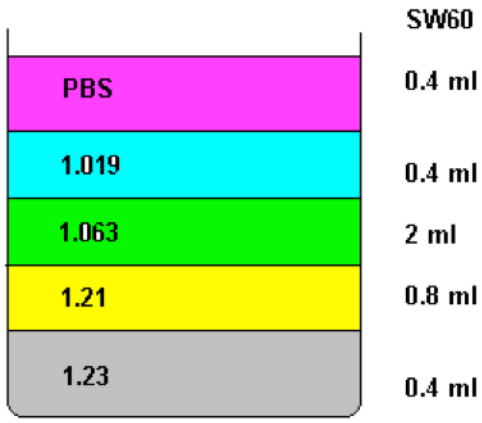

Figure 13: Illustration of tube contents, creating the density gradient.

The Beckman Ultra-Clear Centrifuge Tubes are then carefully loaded into the 44.4 gauge Beckman rotor tubes, and secured into the Beckman SW60 rotor. The rotor is placed into a pre-cooled 4°C Beckman L8-70M Ultracentrifuge. The centrifuge is programmed to spin for 20-24 hours at 4°C, at 28500 rpm.

After the spin is completed, the contents of each tube is separated into ten fractions, the topmost layer becomes fraction #1, the bottom most layer becomes fraction #10, and so on. Separation is achieved through very meticulous micro-pipetting with a P-1000 tip, being careful to take only from the liquid’s surface. In order to get an equal amount in each of the ten fractions, I find that each of my fractions contain between 405 to 407 microliters. Each fraction is now contained in a Fischer 14-961-26 12x75mm glass tube.

At this point, the optical density is measured and recorded for each of the ten fractions. I take 30microliters from each fraction and put it onto the slide of an American Optical Abbe Refractometer.

Next, an EM dialysis buffer is made by combining 37.2g of ammonium acetate, 0.996g ammonium carbonate, 204 microliters of 0.5M EDTA (pH=8), and then filling up to 4L with dH_20. The pH of the buffer is then measured using a Fischer Accument Basic AB15 pH meter. If needed, it is adjusted with 10M sodium hydroxide to a pH of 7.4, then cooled to 4°C.

Each glass tube is covered with a pre-cut piece of water-soaked Spectra/Por Dialysis Membrane, 3500 MWCO. The membrane is held in place by cut out membrane caps. The covered tubes are then secured in a bundle and inverted into a 4L beaker filled with EM dialysis buffer, allowing the fractions to be in contact with the buffer via the membrane. This is left to dialyze overnight at 4°C.

After the EM dialysis, 100 microliters is removed from each fraction and stored at 4°C for later EM analysis. The tubes are then re-covered with the same dialysis membrane and cap, secured and inverted this time into a 4L beaker containing just dH_20. This is left to dialyze overnight at 4°C.

After the water dialysis, 100 microliters is removed from each fraction (whatever is remaining of each fraction is kept at 4°C). The 100 microliters of H_20-dialyzed sample are placed in 1.5mL Eppendorf tubes and dried down to ~20 microliters using Savant Speed Vac SC110 and Savant Universal Vacuum System 400.

Once the samples are concentrated to ~20 microliters each, they are prepped to be run on a SDS-PAGE gel by heating for five minutes at 95-100°C on a VWR Heat Block. The samples are then run at 80-100 volts, until the dye reaches the bottom of the gel. This last step of gel analysis in

its entirety is run according to the protocol for SDS-PAGE gels (detailed in the section "*SDS-polyacrylamide gel electrophoresis (SDS-PAGE)"*).

Concentrating HDL from Flotation

To concentrate HDL from flotation fractions, I use an Amicon Ultra Centrifuge Filter Kit and put together two filter/tube setups. The Eppendorf Centrifuge 5415C placed in a room at 4°C is used to spin 500µL of sample from the fractions (in the filter tube setups) for 3 to 3 ½ minutes at 12,000 rpm. The flow through is dumped off, while the filter and HDL are retained. That same filter/tube combination is now filled with another 500µL of sample and spun again under the same conditions (4°C at 12,000 rpm for 3-3 ½ minutes), and then just as before, the flow through is dumped off and the filter and HDL remain. This process is repeated until all of the product from the flotation has been spun through the filters.

Next, a reverse centrifugation is run, where the filter is inverted and placed inside a new tube. This orientation and combination is spun at 4°C for about 10 minutes at 1,000 rpm. The pooled product, the concentrated HDL from the flotation fractions, is then stored at 4°C.

Two-dimensional Gel Electrophoresis

A two dimensional gel is used for separating α-, pre-β1 and pre-β2 HDL from plasma.

The first thing I do when preparing for the 2D gel is to make the barbital buffer. I dissolve one vial of Sigma B5934-12VL Barbital Buffer powder into one liter of dH20, which makes a 1X solution. This solution is then left at 4°C to dissolve over the course of 30 minutes to an hour.

Once the barbital buffer is dissolved and adequately cooled to 4°C, 0.75 grams of agarose in 100mL of the barbital buffer by microwaving in one-minute increments. Dissolution has occurred

completely once solution appears transparent. I then place the solution in a 55° water bath to cool down.

Next I prepare the gel itself. I begin by clearing the glass plates, which sandwich the gel, with acetone in order to remove any traces of SDS. Then they need to be marked at four points—measuring from the top of the glass, they are marked at 3, 3.5, 5, and 5.5cm. The glass plates are arranged in the Biorad retainer, as they would be for any other gel, and then the 55°C agarose/barbital solution is poured in between the glass plates. A 1.5mm Biorad ten-well comb is submerged ¾ of the way to create the wells.

The next step is to prepare the sample to be run in the gel. Each sample contains 6μL of the 1X barbital buffer solution that was prepared earlier, 2μL of 50% glycerol in H20, 1μL of 1% bromophenol blue/1% xylene (in barbital buffer), and ~1μL of plasma. The amount of plasma put into the sample will vary depending on level of cholesterol of the subject. If the cholesterol is higher than normal, less than 1μL (such as 0.5μL) may be used—and conversely, if the cholesterol is lower than normal, more than 1μL of plasma is used (such as 2μL). All of these reagents are kept on ice. The control sample contains 6μL of the 1X barbital buffer solution that was prepared earlier, 2μL of 50% glycerol in H20, 1μL of 1% bromophenol blue/1% xylene (in barbital buffer), like the plasma sample, but differs here. In the place of plasma, 1μL of 20% BSA (in H20) is added.

I then set up the Biorad bucket apparatus, as with any other gel, but I am sure to wash all of the pieces with dH20 once again in order to remove any and all traces of SDS. After affixing the gel into the apparatus and pouring in the running buffer (the 1X barbital buffer prepared earlier), I gently remove the 10-well comb and load the samples into the wells. I leave one blank well in between each well containing sample.

The gel is allowed to run at 80V at 4°C for about 1.5 hours or until the band of BSA has traveled to the 3cm mark and the band of bromophenol blue has traveled to the 5cm mark.

A second gel is now prepared for each plasma sample well that was run (a second gel is *not* run for the well containing the control). This will be a non-denature gradient gel. These gels are pre-made, Biorad Ready Gel Tris-HCl Gel 161-1393 polyacrylamide gels. After removing the packaging and the wrapping, I use a razor blade to cut along the black line at the bottom of the gel and then pull off this adhesive layer. I remove the comb at the top of the gel and stand it upright on the clamp apparatus from Biorad.

Now, from the first gel, I cut a think strip from the middle of each sample well trail. The line width is controlled and always uniform (~1.5-2mm).

Next, using a style E transfer pipette, I fill the well to the point of overflowing with 3% stacking gel *without SDS*. This stacking gel contains 0.5mL 30% acrylamide, 1.25mL 4X stacking gel solution w/o SDS (Tris .05 gr pH6.8 with HCl in 100mL dH20), 3.25mL dH20, 85µL of 10% APS and 8.5µL TEMED. Once this gel has polymerized, I take the thin strip cut from the agarose gel and lay is horizontally on top of the new-polymerized stack.

The agarose strip is sealed onto the stack by overlaying more agarose solution with a style E transferring pipette, being careful to ensure that there are no bubbles or air between the layers—this is critical.

This gel is now set inside the Biorad bucket/apparatus system, 1X TG Running Buffer (3.028 grams of Tris and 14.413 grams of Glycine in 1 liter of H_20) is added, and it is run at 100-120V at 4°C. This is allowed to run until the band of bromophenol blue has reached the white line at the bottom of the gel, this usually takes about 90 minutes.

The next step is the transfer of the proteins from the gel to a special nitrocellulose membrane, GE Healthcare Amersham Hybond-ECL 0.2µm RPN3032D. Preparation for the transfer includes making a transfer buffer, consisting of 100mL of 10X TG buffer w/o SDS, 200mL of methanol, and 700 mL of ddH_2O. Preparation also includes cutting four pieces of thick, cardstock paper (dimensions 7cm x 9cm) per gel to be transferred, cutting one piece of nitrocellulose membrane (dimensions 6.5cm x 8cm) per gel to be transferred. The nitrocellulose membrane is soaked in water before it is used.

After carefully cutting away the extraneous agarose gel, stack gel and adhesives from the Biorad, the layering is performed. In a pan containing the transfer buffer, all components are stacked and layered in the following order:

- Red plastic end of transfer cassette
- Sponge
- Paper
- Paper
- Nitrocellulose membrane
- Gel
- Paper
- Paper
- Sponge
- Black plastic end of transfer cassette

At this point, it is important to be aware of the alignment of the cassettes into the apparatus and then into the bucket. The black side of the cassette faces the black side of the apparatus and the red side of the cassette faces the white side of the apparatus. The white closure arm of the cassettes is placed upwards.

The transfer is run overnight at 4°C at 35V using the EC Apparatus Corporation EC-105 voltage generator machine.

The next day, as protocol suggests, I continue with a normal Western blot.

Analysis by Western blot

For the Western blot, two CLP glass tubes with screw caps are used for washing the membrane, which is removed from the cassettes in a bath of water or buffer. The CLP glasses are washed with TBS 1X to wet the surface and allow the membrane to stick with ease. The membrane is situated inside the glass so that it lies flat to the surface; *no bubbles* are to be present. The side where the proteins are contained should be facing the inside of the glass so that they are exposed to the liquids to be contained within the glass (this side was marked prior to the stacking and overnight transfer).

Once the membrane is properly placed in the glass tubes, the one-hour blocking buffer wash can begin. The blocking buffer I use for this assay is made of 5% milk in TBST (TBS-tween). For this wash, a volume of 5mL of the blocking buffer is used in each glass tube. The tubes are then allowed to spin in the Biometra Compact Line OV4 penta-rotator for one hour at 37°C, after which time the buffer is dumped out, but the membrane remains in the tube.

The next wash is that of the first antibody. For WTA1 and Mut1, I use human A1, marked "A1740,' stored at -80°C. I make a 1:1000 (antibody:milk buffer) dilution for A1, and then put a 5mL volume of the antibody dilution into each tube. This is allowed to spin at 37°C in the penta-rotator for one hour as well. After one hour, the antibody dilution is removed and the membrane again remains in the glass tube.

Next a series of washes with the milk and TBST blocking buffer are performed. There are three washes total, each at a volume of 5mL per glass tube, and each spinning for 10 minutes in the penta-rotator at 37°C.

It is now time to incubate the membrane in the second antibody. For this second antibody I use a rabbit anti-goat, which is stored at 4°C and diluted to 1:5000 (antibody:milk buffer). Once again, a volume of 5mL is placed into each glass tube and they are allowed to incubate while spinning in the penta-rotator for one hour at 37°C.

After the second antibody wash, the membrane undergoes one final wash with TBS 1X (5mL at 37°C in the penta-rotator) for 5 minutes.

After the blocking and washes, the final component of this assay is the development of the image of the membrane. The first step is to prepare the ECL buffer. I use ~1mL of buffer per membrane. The buffer is made from two pre-made solutions from GE Healthcare. The bottles are light sensitive and are kept at 4°C, the two (white cap and black cap Amersham ECL Western Blotting Analysis System RPN2109 Detection Reagents 1 & 2) are mixed in equal parts, and then pipetted up and down to ensure homogeny. The membrane is then placed on a large square of Fisher brand All Purpose Laboratory Polyvinyl Chloride wrap, and 1mL of the newly-mixed light-sensitive ECL buffer is overlaid carefully but quickly onto the membrane. The remainder of the plastic wrap is folded over onto the membrane, and it is taped to the FisherBiotech Electrophoresis Systems Autoradiography Cassette FBXC 810 cassette board. The cassette is closed quickly to minimize exposure to the light and then it is taken to the dark room for exposure and development. GE Healthcare Amersham Hyperfilm ECL High Performance Chemiluminescence film is placed over the plastic-covered ELC-soaked membrane, then the lid is closed again and the timer is set.

The film is being exposed during this time period. I expose beginning with 10 seconds, and then do another exposure for 1 minute. The time is adjusted further from there based on the resulting developed film. After the timer, the film is placed in the Source One Healthcare Technologies 417288 machine for development. Once the film as been developed, the limits of the membrane are marked and the film is scanned.

Fast Protein Liquid Chromatography (FPLC)

I perform an FPLC (Fast Protein Liquid Chromatography), on samples in order to separate the plasma into 25 separate fractions. The separation occurs according to size, and therefore such fractionation achieves separation of bigger particles from smaller ones. This way, I can measure lipid levels from each fraction and compare between them.

To carry out this assay I use the Pharmacia LKB Smart System, which includes the µ•Peak Monitor, µ•Separation Unit, and µ•Precision Pump. A computer hooked up the Pharmacia system uses the KKLP software to control the apparatus. The first step in running this assay to "wash" the column with PBS. I run PBS through the column for two levels by selecting *Manual→Pump→Conc. B*, and then entering a value of 100%, followed by selecting *Manual→Pump→Flow*, and setting the flow between 60 and 80µL/min (normally I use 60, since it produces less pressure in the column to be run at a lower flow rate).

While the wash is running, I fill the cylinder receptacle with 0.5mL MCT Graduated Natural Eppendorf tubes labeled 1-25 (one for each fraction). Also while the wash is ongoing, I prepare the sample by taking 20µL of plasma and mixing in 40µL PBS and then giving it a quick spin in the Eppendorf Centrifuge 5415C.

Once the wash has completed, I wash the Hamilton 250µL Sample Gastight #1725 Lock Syringe with PBS, then load my sample into the syringe. After ensuring that there are no bubbles in the syringe (as they will cause high pressure in the machine and break it), I inject the sample from the syringe into the column carefully and slowly. I select *Run* from the actions menu in the KKLP software and make sure that throughout the entire run the pressure does not exceed 1.2 MPa.

Once the method has ended, all of the samples will have been distributed into 25 fractions, and each of the pre-labeled tubes will be full. After spinning the fractions in the Eppendorf Centrifuge 5415C, the fractions are measured for their lipid content using the standard protocol for Lipid Panel Measurements (see separately outlined protocol for more details). The only difference between the standard protocol for measuring lipid levels and that used here for measuring the lipid content of the fractions of one sample is that here I load the entire volume of the sample well with sample, as opposed to 3-5µL of sample and the rest PBS.

Measuring Serum Lipid Profiles

In order to evaluate how much Total Cholesterol (TC), Triglycerides (TG), Phospsolipids (PL), or Free Cholesterol (FC) there is in a sample, I conduct a lipids panel assay. This is done by essentially placing the sample in a grid well plate and then using a plate reader to evaluate the lipid contents of the plasma. The plates I use are 96-well plates, and therefore I can comfortably get lipid-content data for ~60 different samples—but, it is capable of obtaining information on up to 90 samples, if one chooses to use the wells on the perimeter of the plate.

The first thing I do for this assay is to outline my grid well plate on paper. This way I know the exact contents of each well. This is usually how my plate looks:

Table 2A: Sample grid plate for lipid panel analysis of plasma. *Blank*=B2 is always the blank well and contains only PBS, *smpl*^{x}=a single sample of plasma, *std*=standard solution for the assay.

	1	2	3	4	5	6	7	8	9	10	11	12
A												
B	blank	smpl^{1}	smpl^{2}	smpl^{3}	smpl^{4}	smpl^{5}	smp^{l6}	smp^{l7}	smp^{l8}	smp^{l9}	smpl^{10}	
C	std	smpl^{11}	smpl^{12}	smpl^{13}	smpl^{14}	smpl^{15}	smpl^{16}	smpl^{17}	smpl^{18}	etc.		
D	std											
E	std											
F	std											
G	std											
H												

Next, I add the appropriate amount of sample to each assigned sample well. If measuring TC or TG, I load 3µL of sample into each well. If measuring PL or FC, I load 5µL of sample into each well. The total volume of each well equals 20µL for TC and FC assays, 25µL for TG, and 15µL PL assays, therefore the corresponding amount of PBS is added into each sample well to fill it to the required volume (17µL for TC, 22µL for TG, 15µL for FC, and 10µL for PL).

Then I fill the blank well (always well #B2) with only PBS to the required volume for the assay (volumes stated above). I also fill the assigned standard wells with the appropriate standard

solution. The standard solution for TC is Wako 439-17501 Cholesterol E Standard Solution diluted to 50mg/dL, for TG is Sigma-Aldrich Glycerol Standard Solution G7793-5ML 077K6164 equivalent triolein concentration 2.5 mg/mL, for PL is Wako 433-36201 Phospholipids C Standard 300mg/dL, and for FC is Wako 435-35801 Free Cholesterol E Standard Solution 100mg/dL. The amounts per well can be found on the chart below.

Table 2B: Standards, volume, color reagent and plate reader program.

TC, TG, FC & PL measurements							
TC (50 mg/dl)		TG		FC		PL	
Std	PBS	Std	PBS	Std	PBS	Std	PBS
0	20	0	25	0	20	0	15
3	17	3	22	1	19	2	13
5	15	5	20	2.5	17.5	4	11
10	10	10	15	5	15	10	5
20	0	15	10	10	10	15	0
				20	0		
20 µl total		25 µl total		20 µl total		15 µl total	
300 µl TCholE		300 µl TG infinity		300 µl FC Reagent		300 µl PL Reagent	
37^{o}C for 5 min		37^{o}C for 10 min		37^{o}C for 5 min		37^{o}C for 5 min	

31 ASC	43 ASTg	31 ASC	31 ASC

The final addition to the plate is the color reagent in each well (the empty wells need not be filled with color reagent). Each well receives 300μL of color reagent. For TC I use Wako 439-17501 Cholesterol E Buffer solution. For TG I use Fischer Thermo Scientific TR22421 Infinity Triglycerides. For PL I use Wako 433-36201 Phospholipids C Buffer Reagent plus Color Reagent. For FC I use Wako 435-35801 Free Cholesterol E Buffer Solution plus Color Reagent.

Before taking the plate to be read, it is incubated at 37°C for 5 minutes (with the exception of a TG plate, which is incubated for 10 minutes). After the incubation, and after ensuring that there are no bubbles in any of the wells (as they can introduce errors in the reading), the plate is inserted into the plate reader. The program used for the TC, FC, and PL is 31 ASC while the program used to read the TG assay is 43ASTg. The machine is hooked up to a printer, which gives the blank-corrected values for each well.

The values given for the wells containing the Standard Solutions are used to create a standard curve and find the y=mx+b equation, which is used to manipulate the rest of the data to get it into workable numbers. The values printed out for each sample-containing well are then adjusted with a few equations to give values of mg/dL.

Measuring Relative Hepatic mRNA

Isolation of RNA from the tissue sample

Initially, al instruments, tools, surfaces, and gloves are sprayed with Ambion RNase Zap (9780.9782), which will destroy any nucleases and help ensure a successful RNA extraction with accurate expressions levels in the downstream analyses.

All samples from which RNA is to be isolated is taken out of the -80°C freezer and placed on ice. The samples from which I always collect RNA are livers. To each tissue sample, 1mL of Trizol is added. The screw cap is placed back on the tube and it remains on ice (the tubes that I use for collecting the livers are Fisherbrand Microcentrifuge Tubes, 27-707-354, 2mL conical cap tube with tethered cap and o-ring).

Next, each tube is placed inside the Biospec Products Mini BeadBeater homogenizer, which is turned on for 30 seconds and shakes the tube with such vigor that it pulverizes the tissue (effectively homogenizing the sample). After the homogenization each tube is returned to the ice.

Thirty seconds after the homogenization, 100µL of chloroform is added into each tube, and that tube is placed back into the homogenizer for 10 seconds. It is then returned to the ice.

Once this routine has been done on all of the samples, they are spun in an Eppendorf Centrifuge 5415C at room temperature for 15 minutes at 13,000 rmp. After the centrifugation the sample will have separated into RNA (the top phase), DNA (the middle band), and cell components (proteins, membranes, etc. on the bottom phase). The upper phase is collected, being very careful to collect only the RNA and leave all of the DNA. Usually, the quantity of RNA collected is about 350µL. The RNA from each sample is placed in its own new, sterile eppendorf 1.5mL tube. The

same volume of isopropanol is now added to each tube (again, it will be around 350µL). The tubes are mixed by hand, being inverted over and over a few times.

The samples are spun at room temperature for 15 minutes at 13,000 rpm once more. The supernatant is then dumped off while the pellet remains in the bottom of the tube. To the tube, 0.5mL of 70% RNase-free ethanol (in DEPC water), and the tubes are spun at room temperature for five minutes at 13,000 rpm.

The supernatant is removed by suction since the resultant pellet is so fragile at this point. The caps are left open, and the pellets are left to dry all of the way under the hood for approximately 30 minutes.

At this point the pellet is resuspended in 100µL of DEPC water. The DEPC water is made up ahead of time by putting 1mL of DEPC in 1L of water while stirring inside the hood, it is left stirring in 4°C over night and then autoclaved the next day.

The tubes containing the pellets in DEPC water are placed on a 65°C heat block (Lab-Line MultiBlok Heater) for five minutes. At five minutes, the samples are checked for dissolution by pipetting. Once dissolved, the samples are placed back on ice, or stored in -80°C if one cannot continue with the procedure at the present time.

The next step is to measure the RNA by photometry with a dilution of 1:250. The UV reader that I use is a Beckman DU 350 Life Science UV/Vis Spectrophotometer. The dilution is made by adding 4µL of each sample to 996µmL of water. A control tube is also made filled with 1,000µL of water. All of the samples go for a quick spin in the centrifuge, and then the readings begin (control first) by putting the sample in a square glass tube (cuvette) and then into the machine for reading. It is important to wash the cuvette with water and ethanol between each reading.

RT-PCR Procedure

In order to complete the expression levels of certain genes in the tissues, cDNA is made from the RNA that was extracted from the tissues. This accomplished by using reverse transcriptase PCR (RT-PCR). The concentration will be 0.1µg/µL, so the first step is convert the values in µg/mL from the photometry reading of the RNA into µg/µL. Since the photometry readings gave me the concentrations of the samples, I can calculate the volumes needed to reach the proper ratio by using the known concentrations and volumes from the samples that were read.

In a sterile eppendorf, the corresponding volumes of sample and water are combined to give the 0.1µg/µL dilution for each sample. I flick and quick spin the samples to make sure that they are adequately mixed. At this point, if need be, one can store the samples in -80°C or carry on with further steps.

For the reaction to take place and the RT-PCR to be successful, the following reagents are combined in a new, sterile eppendorf 1.5mL for each sample:

10 µl of RNA (0.1 µg/µl)

2 µl 10x RT buffer

0.8 µl 25x dNTPs (100 mM)

1 µl Oligo-dT

1 µl 18S

1 µl Reverse Transcriptase

1 µl RNAse inhibitor

3.2 µl DEPC H_2O or RNAse-free water

20 µl total volume

It is important to remember that the reverse transcriptase and the RNase inhibitor are very sensitive and they should only be taken out as they are needed, not thawed on ice as all of the other reagents are.

A control tube, without RNase, but with transcriptase, is also made and run with the other samples. The remaining RNA at the 0.1μg/μL dilution can be stored in -80°C.

At this point the RT-PCR is run. All of the samples are loaded into the MJ Research PTC-200 Peltier Thermal Cycler and the machine is activated. The first cycle runs for 10 minutes at 25°C, the second for 120 minutes at 37°C, the third for 5 minutes at 85°C, and fourth can run indefinitely at 4°C until it is finished.

Once the cycles have finished, the product in the tubes is cDNA, which can now be used to run a real time PCR, or quantitative PCR (qPCR), or it can be stored at -20°C until one is ready to run the qPCR.

qPCR Procedure

To run a real time PCR, or qPCR, I first need to dilute the cDNA that was made in the RT-PCR from the RNA extracted from my tissue samples. This dilution is made with nuclease-free water down to 1:500.

The cDNA samples are kept on ice while preparation of the sterile eppendorf 1.5mL tubes takes place. 500μL of nuclease-free water and 1μL of cDNA sample is put into each eppendorf, then are flicked and quick spun to mix, and then placed on ice to be kept cold while the master mix for the qPCR reaction is being prepared. Each well of the qPCR plate will contain:

10 µl 2x Reaction mix

0.5 µl primer (e.g. LCAT)

0.5 µl 18S primer

8 µl H_2O (nuclease-free)

19 µl total volume

Enough master mix should be prepared so that there is enough extra for 5-10 wells. The mix goes for a quick spin in the centrifuge.

Next, 1µL of the diluted cDNA sample and 19µL of the master mix are put into each Bioplastics AB17500 EU Frosted Sub Skirted QPCR 96 well plate, making for a total well volume of 20µL. Most of time I do a triple run, meaning that each sample will be loaded a total of three separate times in three separate wells. Once the plate is full it is covered with an optical adhesive cover membrane by Applied Biosystems no. 4360954, and then cover it with aluminum foil to avoid any light sensitive reactions. Air is forced around the bottom of the plate to remove any dust. The plate is now taken to a large centrifuge designed for multi-well plates, such as the Sigma 4-15C. The plate is spun usually for only about 10 seconds, and then it is recovered and taken to the PCR machine that will run the reaction to give the real time PCR results.

After inserting the plate into the machine, the 7300 System SOS Software to set up the reaction. The reaction usually takes about 1 hour and 50 minutes from beginning to end. The results will be stored on the computer to which the machine is attached and on which the software was run.

RESULTS

Designation of Separate Rounds of Experiments

The results of two sets of experiments will be described here, since it is the cumulative data from which conclusions will be drawn. The first set (referred to henceforth as Project I) used apoA-I -/- x apoE -/- mice infected with either WT apoA-I or mutant apoA-I [L218A/L219A/V221A/L222A] adenoviruses. The second set of experiments (referred to henceforth as Project II) used apoA-I -/- x apoE -/- mice infected with either WT apoA-I, mutant apoA-I [L218A/L219A/V221A/L222A] or mutant apoA-I [L218A/L219A/V221A/L222A] plus LCAT.

The scope of Project II was to confirm the data of Project I, and in addition, examine whether LCAT could restore HDL formation by the mutant apoA-I[L218A/L219A/V221A/L222A].

Amplification, Isolation, and Titration of the recombinant adenoviruses

HEK293 cells grown to about 70% confluence in T175 flasks are initially infected with the apoA-I [L218A/L219A/V221A/L222A] adenovirus stock, and the wild type apoA-I virus stock. After incubation the lysate is spun and the pellet of infected cells are purified by CsCl gradient ultracentrifugation. Aliquots are prepared, and from these the viral titre is calculated with a plaque assay. Detailed instructions for these procedures are found in the Materials and Methods section of the text.

The titres of my viruses were as indicated in the following table.

Table 3: Titres of adenoviruses in plaque-forming units per micro liter.

	Titre
apoA-I wild type	9.5×10^7 pfu/μL
apoA-I [L218A/L219A/V221A/L222A]	1.35×10^7 pfu/μL
LCAT	3×10^7 pfu/μL

Expression of the apoA-I transgene following adenovirus infection

Four days postinfection with adenoviruses (apoA-I WT, apoA-I [L218A/L219A/V221A/L222A], and apoA-I [L218A/L219A/V221A/L222A] plus LCAT), apoA-I -/- x apoE -/- mice were sacrificed and RNA was isolated from their livers. Relative expression of these transgenes was determined using qRT-PCR. Detailed instructions for this procedure are found in the Materials and Methods section of the text.

The analysis for Project I showed that in representative mice the relative expressions of the wild type and the mutant apoA-I [L218A/L219A/V221A/L222A] were comparable in individual mice, with the expression of the mutant being higher in one mouse (Table 5 and Figure 14). This allows us to draw the conclusion that any differences in the phenotype will not be due to reduced expression of the mutant apoA-I.

The analysis for Project II showed that in representative mice the relative expressions of the wild type and the mutant apoA-I [L218A/L219A/V221A/L222A] were comparable, whereas the relative expression of the apoA-I [L218A/L219A/V221A/L222A] plus LCAT was 42% of the WT apoA-I (Table 5 and Figure 15). Dosages for each adenovirus used are outlined in the table below (Table 4).

Table 4: Doses of adenoviruses used in Project I and II, in plaque-forming units per micro liter.

	Dose
apoA-I wild type	1×10^9 pfu
apoA-I [L218A/L219A/V221A/L222A]	1×10^9 pfu
apoA-I [L218A/L219A/V221A/L222A] plus LCAT	4×10^8 pfu for LCAT 9×10^8 pfu for apoA-I[L218A/L219A/V221A/L222A]

Serum lipoprotein profile

Four days post-infection with adenoviruses (apoA-I WT, apoA-I [L218A/L219A/V221A/L222A], and apoA-I [L218A/L219A/V221A/L222A] plus LCAT), the plasma lipids from apoA-I -/- x apoE -/- mice were determined as described in the Materials and Methods section of this text.

In Project I, all of the mice had triglycerides in the normal range, under 100 mg/dL. All but one of the mice expressing the mutant apoA-I had normal total cholesterol levels, between 200-300 mg/dL, while the one WT and one of the mutant mice had high total cholesterol levels, >300 mg/dL.

In Project II, all of the mice regardless of which adenovirus they expressed had high total cholesterol levels. All of the WT mice developed high triglycerides, while none of the mice in the mutant groups did, as was anticipated due to the deficiency of apoE.

The following tables show the mean values for the combined total cholesterol and triglyceride levels, with standard deviations, expressed in mg/dL (Project I, table 5; Project II, table 6).

Table 5: Project I plasma lipids and hepatic mRNA levels of apoA-I -/- x apoE -/- mice expressing wild type (WT) and mutant forms of apoA-I obtained four days post-infection.

Protein Expressed	Total Cholesterol *mg/dL*	Triglycerides *mg/dL*	Relative apoA-I mRNA *%*
WT apoA-I n=1	378	70	100
apoA-I [L218A/L219A/V221A/ L222A] n=3	268 ± 41	7 ± 2	92 ± 15

Values are means ± standard deviation, where n=1-3. Expression of LCAT was also confirmed by RT-PCR.

Table 6: Project II plasma lipids and hepatic mRNA levels of apoA-I -/- x apoE -/- mice expressing wild type (WT) and mutant forms of apoA-I obtained four days post-infection.

Protein Expressed	Total Cholesterol *mg/dL*	Triglycerides *mg/dL*	Relative apoA-I mRNA *%*
WT apoA-I n=3	1343 ± 104	294 ± 129	100 ± 13
apoA-I [L218A/L219A/V221A/ L222A] n=2	778 ± 52	18 ± 2	92 ± 23
apoA-I [L218A/L219A/V221A/ L222A] plus LCAT n=3	1511 ± 140	24 ± 12	42 ± 3

Values are means ± standard deviation, where n=2-3. Expression of LCAT was also confirmed by RT-PCR.

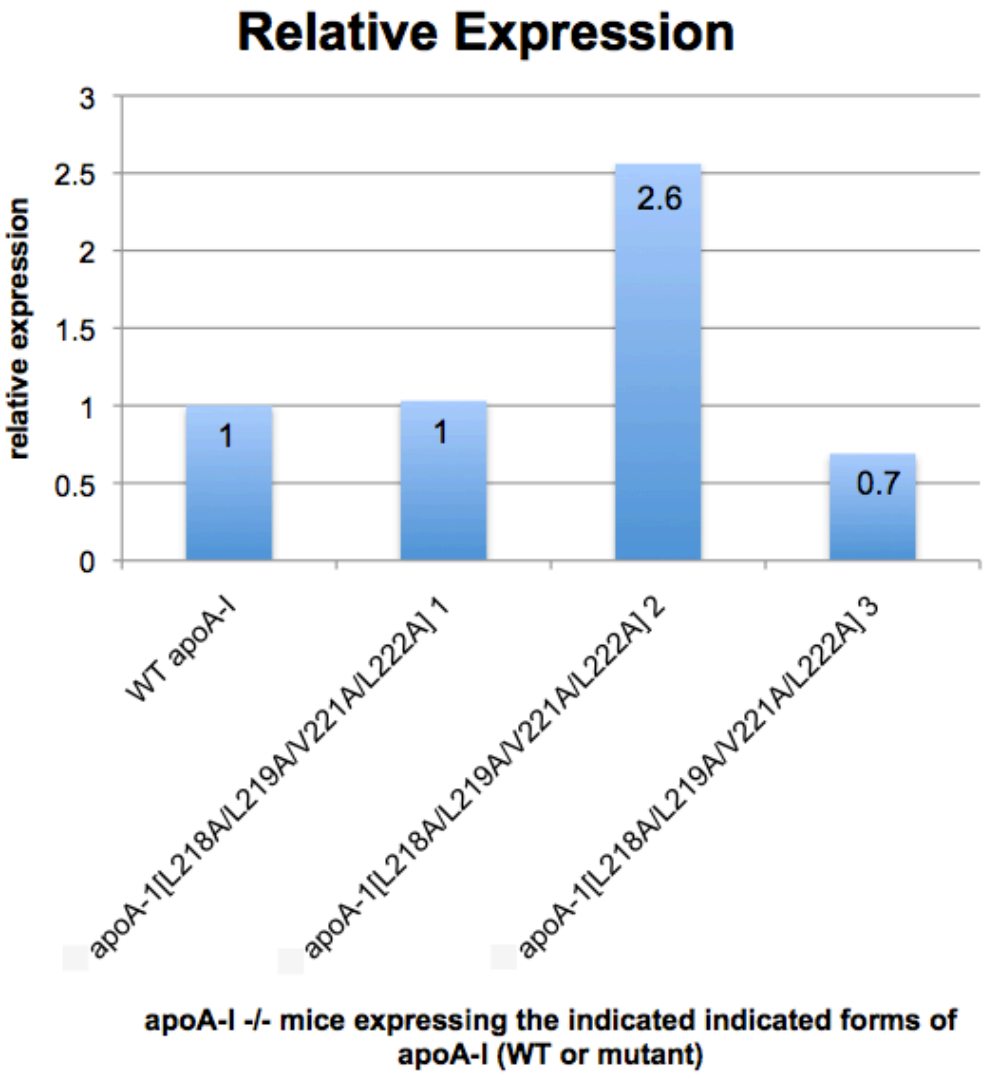

Figure 14: Project I relative expression of apoA-I mRNA in individual mice infected with adenoviruses expressing wild type (WT) apoA-I or mutant apoA-I (apoA-I [L218A/L219A/V221A/L222A].

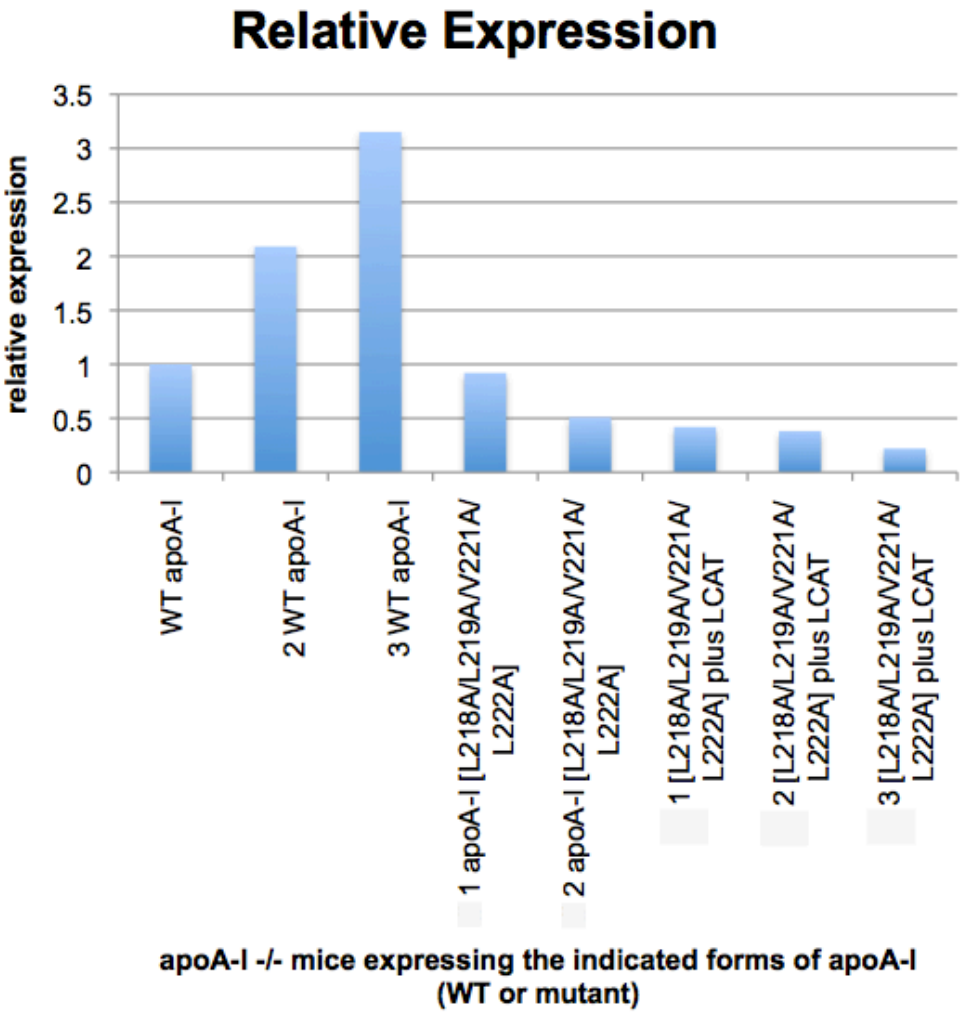

Figure 15: Project II relative expression of apoA-I mRNA in individual mice infected with adenoviruses expressing wild type (WT) apoA-I, mutant apoA-I (apoA-I [L218A/L219A/V221A/L222A] or apoA-I [L218A/L219A/V221A/L222A] plus LCAT).

FPLC profiles of plasma

FPLC analysis on the plasma collected from apoA-I -/- x apoE -/- mice four days post-infection with adenovirus expressing either WT or mutant apoA-I or mutant apoA-I plus LCAT was performed as described in detail in the Materials and Methods section of this text.

Results from Project I indicate that the mice expressing the WT apoA-I, cholesterol was distributed in the VLDL region and the HDL region, with the characterizing HDL peak appearing in fractions ~13-22. The mutant apoA-I [L218A/L219A/V221A/L222A] did not exhibit an HDL peak, but rather the cholesterol is distributed in the VLDL/IDL region (Figure 16).

Results from Project II indicate that the mice expressing the WT apoA-I, cholesterol was distributed in the VLDL region and the HDL region, with the characterizing HDL peak appearing in fractions ~13-22. The mutant apoA-I [L218A/L219A/V221A/L222A] did not exhibit an HDL peak, but rather the cholesterol is distributed mainly in the VLDL region. Similarly, the mutant apoA-I [L218A/L219A/V221A/L222A] plus LCAT showed no peak in the HDL region. The cholesterol was distributed in the VLDL region and had an additional pronounced shoulder spanning the VLDL/IDL/LDL region (Figure 17).

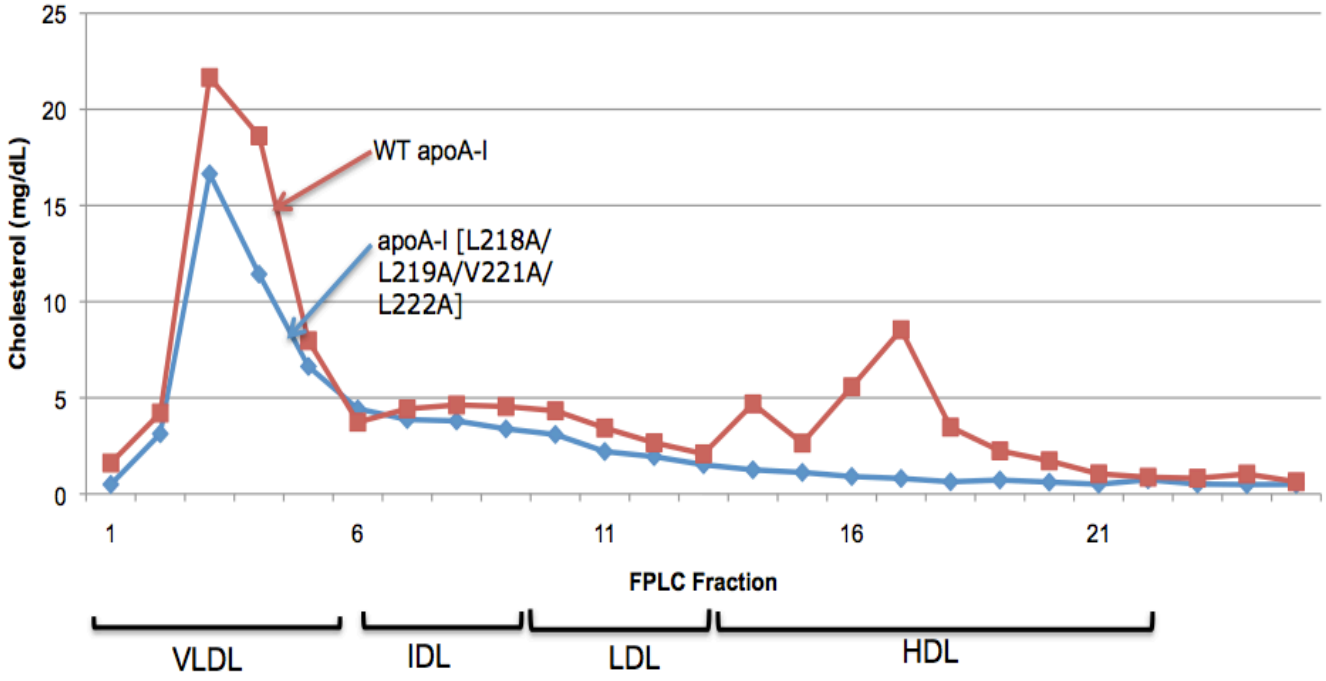

Figure 16: Project I FPLC profiles of total cholesterol of apoA-I -/- x apoE -/- mice infected with adenoviruses expressing the wild type (WT) apoA-I or the mutant apoA-I [L218A/L219A/V221A/L222A], as indicated. [Relative expression levels of Project I are depicted in Figure 14]

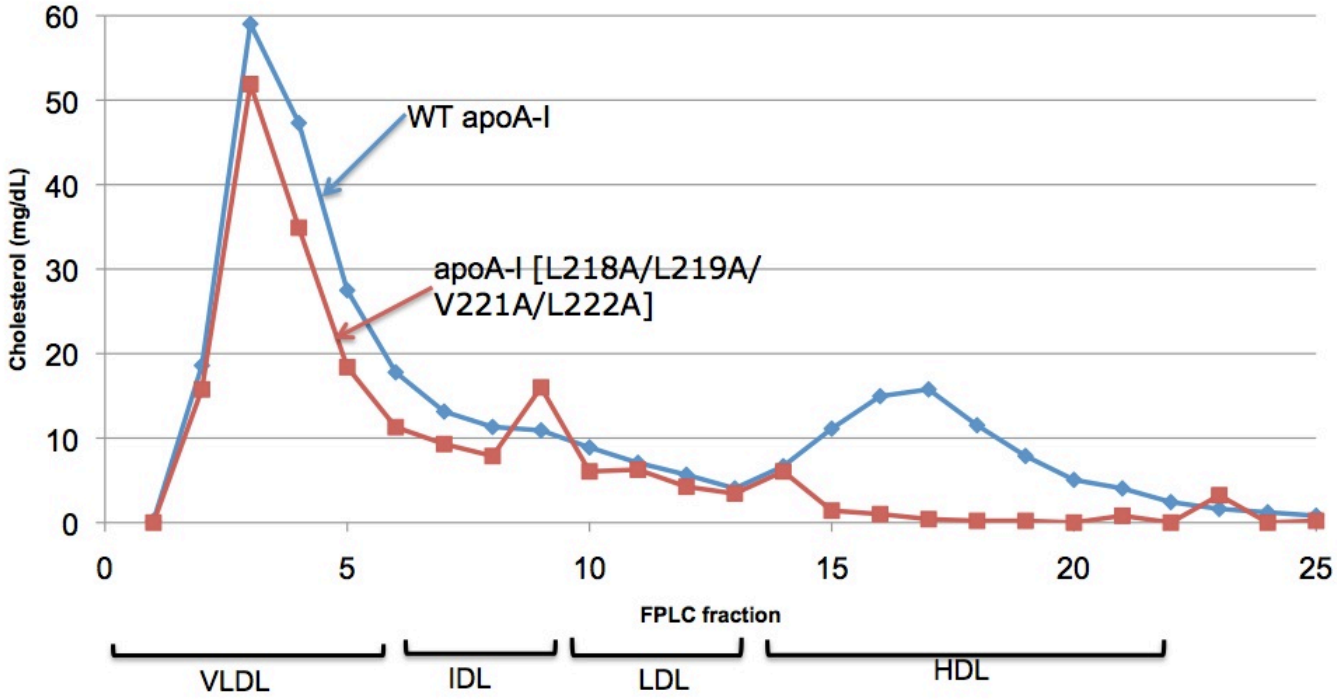

Figure 17: Project II FPLC profiles of total cholesterol of apoA-I -/- x apoE -/- mice infected with adenoviruses expressing the wild type (WT) apoA-I or the mutant apoA-I [L218A/L219A/V221A/L222A], as indicated. [Relative expression levels of Project II are depicted in Figure 15]

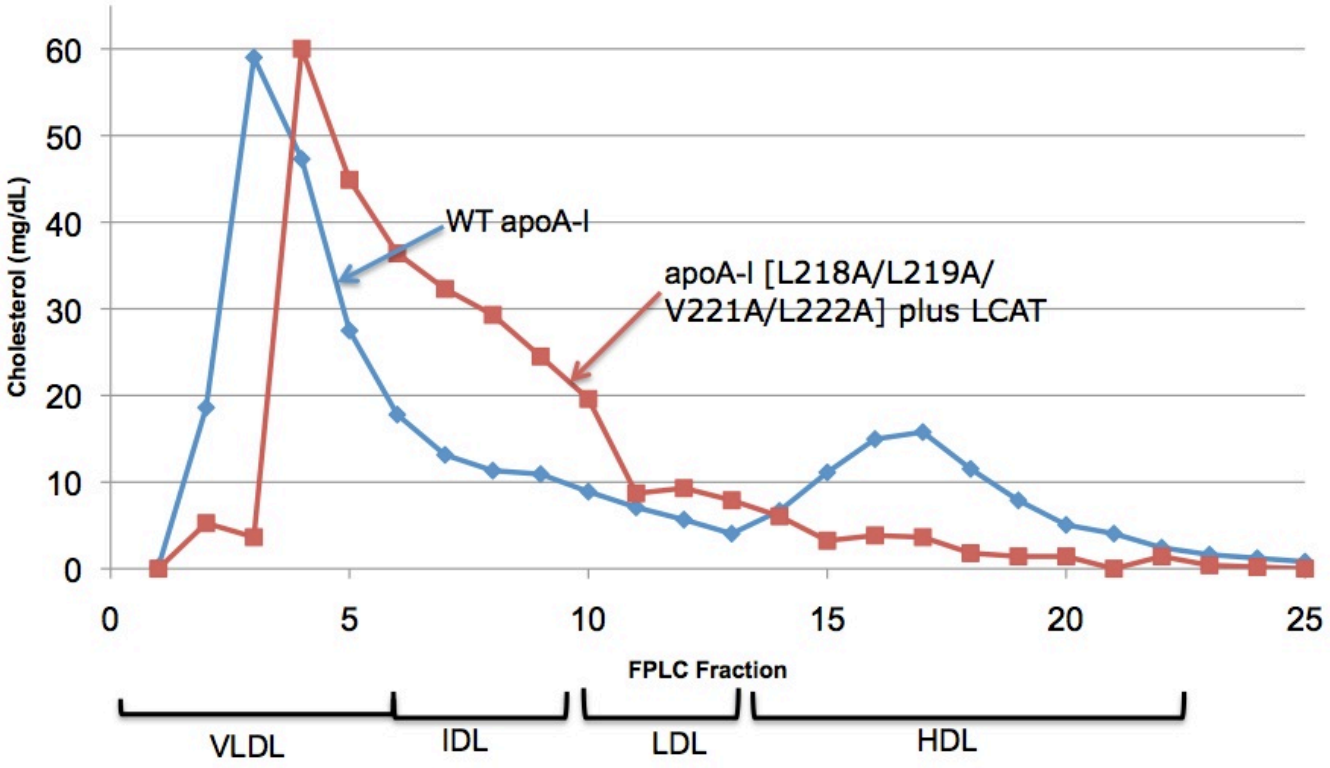

Figure 18: Project II FPLC profiles of total cholesterol of apoA-I -/- x apoE -/- mice infected with adenoviruses expressing the wild type (WT) apoA-I or the mutant apoA-I [L218A/L219A/V221A/L222A] plus LCAT, as indicated. [Relative expression levels of Project II are depicted in Figure 15]

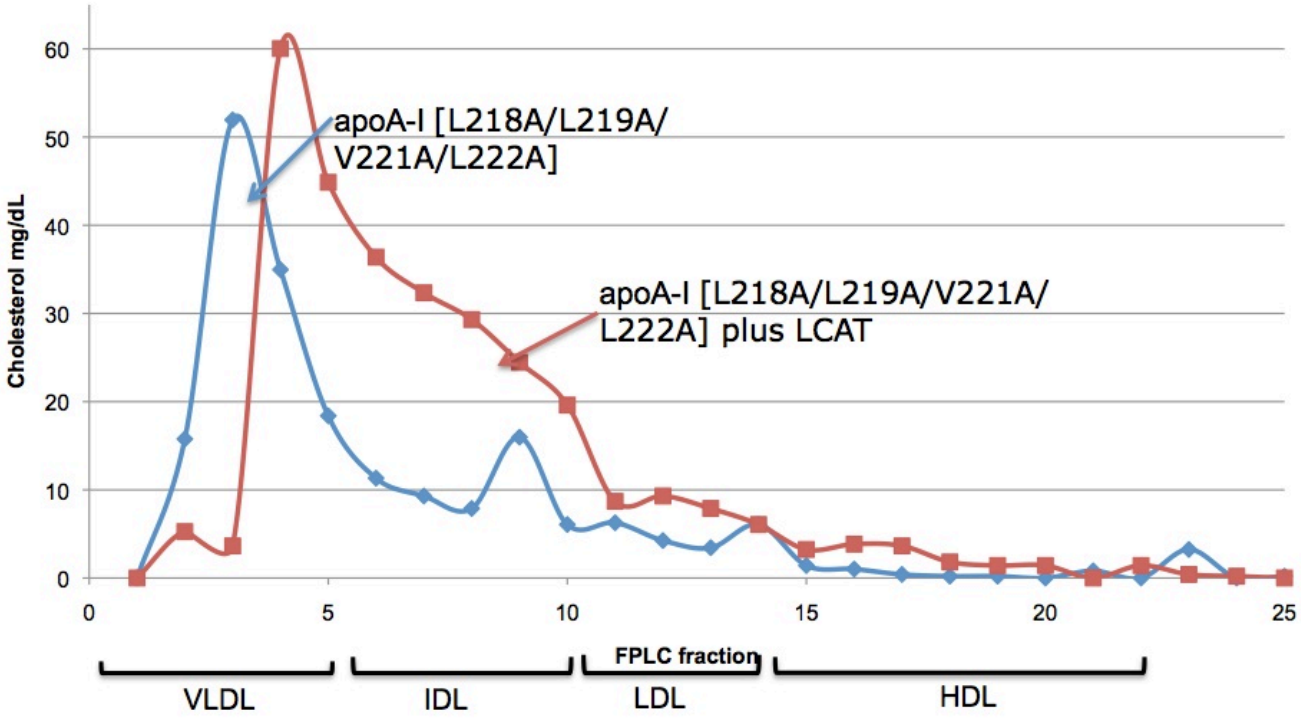

Figure 19: Project II FPLC profiles of total cholesterol of apoA-I -/- x apoE -/- mice infected with adenoviruses expressing the wild type (WT) apoA-I or the mutant apoA-I [L218A/L219A/V221A/L222A] plus LCAT, as indicated. [Relative expression levels of Project II are depicted in Figure 15]

Fractionation of plasma by density gradient ultracentrifugation: SDS-PAGE and electromicroscopy analyses

Plasma taken from apoA-I -/- x apoE -/- mice four days post infection with adenovirus expressing either WT or mutant apoA-I or mutant apoA-I plus LCAT was subject to fractionation by density gradient ultracentrifugation, and then the resultant fractions were analyzed by SDS-PAGE and electromicroscopy. In EM analysis, the expected size range for HDL particles is 8-12nm, for LDL particles is 15-25nm, for VLDL particles is 40-80, and anything above 90 is lymph or other remnant particle. These procedures were carried out according to the details written in the Materials and Methods section of this text.

According to the SDS-PAGE gel, the plasma from the mice expressing the WT apoA-I showed its apoA-I content to be predominantly distributed in the HDL3 region and to a lesser extent in the HDL2, LDL, and IDL regions. This was the case for the SDS-PAGE analyses of the fractions in both Project I and Project II (Figure 20 A & B). Electromicroscopic analysis was performed on the WT apoA-I only in Project I. For electromicroscopy analysis on this plasma, fractions 2 & 3 were pooled, as were 4 & 5 and 6 & 7 (fraction 8 was analyzed on its own). In fractions 2 & 3, the majority of the particles are 20-50nm in diameter, an occasional vesicle can be seen, and no disks are apparent. In fractions 4 & 5, HDL, LDL, and VLDL sized particles (8-12, 15-25, and 40-80nm respectively) are seen. Mostly, the particles here are HDL sized. In fractions 6 & 7, a homogeneous population of spherical HDL-sized particles (8-12nm) are seen, with a few larger-sized particles. Lastly, in fraction 8, a more heterogeneous population than fractions 6 & 7 is seen, there are smaller particles, but mostly free protein (Figure 20 C).

The SDS-PAGE gel from the plasma from the mice expressing the mutant apoA-I [L218A/L219A/V221A/L222A] from Project I and II showed that the apoA-I content is distributed in the IDL, LDL, HDL2 and HDL3 regions (Figure 21 A). Similar distribution of apoA-I was observed in Project II (Figure 21 C).

For the electromicroscopy analysis on the mutant apoA-I [L218A/L219A/V221A/L222A] in Project I, fractions 2 & 3 were pooled, as were 4 & 5 and 6 & 7 (fraction 8 was analyzed on its own). In fractions 2 & 3 most of the particles seen are 20-50nm, with the appearance of some vesicles and collapsed vesicles, but no disks. Fractions 4 & 5 reveal mostly LDL-sized particles, with some in the larger in VLDL range. A few vesicles (collapsed) are seen as well as the formation of some discoidal particles. Fractions 6 & 7 show many round particles including vesicles (some as large as 100nm), and evidence of a few disks. In fraction 8 some round particles and vesicles are seen, along with some free protein, but no disks (Figure 21 B). The EM analysis for apoA-I [L218A/L219A/V221A/L222A] in Project II was performed on four pooled samples; 2 & 3, 4 & 5, 6 & 7, and 8 & 9. In sample 2 & 3 LDL and VLDL-sized (~20-50nm) particles are seen, with some vesicles appearing as well. In fraction 4 & 5 there are predominately LDL-sized particles, with some VLDL-sized. In fraction 6 & 7, a few disks are seen in the presence of LDL-sized particles as well as some HDL-sized particles. Fraction 8 & 9 consists of almost exclusively free protein (Figure 21 D).

According to the SDS-PAGE gel, the plasma from the mice expressing the mutant apoA-I [L218A/L219A/V221A/L222A] plus LCAT from Project II, the apoA-I content is distributed in the IDL, LDL, HDL2, and HDL3 regions (Figure 22 A). The electromicroscopy from this plasma was performed on four pooled samples; 2 & 3, 4 & 5, 6 & 7, and 8 & 9. Fraction 2 & 3 show LDL and VLDL-sized particles, ~20-50nm, while fraction 4 & 5 shows LDL and small HDL-sized particles.

Fraction 6 & 7 show a homogenous population of round small sized HDL particles. Fraction 8 & 9 show some small HDL sized particles as well as some free protein (Figure 22 B).

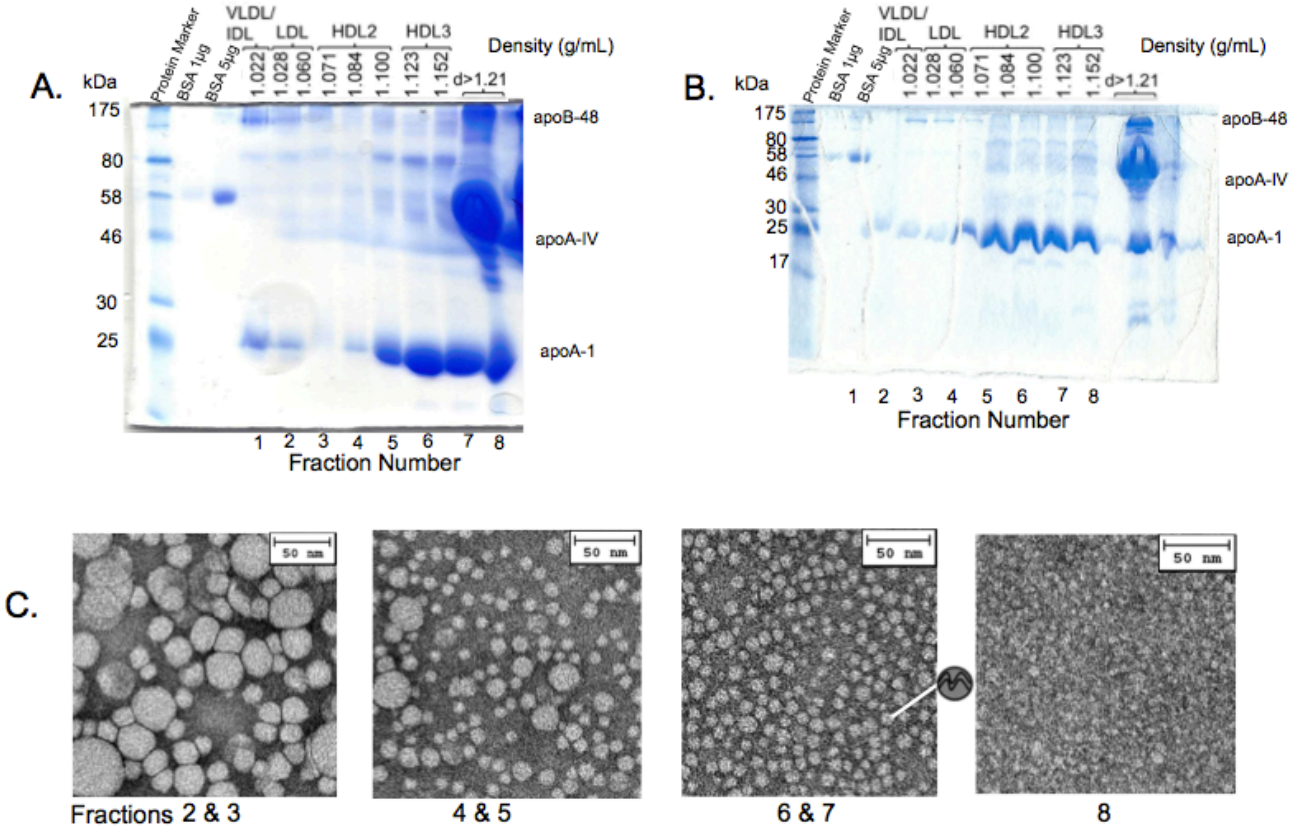

Figure 20: Analyses of plasma of apoA-I -/- x apoE -/- mice infected with adenovirus expressing wild type (WT) apoA-I by density gradient ultracentrifugation, followed by SDS-PAGE analysis of the ultracentrifugation fractions (A: Project I, B: Project II), and electromicroscopy images of fractions 2 & 3, 4 & 5, 6 & 7, and 8 (C). [Relative expression levels of Project I are depicted in Figure 14] [Relative expression levels of Project II are depicted in Figure 15]

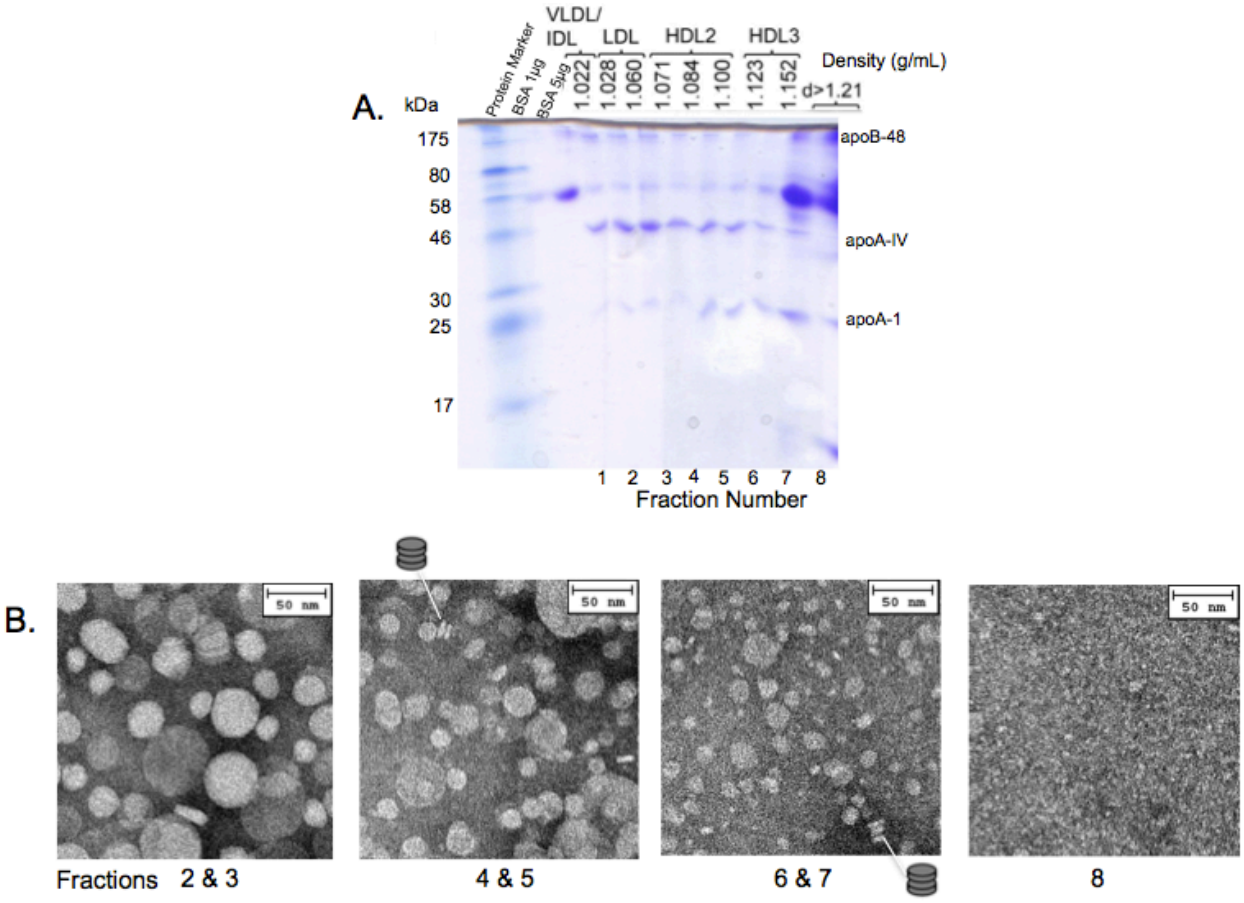

Figure 21 A & B: Project I analyses of plasma of apoA-I -/- x apoE -/- mice infected with adenovirus expressing mutant apoA-I [L218A/L219A/V221A/L222A] by density gradient ultracentrifugation, followed by SDS-PAGE analysis of the ultracentrifugation fractions (A), and electromicroscopy images of fractions 2 & 3, 4 & 5, 6 & 7, and 8 (B). [Relative expression levels of Project I are depicted in Figure 14] [Relative expression levels of Project II are depicted in Figure 15]

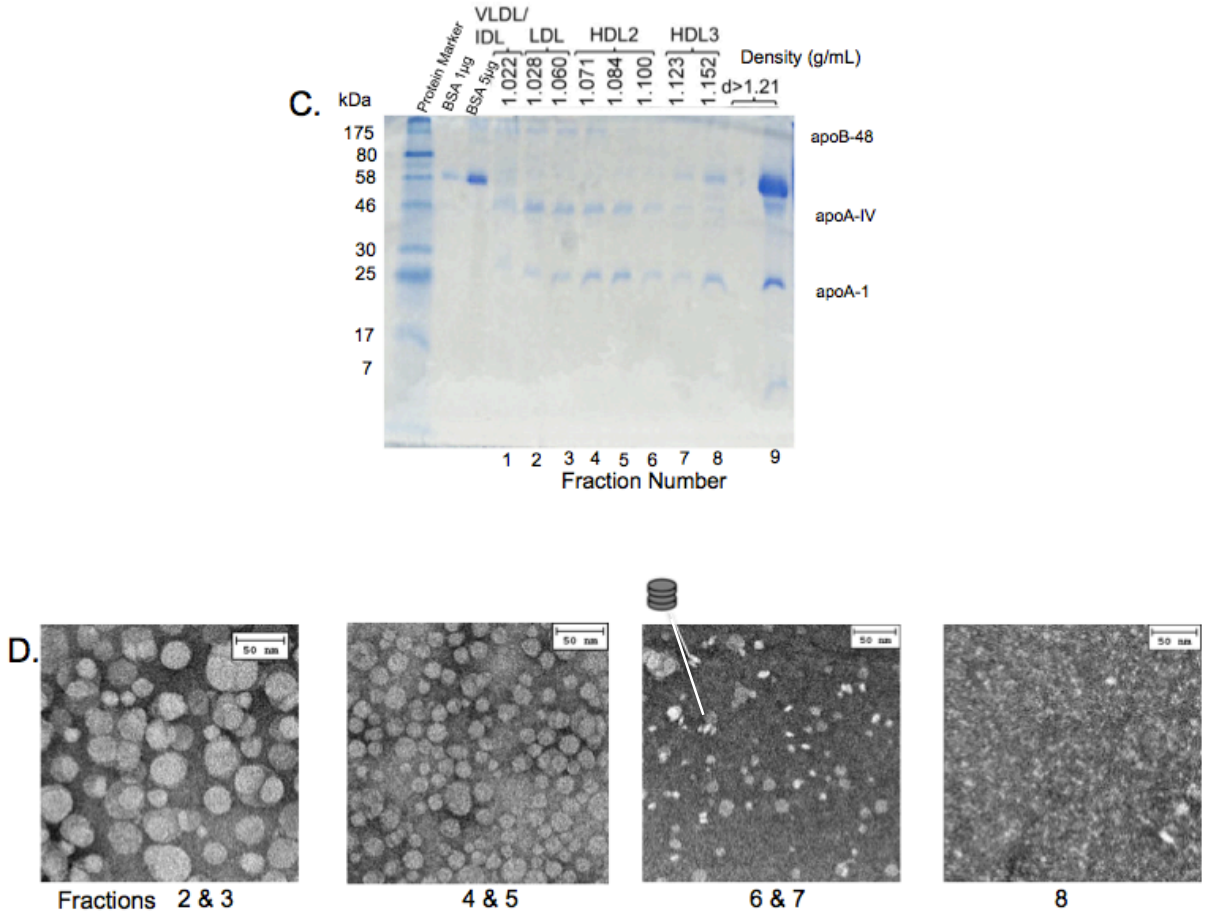

Figure 21 C & D: Project II analyses of plasma of apoA-I -/- x apoE -/- mice infected with adenovirus expressing mutant apoA-I [L218A/L219A/V221A/L222A] by density gradient ultracentrifugation, followed by SDS-PAGE analysis of the ultracentrifugation fractions (C), and electromicroscopy images of fractions 2 & 3, 4 & 5, 6 & 7, and 8 (D). [Relative expression levels of Project I are depicted in Figure 14] [Relative expression levels of Project II are depicted in Figure 15]

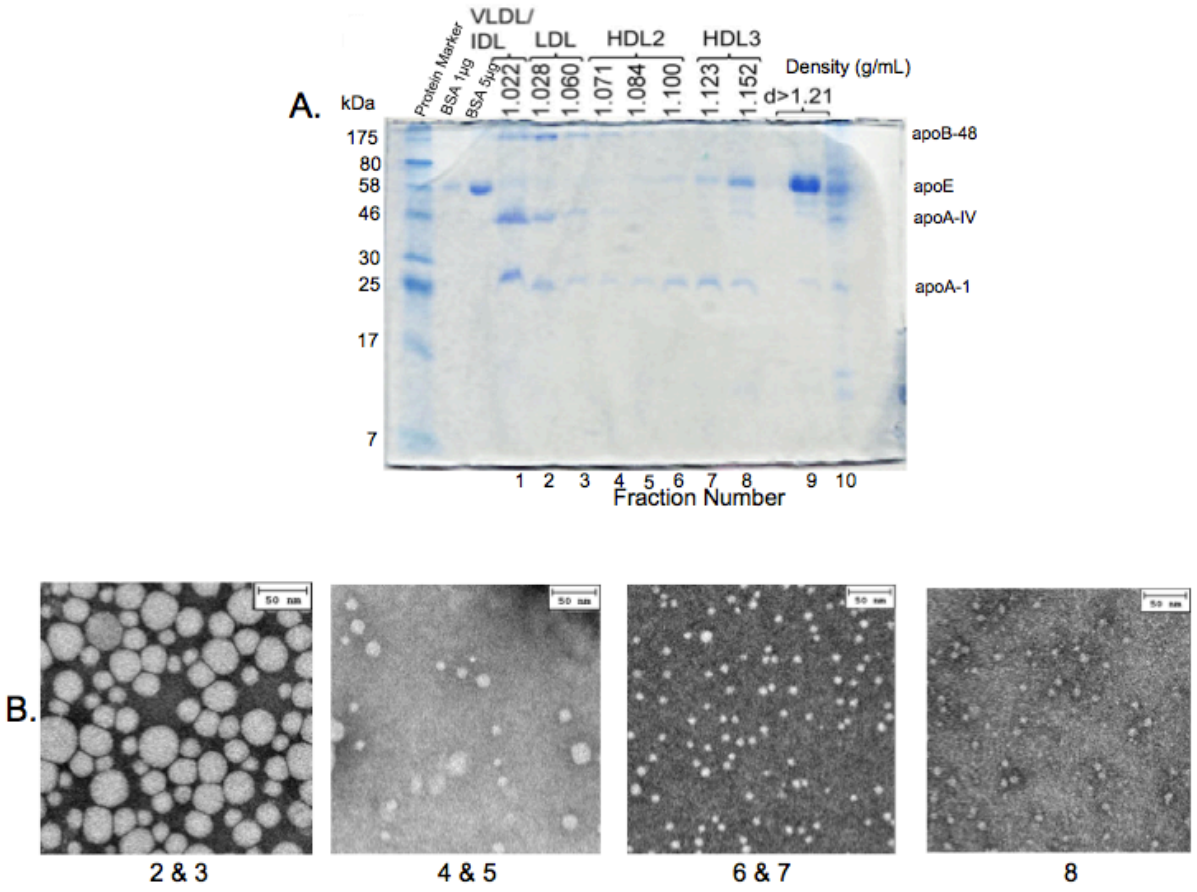

Figure 22: Analyses of plasma of apoA-I -/- x apoE -/- mice infected with adenovirus expressing mutant apoA-I [L218A/L219A/V221A/L222A] plus LCAT by density gradient ultracentrifugation, followed by SDS-PAGE analysis of the ultracentrifugation fractions (A), and electromicroscopy images of fractions 2 & 3, 4 & 5, 6 & 7, and 8 (B). [Relative expression levels of Project II are depicted in Figure 15]

Two-dimensional gel electrophoresis

A two-dimensional gel electrophoresis assay was performed (according to the specifications outlined in the Materials and Methods section of this text) on the plasma taken from apoA-I -/- x apoE -/- mice four days post infection with adenoviruses expressing either WT or mutant apoA-I or mutant apoA-I plus LCAT. For the WT apoA-I, normal alpha (α) subpopulations were apparent (α1, α 2, α 3) and pre-β HDL particles were also present (Figure 23 A). Both apoA-I [L218A/L219A/V221A/L222A] and apoA-I [L218A/L219A/V221A/L222A] plus LCAT formed predominantly pre-β HDL particles, with little to no evidence of any α subpopulations (Figure 23 B & C). The outcome of the two-dimensional gel electrophoresis for both project, I and II, were the same. Therefore, one representative film was chosen for each group.

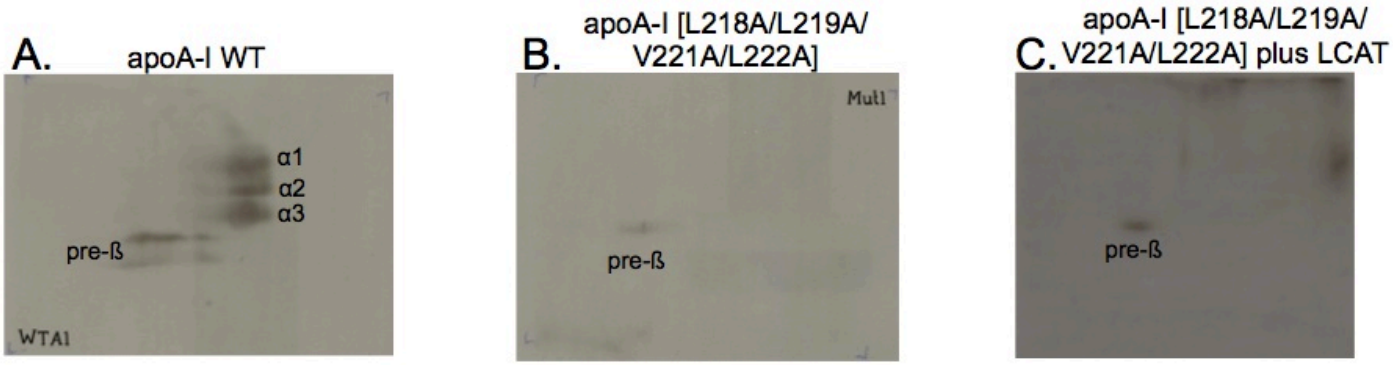

Figure 23: Two-dimensional gel electrophoresis and Western blot analysis of plasma of apoA-I -/- x apoE -/- mice infected with adenovirus expressing wild type apoA-I (A), mutant apoA-I [L218A/L219A/V221A/L222A] (B), or mutant apoA-I [L218A/L219A/V221A/L222A] plus LCAT (C).

DISCUSSION

Why apoA-I[L218A/L219A/V221A/L222A]?

Being the major protein of HDL, apoA-I, when mutated, causes disruption of the biogenesis of HDL and can alter the functionality of HDL (A Chroni 2003 and 2007). Deletion of amino acid residues 187-243 (carboxy terminal helices 8-10; apoA-I[Δ(187-243)] or apoA-I[Δ(210-243)] resulted in impaired binding ability of mutant protein to macrophages, and a reduced ability to promote cholesterol and phospholipid efflux (185, 186). Hydrophobic amino acid substitution of apoA-I within this domain, L222K, F225K, and F229K has been shown to diminish apoA-I's ability to associate with HDL and phospholipids (*127*). ApoA-I mutants with hydrophobic residue substitutions, apoA-I[L211V/L214V/L218V/L219V] and apoA-I[L222K/F225K/F229K], also lack the ability to create mature spherical HDL particles in vivo, instead discoidal HDL particles accumulate in the plasma of these mutants (187). The 220-231 domain of apoA-I was found to be highly conserved evolutionarily—much more so than other domains of apoA-I(188), and chemical cross-linking and immunoprecipitation studies suggest that apoA-I carboxy terminal region 220-231 deletions reduce the ability of apoA-I to crosslink to ABCA1 (189).

Based on the data summarized above, the Zannis group explored the ability of apoA-I mutants lacking amino- and carboxy-terminal domains to promote cholesterol and phospholipid efflux from macrophages. They found that apoA-I's carboxy-terminal domain including amino acid residues 220-231 is required for ABCA1-mediated cholesterol efflux by apoA-I, and such mutants do not form HDL in vivo (*66*). A potential explanation for the inability of the apoA-I mutants lacking the 220-232 region is centered around the finding that this mutant has a limited capacity to promote cholesterol efflux and form pre-β-HDL precursors, and also a reduced solubilization of

DMPC mulitlamellar vesicles (*66*).This investigation lead to the conclusion that proper lipid efflux involves a functional interaction between ABCA1 and intact apoA-I, and that this efflux is required for the formation of HDL precursors which mature into HDL particles.

Further exploring the apoA-I[Δ(185−243)], apoA-I[Δ(220−243)], and apoA-I[Δ(232−243)] mutants, the Zannis group found that deletions in these regions of apoA-I prevent the biogenesis of normal α-HDL particles, but they allow the formation of pre-β-HDL particles by processes that appear to be independent of interactions between apoA-I and ABCA1 (190).

Objective

The overall objective of my studies on apoA-I[L218A/L219A/V221A/L222A] was to further the studies already completed by the Zannis lab, thereby advancing understanding of the importanace of the 220-232 carboxy terminal domain of apoA-I. I focused specifically on the 218-222 region, aiming to assess the importance of these specific amino acid residues of apoA-I in the biogenesis of HDL by expressing the mutant in apoA-I -/- x apoE -/- mice. This study is based on the theory that HDL biogenesis as a continuous pathway where HDL, apoA-I, and other proteins interact. The successful biogenesis of HDL requires the initial interaction between apoA-I and ABCA1 to promote the lipidation of apoA-I. The nascent particles thus formed are acted upon by LCAT, creating mature and fully functional HDL (66, 191, 192). Numerous studies show that in both humans and animals, HDL does not form in the absence of normal apoA-I or ABCA1 (57, 192, 193). ABCA1/apoA-I interactions in the liver have been implicated not only in the initial lipidation of apoA-I, but in the maturation of nascent pre-β-HDL particles to mature sphperical α-HDL particles (194, 195), and it is known that interaction with apoproteins stabilizes ABCA1, retarding its degradation (196, 197).

My work is an extension of recent, unpublished data from the Zannis lab. These data, obtained in apoA-I -/- mice, shows a great reduction in plasma total cholesterol and apoA-I levels in mice injected with adenovirus expressing the apoA-I[L218A/L219A/V221A/L222A], compared to the apoA-I WT. These experiments also showed the mutant apoA-I has a shifted distribution of apoA-I accompanied by a significant increase in mouse apoE that floats in the HDL2, HDL3 region. The EM of the apoA-I[L218A/L219A/V221A/L222A] mutant showed presence of HDL-sized particles, some of which could be apoE-containing HDL (*68*). These mice also form pre-β and α-4 HDL particles.

The presence of mouse apoE may stabilize ABCA1, and allow the formation of HDL particles that contain mouse apoE or apoA-I[L218A/L219A/V221A/L222A]. This presence of apoE could account for the findings of the previous study that suggest HDL formation in the mice expressing the apoA-I[L218A/L219A/V221A/L222A] mutation, determined by EM analysis and 2D gel electrophoresis. My experiments have all been performed in double knockout mice, apoA-I -/- x apoE -/- to overcome the potential contribution of apoE in the formation of apoE-containing HDL particles as well as the stablilization of ABCA1.

Project I: Ability of mutant apoA-I[L218A/L219A/V221A/L222A] to form HDL

For Project I, the total plasma cholesterol levels of mice injected with adenovirus expressing apoA-I[L218A/L219A/V221A/L222A] were lower than that for the mice injected with adenovirus expressing wild type apoA-I. Previous, unpublished data showed that the apoA-I[L218A/L219A/V221A/L222A] mutant has lower levels of plasma total cholesterol than apoA-I WT, most likely due to the overall decrease in HDL cholesterol (as determined by FPLC analysis and density gradient ultracentrifugation analysis).

Formation of HDL

The formation of HDL was assessed by the presence of an HDL cholesterol peak, and the presence of apoA-I in the HDL fraction following the fractionation of plasma by FPLC. The FPLC analysis shows the presence of an HDL cholesterol peak in mice expressing the wild type apoA-I and absence of such a peak in mice expressing the apoA-I mutant. Density gradient ultracentrifugation of plasma shows that in the mice expressing the WT apoA-I, the HDL region is enriched with apoA-I. Conversely in the mice expressing the mutant apoA-I[L218A/L219A/V221A/L222A], there are lower levels of apoA-I, as well as presence of apoA-IV in all lipoprotein fractions.

Electromicroscopy analysis of Project I showed that there are a few discoidal particles present in the plasma of the mutant apoA-I[L218A/L219A/V221A/L222A], but that this mutant failed to promote the formation of spherical HDL particles. The plasma from the wild type apoA-I showed clear spherical HDL particle formation.

Additionally, two dimensional gel electrophoresis of plasma showed that the expression of apoA-I[L218A/L219A/V221A/L222A] promoted the formation of pre-β HDL particles, but not α-HDL particles. The wild type apoA-I promoted formation of a few pre-β HDL particles, but predominantly α-HDL particles (α1, α2, and α3). The lack of α-HDL particles in the mutant apoA-I[L218A/L219A/V221A/L222A] plasma could explain the low levels of plasma HDL. Together these data further support the notion that the L218, L219, V221, and L222 amino acids of apoA-I are crucial for the formation of mature HDL particles.

The data indicate that in apoA-I -/- x apoE -/- mice expressing apoA-I[L218A/L219A/V221A/L222A], the mutant protein forms immature discoidal particles. Previous studies showed that lipid-free apoA-I or partially lipidated apoA-I forms can be catabolized rapidly by the kidney (194, 198, 199), thus providing a possible explanation as to why low levels of plasma HDL are observed in the mutant.

It can be suggested that in the previous experiments, the presence of the mutant apoA-I, the mouse apoE had the opportunity to be lipidated and form apoE-containing HDL particles. Potential stabilization of ABCA1 due to ites interaction with apoE may allow interaction with apoA-I as well as the formation of α-4 HDL particles. Such findings are not observed when double knockout mice are used.

Project II: Ability of LCAT to restore formation of HDL particles in mice expressing the mutant apoA-I[L218A/L219A/V221A/L222A]

The experiments performed four days post-infection were to confirm the findings of Project I pertinent to the ability of the mutant protein to promote formation of mature HDL particles, and additionally to see if the expression of LCAT could rescue the phenotype of the apoA-I[L218A/L219A/V221A/L222A] mutant.

Rationale: Why LCAT may be able to rescue phenotype

The rate-limiting step of HDL biogenesis seems to be the initial lipidation of apoA-I, taking place in the liver with seemingly little contribution from the peripheral tissues (194, 195, 200). ABCA1 interacts with apoA-I and even pre-β HDL particles to enrich them further with cholesterol,

thus increases the stability of ABCA1 (194, 195, 200). It has also been shown that in mice liver-specific inactivation of ABCA1 reduces plasma HDL (194, 195), suggesting that other proteins produced by the liver may be required for the maturation of HDL—one such protein being LCAT.

If LCAT has an impact on the biogenesis of HDL in mice expressing the apoA-I[L218A/L219A/V221A/L222A] mutant, we expect to see the phenotype of the mutant become more like the that of the WT apoA-I. If LCAT has no effect, if it cannot cause maturation of the particle, then we can surmise that the defect in the pathway of biogenesis is actually the initial interaction of apoA-I with ABCA1.

Plasma lipids

In Project II the mice expressing apoA-I[L218A/L219A/V221A/L222A] had lower total plasma cholesterol levels than did the mice expressing WT apoA-I—however, mice expressing the apoA-I[L218A/L219A/V221A/L222A] plus LCAT had higher total plasma cholesterol levels than mice expressing the wild type. It should be noted that all of the mice from Project II had relatively high levels of total cholesterol.

Formation of HDL

The FPLC analysis showed that mice expressing the mutant apoA-I[L218A/L219A/V221A/L222A] did not exhibit an HDL cholesterol peak, while mice expressing WT apoA-I did. In mice expressing apoA-I[L218A/L219A/V221A/L222A] plus LCAT the FPLC profile was shifted to the higher densities and contained a shoulder in the IDL-LDL region. Similar

to Project I, density gradient ultracentrifugation of plasma showed that in the mice expressing the WT apoA-I, the HDL regions are enriched with apoA-I. Conversely, in the mice expressing the mutant apoA-I[L218A/L219A/V221A/L222A] there are lower levels of apoA-I in the HDL region, and additionally apoA-IV is distributed in all lipoprotein fractions.

The two-dimensional gel electrophoresis analysis of the plasma showed no distinguishable difference in the formation of HDL subpopulations between the mice expressing apoA-I[L218A/L219A/V221A/L222A] and those expressing apoA-I[L218A/L219A/V221A/L222A] plus LCAT. They show formation of only pre-β HDL particles, no α particles. Again, the WT apoA-I showed formation of pre-β HDL particles as well as α1, α2, and α3-HDL particles.

Electromicroscopy analysis of plasma from the wild type apoA-I showed clear spherical HDL particle formation, while once again, in the plasma of the mutant apoA-I[L218A/L219A/V221A/L222A] there are a few discoidal particles present, but no clear evidence of spherical HDL particle formation. However, mice expressing the apoA-I[L218A/L219A/V221A/L222A] plus LCAT mutant formed spherical small HDL particles, indicating that the phenotype of the apoA-I[L218A/L219A/V221A/L222A] mutant can be partially restored by the expression of LCAT.

Our findings suggest that, while the LCAT treatment did not cause any substantial increase in the HDL or apoA-I levels in mice expressing the apoA-I[L218A/L219A/V221A/L222A] mutant according to the density gradient ultracentrifugation analysis, it did allow for the discoidal particles produced by the mutant to be converted to spherical particles. On the other hand, the FPLC analysis showed that even when the apoA-I[L218A/L219A/V221A/L222A] mutant is treated with LCAT, there is still no evidence of an HDL cholesterol peak. It seems that the LCAT treatment can

partially, but not completely, rescue the phenotype of the mutant apoA-I[L218A/L219A/V221A/L222A]. It is possible that the HDL particles formed fuse with apoB-containing particles and contribute to the observed HDL cholesterol shoulder seen in the IDL region.

CONCLUSIONS

Substitution of the hydrophobic residues 220-232 of the apoA-I protein by alanine (specifically the highly conserved 218-222 region) causes a disruption in the biogenesis of HDL. Lipidated particles that contain apoA-I[L218A/L219A/V221A/L222A] exist in the form of pre-β HDL particles. These particles are unstable and are most likely subjected to fast catabolism, thus explaining he low HDL levels of the mice expressing this mutation. It appears that the mutation has caused a block in the conversion of nascent HDL particles to mature particles. This defect appears to be due to inability of the endogenous LCAT to rapidly convert the discoidal particles containing this mutant to mature particles. Excess of LCAT provided by co-infection of the apoA-I -/- x apoE -/- mice overcomes this block (Figure 24).

The absence of both apoA-I and apoE in the double knockout mice used in these experiments caused ABCA1 to be less stable. The instability of ABCA1 leads to a reduced initial lipidation of the apoA-I[L218A/L219A/V221A/L222A] mutant, preventing further lipidation and maturation of the particles. When the mutant apoA-I apoA-I[L218A/L219A/V221A/L222A] is treated with LCAT, the conversion of discoidal to spherical particles takes place, and the aberrant HDL phenotype generated by the mutant apoA-I[L218A/L219A/V221A/L222A] is partially restored.

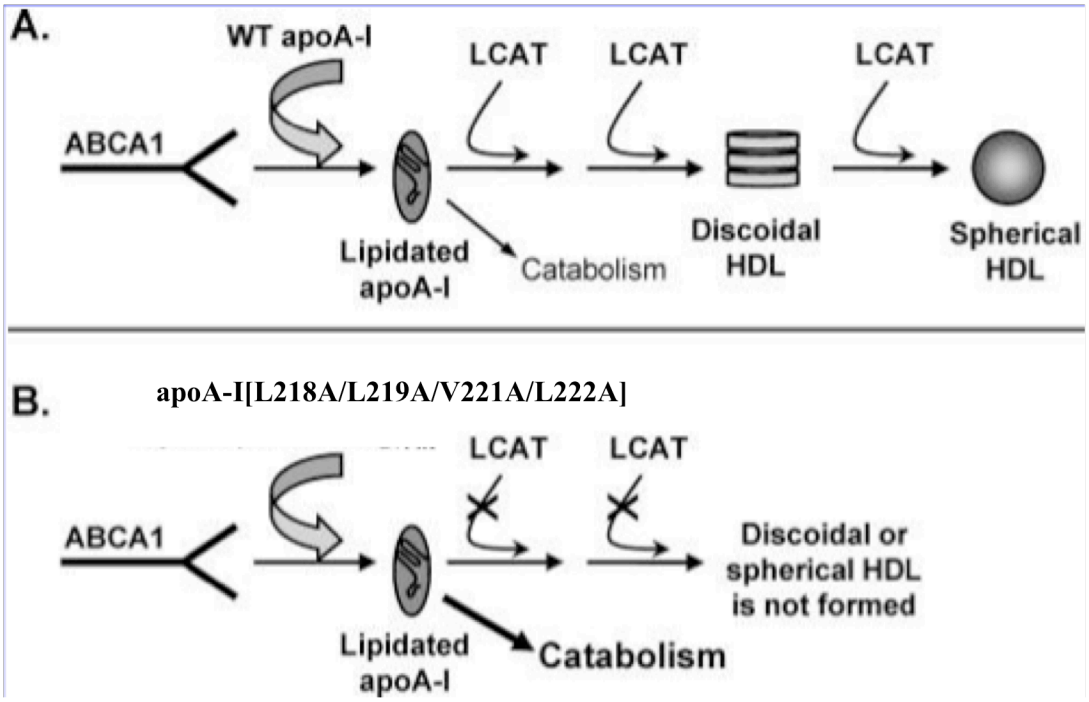

Figure 24: Adapted from (*68*). Schematic representation showing the pathway of biogenesis of HDL and how the two mutations affect the esterification of cholesterol of the pre-beta HDL particles and prevent their conversion to discoidal and spherical HDL, thus promoting their catabolism.

Reference List

1. Castelli,W.P. (1984) Epidemiology of coronary heart disease: the Framingham study, *Am. J. Med. 76*, 4-12.

2. Okajima,F., Sato,K., and Kimura,T. (2009) Anti-atherogenic actions of high-density lipoprotein through sphingosine 1-phosphate receptors and scavenger receptor class B type I, *Endocr. J. 56*, 317-334.

3. Parker,T.S., Levine,D.M., Chang,J.C., Laxer,J., Coffin,C.C., and Rubin,A.L. (1995) Reconstituted high-density lipoprotein neutralizes gram-negative bacterial lipopolysaccharides in human whole blood, *Infect. Immun. 63*, 253-258.

4. Singh,I.P., Chopra,A.K., Coppenhaver,D.H., Ananatharamaiah,G.M., and Baron,S. (1999) Lipoproteins account for part of the broad non-specific antiviral activity of human serum, *Antiviral Res. 42*, 211-218.

5. Vanhollebeke,B. and Pays,E. (2010) The trypanolytic factor of human serum: many ways to enter the parasite, a single way to kill, *Mol. Microbiol. 76*, 806-814.

6. Guo,Z.G., Li,C., Zhong,J.K., Tu,Y., and Xie,D. (2012) Laboratory investigation of dysfunctional HDL, *Chem. Phys. Lipids 165*, 32-37.

7. Nakamura,K., Kennedy,M.A., Baldan,A., Bojanic,D.D., Lyons,K., and Edwards,P.A. (2004) Expression and regulation of multiple murine ATP-binding cassette transporter G1

mRNAs/isoforms that stimulate cellular cholesterol efflux to high density lipoprotein, *J. Biol. Chem. 279*, 45980-45989.

8. Gu,X., Kozarsky,K., and Krieger,M. (2000) Scavenger receptor class B, type I-mediated [3H]cholesterol efflux to high and low density lipoproteins is dependent on lipoprotein binding to the receptor, *J. Biol. Chem. 275*, 29993-30001.

9. Seetharam,D., Mineo,C., Gormley,A.K., Gibson,L.L., Vongpatanasin,W., Chambliss,K.L., Hahner,L.D., Cummings,M.L., Kitchens,R.L., Marcel,Y.L., Rader,D.J., and Shaul,P.W. (2006) High-density lipoprotein promotes endothelial cell migration and reendothelialization via scavenger receptor-B type I, *Circ. Res. 98*, 63-72.

10. Mineo,C., Yuhanna,I.S., Quon,M.J., and Shaul,P.W. (2003) High density lipoprotein-induced endothelial nitric-oxide synthase activation is mediated by Akt and MAP kinases, *J. Biol. Chem. 278*, 9142-9149.

11. Nofer,J.R., Levkau,B., Wolinska,I., Junker,R., Fobker,M., von,E.A., Seedorf,U., and Assmann,G. (2001) Suppression of endothelial cell apoptosis by high density lipoproteins (HDL) and HDL-associated lysosphingolipids, *J. Biol. Chem. 276*, 34480-34485.

12. Okura,H., Yamashita,S., Ohama,T., Saga,A., Yamamoto-Kakuta,A., Hamada,Y., Sougawa,N., Ohyama,R., Sawa,Y., and Matsuyama,A. (2010) HDL/apolipoprotein A-I binds to macrophage-derived progranulin and suppresses its conversion into proinflammatory granulins, *J. Atheroscler. Thromb. 17*, 568-577.

13. Cockerill,G.W., Rye,K.A., Gamble,J.R., Vadas,M.A., and Barter,P.J. (1995) High-density lipoproteins inhibit cytokine-induced expression of endothelial cell adhesion molecules, *Arterioscler. Thromb. Vasc. Biol. 15*, 1987-1994.

14. Murphy,A.J., Woollard,K.J., Hoang,A., Mukhamedova,N., Stirzaker,R.A., McCormick,S.P., Remaley,A.T., Sviridov,D., and Chin-Dusting,J. (2008) High-density lipoprotein reduces the human monocyte inflammatory response, *Arterioscler. Thromb. Vasc. Biol. 28*, 2071-2077.

15. Dole,V.S., Matuskova,J., Vasile,E., Yesilaltay,A., Bergmeier,W., Bernimoulin,M., Wagner,D.D., and Krieger,M. (2008) Thrombocytopenia and platelet abnormalities in high-density lipoprotein receptor-deficient mice, *Arterioscler. Thromb. Vasc. Biol. 28*, 1111-1116.

16. Navab,M., Hama,S.Y., Anantharamaiah,G.M., Hassan,K., Hough,G.P., Watson,A.D., Reddy,S.T., Sevanian,A., Fonarow,G.C., and Fogelman,A.M. (2000) Normal high density lipoprotein inhibits three steps in the formation of mildly oxidized low density lipoprotein: steps 2 and 3, *J. Lipid Res. 41*, 1495-1508.

17. Navab,M., Hama,S.Y., Cooke,C.J., Anantharamaiah,G.M., Chaddha,M., Jin,L., Subbanagounder,G., Faull,K.F., Reddy,S.T., Miller,N.E., and Fogelman,A.M. (2000) Normal high density lipoprotein inhibits three steps in the formation of mildly oxidized low density lipoprotein: step 1, *J. Lipid Res. 41*, 1481-1494.

18. Murphy,A.J., Westerterp,M., Yvan-Charvet,L., and Tall,A.R. (2012) Anti-atherogenic mechanisms of high density lipoprotein: Effects on myeloid cells, *Biochim. Biophys. Acta 1821*, 513-521.

19. Elsoe,S., Ahnstrom,J., Christoffersen,C., Hoofnagle,A.N., Plomgaard,P., Heinecke,J.W., Binder,C.J., Bjorkbacka,H., Dahlback,B., and Nielsen,L.B. (2012) Apolipoprotein M binds oxidized phospholipids and increases the antioxidant effect of HDL, *Atherosclerosis 221*, 91-97.

20. Gordon,D.J., Probstfield,J.L., Garrison,R.J., Neaton,J.D., Castelli,W.P., Knoke,J.D., Jacobs,D.R., Jr., Bangdiwala,S., and Tyroler,H.A. (1989) High-density lipoprotein cholesterol and cardiovascular disease. Four prospective American studies, *Circulation 79*, 8-15.

21. Kilpatrick,R.D., McAllister,C.J., Kovesdy,C.P., Derose,S.F., Kopple,J.D., and Kalantar-Zadeh,K. (2007) Association between serum lipids and survival in hemodialysis patients and impact of race, *J. Am. Soc. Nephrol. 18*, 293-303.

22. Tolle,M., Huang,T., Schuchardt,M., Jankowski,V., Prufer,N., Jankowski,J., Tietge,U.J., Zidek,W., and van der Giet,M. (2012) High-density lipoprotein loses its anti-inflammatory capacity by accumulation of pro-inflammatory-serum amyloid A, *Cardiovasc. Res. 94*, 154-162.

23. de la Llera,M.M., McGillicuddy,F.C., Hinkle,C.C., Byrne,M., Joshi,M.R., Nguyen,V., Tabita-Martinez,J., Wolfe,M.L., Badellino,K., Pruscino,L., Mehta,N.N., Asztalos,B.F., and

Reilly,M.P. (2012) Inflammation modulates human HDL composition and function in vivo, *Atherosclerosis 222*, 390-394.

24. Drew,B.G., Rye,K.A., Duffy,S.J., Barter,P., and Kingwell,B.A. (2012) The emerging role of HDL in glucose metabolism, *Nat. Rev. Endocrinol. 8*, 237-245.

25. Barter,P.J., Caulfield,M., Eriksson,M., Grundy,S.M., Kastelein,J.J., Komajda,M., Lopez-Sendon,J., Mosca,L., Tardif,J.C., Waters,D.D., Shear,C.L., Revkin,J.H., Buhr,K.A., Fisher,M.R., Tall,A.R., and Brewer,B. (2007) Effects of torcetrapib in patients at high risk for coronary events, *N. Engl. J. Med. 357*, 2109-2122.

26. Kastelein,J.J., van Leuven,S.I., Burgess,L., Evans,G.W., Kuivenhoven,J.A., Barter,P.J., Revkin,J.H., Grobbee,D.E., Riley,W.A., Shear,C.L., Duggan,W.T., and Bots,M.L. (2007) Effect of torcetrapib on carotid atherosclerosis in familial hypercholesterolemia, *N. Engl. J. Med. 356*, 1620-1630.

27. van der Steeg,W.A., Holme,I., Boekholdt,S.M., Larsen,M.L., Lindahl,C., Stroes,E.S., Tikkanen,M.J., Wareham,N.J., Faergeman,O., Olsson,A.G., Pedersen,T.R., Khaw,K.T., and Kastelein,J.J. (2008) High-density lipoprotein cholesterol, high-density lipoprotein particle size, and apolipoprotein A-I: significance for cardiovascular risk: the IDEAL and EPIC-Norfolk studies, *J. Am. Coll. Cardiol. 51*, 634-642.

28. Vazquez,E., Sethi,A.A., Freeman,L., Zalos,G., Chaudhry,H., Haser,E., Aicher,B.O., Aponte,A., Gucek,M., Kato,G.J., Waclawiw,M.A., Remaley,A.T., and Cannon,R.O., III (2012) High-density lipoprotein cholesterol efflux, nitration of apolipoprotein A-I, and endothelial function in obese women, *Am. J. Cardiol. 109*, 527-532.

29. Zannis,V.I., Zanni,E.E., Papapanagiotou,D., Kardassis,D., and Chroni,A. ApoA-I functions and synthesis of HDL: Insights from mouse models of human HDL metabolism, High-Density Lipoproteins. 237-265. 2006. From Basic Biology to Clinical Aspects, Weinheim, Wiley-VCH.

Ref Type: Generic

30. Zannis,V.I., Chroni,A., and Krieger,M. (2006) Role of apoA-I, ABCA1, LCAT, and SR-BI in the biogenesis of HDL, *J. Mol. Med. (Berl) 84*, 276-294.

31. Tsompanidi,E.M., Brinkmeier,M.S., Fotiadou,E.H., Giakoumi,S.M., and Kypreos,K.E. (2010) HDL biogenesis and functions: role of HDL quality and quantity in atherosclerosis, *Atherosclerosis 208*, 3-9.

32. Mineo,C. and Shaul,P.W. (2003) HDL stimulation of endothelial nitric oxide synthase: a novel mechanism of HDL action, *Trends Cardiovasc. Med. 13*, 226-231.

33. Gong,M., Wilson,M., Kelly,T., Su,W., Dressman,J., Kincer,J., Matveev,S.V., Guo,L., Guerin,T., Li,X.A., Zhu,W., Uittenbogaard,A., and Smart,E.J. (2003) HDL-associated estradiol stimulates endothelial NO synthase and vasodilation in an SR-BI-dependent manner, *J. Clin. Invest 111*, 1579-1587.

34. Nofer,J.R., van der Giet,M., Tolle,M., Wolinska,I., von Wnuck,L.K., Baba,H.A., Tietge,U.J., Godecke,A., Ishii,I., Kleuser,B., Schafers,M., Fobker,M., Zidek,W., Assmann,G., Chun,J., and Levkau,B. (2004) HDL induces NO-dependent vasorelaxation via the lysophospholipid receptor S1P3, *J. Clin. Invest 113*, 569-581.

35. Nofer,J.R., Junker,R., Pulawski,E., Fobker,M., Levkau,B., von,E.A., Seedorf,U., Assmann,G., and Walter,M. (2001) High density lipoproteins induce cell cycle entry in vascular smooth muscle cells via mitogen activated protein kinase-dependent pathway, *Thromb. Haemost. 85*, 730-735.

36. Norata,G.D., Callegari,E., Marchesi,M., Chiesa,G., Eriksson,P., and Catapano,A.L. (2005) High-density lipoproteins induce transforming growth factor-beta2 expression in endothelial cells, *Circulation 111*, 2805-2811.

37. Norata,G.D. and Catapano,A.L. (2005) Molecular mechanisms responsible for the antiinflammatory and protective effect of HDL on the endothelium, *Vasc. Health Risk Manag. 1*, 119-129.

38. Clay,M.A., Pyle,D.H., Rye,K.A., Vadas,M.A., Gamble,J.R., and Barter,P.J. (2001) Time sequence of the inhibition of endothelial adhesion molecule expression by reconstituted high density lipoproteins, *Atherosclerosis 157*, 23-29.

39. Kleemann,R., Zadelaar,S., and Kooistra,T. (2008) Cytokines and atherosclerosis: a comprehensive review of studies in mice, *Cardiovasc. Res. 79*, 360-376.

40. Park,S.H., Park,J.H., Kang,J.S., and Kang,Y.H. (2003) Involvement of transcription factors in plasma HDL protection against TNF-alpha-induced vascular cell adhesion molecule-1 expression, *Int. J. Biochem. Cell Biol. 35*, 168-182.

41. Xia,P., Vadas,M.A., Rye,K.A., Barter,P.J., and Gamble,J.R. (1999) High density lipoproteins (HDL) interrupt the sphingosine kinase signaling pathway. A possible

mechanism for protection against atherosclerosis by HDL, *J. Biol. Chem. 274*, 33143-33147.

42. Diederich,W., Orso,E., Drobnik,W., and Schmitz,G. (2001) Apolipoprotein AI and HDL(3) inhibit spreading of primary human monocytes through a mechanism that involves cholesterol depletion and regulation of CDC42, *Atherosclerosis 159*, 313-324.

43. Gonzalez-Diez,M., Rodriguez,C., Badimon,L., and Martinez-Gonzalez,J. (2008) Prostacyclin induction by high-density lipoprotein (HDL) in vascular smooth muscle cells depends on sphingosine 1-phosphate receptors: effect of simvastatin, *Thromb. Haemost. 100*, 119-126.

44. Liu,D., Ji,L., Tong,X., Pan,B., Han,J.Y., Huang,Y., Chen,Y.E., Pennathur,S., Zhang,Y., and Zheng,L. (2011) Human apolipoprotein A-I induces cyclooxygenase-2 expression and prostaglandin I-2 release in endothelial cells through ATP-binding cassette transporter A1, *Am. J. Physiol Cell Physiol 301*, C739-C748.

45. Besler,C., Heinrich,K., Rohrer,L., Doerries,C., Riwanto,M., Shih,D.M., Chroni,A., Yonekawa,K., Stein,S., Schaefer,N., Mueller,M., Akhmedov,A., Daniil,G., Manes,C., Templin,C., Wyss,C., Maier,W., Tanner,F.C., Matter,C.M., Corti,R., Furlong,C., Lusis,A.J., von,E.A., Fogelman,A.M., Luscher,T.F., and Landmesser,U. (2011) Mechanisms underlying adverse effects of HDL on eNOS-activating pathways in patients with coronary artery disease, *J. Clin. Invest 121*, 2693-2708.

46. Oh,J., Riek,A.E., Weng,S., Petty,M., Kim,D., Colonna,M., Cella,M., and Bernal-Mizrachi,C. (2012) Endoplasmic reticulum stress controls M2 macrophage differentiation and foam cell formation, *J. Biol. Chem. 287*, 11629-11641.

47. Ito,J., Nagayasu,Y., Kheirollah,A., Abe-Dohmae,S., and Yokoyama,S. (2011) ApoA-I enhances generation of HDL-like lipoproteins through interaction between ABCA1 and phospholipase Cgamma in rat astrocytes, *Biochim. Biophys. Acta 1811*, 1062-1069.

48. Maejima,T., Sugano,T., Yamazaki,H., Yoshinaka,Y., Doi,T., Tanabe,S., and Nishimaki-Mogami,T. (2011) Pitavastatin increases ABCA1 expression by dual mechanisms: SREBP2-driven transcriptional activation and PPARalpha-dependent protein stabilization but without activating LXR in rat hepatoma McARH7777 cells, *J. Pharmacol. Sci. 116*, 107-115.

49. Grun,F., Watanabe,H., Zamanian,Z., Maeda,L., Arima,K., Cubacha,R., Gardiner,D.M., Kanno,J., Iguchi,T., and Blumberg,B. (2006) Endocrine-disrupting organotin compounds are potent inducers of adipogenesis in vertebrates, *Mol. Endocrinol. 20*, 2141-2155.

50. Cui,H., Okuhira,K., Ohoka,N., Naito,M., Kagechika,H., Hirose,A., and Nishimaki-Mogami,T. (2011) Tributyltin chloride induces ABCA1 expression and apolipoprotein A-I-mediated cellular cholesterol efflux by activating LXRalpha/RXR, *Biochem. Pharmacol. 81*, 819-824.

51. Ng,K.M., Lee,Y.K., Lai,W.H., Chan,Y.C., Fung,M.L., Tse,H.F., and Siu,C.W. (2011) Exogenous expression of human apoA-I enhances cardiac differentiation of pluripotent stem cells, *PLoS. One. 6*, e19787.

52. PULLMAN,M.E. and MONROY,G.C. (1963) A NATURALLY OCCURRING INHIBITOR OF MITOCHONDRIAL ADENOSINE TRIPHOSPHATASE, *J. Biol. Chem. 238*, 3762-3769.

53. Genoux,A., Pons,V., Radojkovic,C., Roux-Dalvai,F., Combes,G., Rolland,C., Malet,N., Monsarrat,B., Lopez,F., Ruidavets,J.B., Perret,B., and Martinez,L.O. (2011) Mitochondrial inhibitory factor 1 (IF1) is present in human serum and is positively correlated with HDL-cholesterol, *PLoS. One. 6*, e23949.

54. Brewer,H.B., Jr., Fairwell,T., LaRue,A., Ronan,R., Houser,A., and Bronzert,T.J. (1978) The amino acid sequence of human APOA-I, an apolipoprotein isolated from high density lipoproteins, *Biochem. Biophys. Res. Commun. 80*, 623-630.

55. Arinami,T., Hirano,T., Kobayashi,K., Yamanouchi,Y., and Hamaguchi,H. (1990) Assignment of the apolipoprotein A-I gene to 11q23 based on RFLP in a case with a partial deletion of chromosome 11, del(11)(q23.3----qter), *Hum. Genet. 85*, 39-40.

56. Mei,X. and Atkinson,D. (2011) Crystal structure of C-terminal truncated apolipoprotein A-I reveals the assembly of high density lipoprotein (HDL) by dimerization, *J. Biol. Chem. 286*, 38570-38582.

57. Williamson,R., Lee,D., Hagaman,J., and Maeda,N. (1992) Marked reduction of high density lipoprotein cholesterol in mice genetically modified to lack apolipoprotein A-I, *Proc. Natl. Acad. Sci. U. S. A 89*, 7134-7138.

58. Zannis,V.I., Cole,F.S., Jackson,C.L., Kurnit,D.M., and Karathanasis,S.K. (1985) Distribution of apolipoprotein A-I, C-II, C-III, and E mRNA in fetal human tissues. Time-

dependent induction of apolipoprotein E mRNA by cultures of human monocyte-macrophages, *Biochemistry 24*, 4450-4455.

59. Benoit,P., Emmanuel,F., Caillaud,J.M., Bassinet,L., Castro,G., Gallix,P., Fruchart,J.C., Branellec,D., Denefle,P., and Duverger,N. (1999) Somatic gene transfer of human ApoA-I inhibits atherosclerosis progression in mouse models, *Circulation 99*, 105-110.

60. Rubin,E.M., Krauss,R.M., Spangler,E.A., Verstuyft,J.G., and Clift,S.M. (1991) Inhibition of early atherogenesis in transgenic mice by human apolipoprotein AI, *Nature 353*, 265-267.

61. Plump,A.S., Scott,C.J., and Breslow,J.L. (1994) Human apolipoprotein A-I gene expression increases high density lipoprotein and suppresses atherosclerosis in the apolipoprotein E-deficient mouse, *Proc. Natl. Acad. Sci. U. S. A 91*, 9607-9611.

62. Knowlton,N., Wages,J., Centola,M., and Alaupovic,P. (2012) Apolipoprotein-defined lipoprotein abnormalities in rheumatoid arthritis patients and their potential impact on cardiovascular disease, *Scand. J. Rheumatol. 41*, 165-169.

63. Shao,B., Pennathur,S., and Heinecke,J.W. (2012) Myeloperoxidase targets apolipoprotein A-I, the major high density lipoprotein protein, for site-specific oxidation in human atherosclerotic lesions, *J. Biol. Chem. 287*, 6375-6386.

64. Shao,B. and Heinecke,J.W. (2011) Impact of HDL oxidation by the myeloperoxidase system on sterol efflux by the ABCA1 pathway, *J. Proteomics. 74*, 2289-2299.

65. Tabet,F., Lambert,G., Cuesta Torres,L.F., Hou,L., Sotirchos,I., Touyz,R.M., Jenkins,A.J., Barter,P.J., and Rye,K.A. (2011) Lipid-free apolipoprotein A-I and discoidal reconstituted

high-density lipoproteins differentially inhibit glucose-induced oxidative stress in human macrophages, *Arterioscler. Thromb. Vasc. Biol. 31*, 1192-1200.

66. Chroni,A., Liu,T., Gorshkova,I., Kan,H.Y., Uehara,Y., von,E.A., and Zannis,V.I. (2003) The central helices of ApoA-I can promote ATP-binding cassette transporter A1 (ABCA1)-mediated lipid efflux. Amino acid residues 220-231 of the wild-type ApoA-I are required for lipid efflux in vitro and high density lipoprotein formation in vivo, *J. Biol. Chem. 278*, 6719-6730.

67. Koukos,G., Chroni,A., Duka,A., Kardassis,D., and Zannis,V.I. (2007) Naturally occurring and bioengineered apoA-I mutations that inhibit the conversion of discoidal to spherical HDL: the abnormal HDL phenotypes can be corrected by treatment with LCAT, *Biochem. J. 406*, 167-174.

68. Koukos,G., Chroni,A., Duka,A., Kardassis,D., and Zannis,V.I. (2007) LCAT can rescue the abnormal phenotype produced by the natural ApoA-I mutations (Leu141Arg)Pisa and (Leu159Arg)FIN, *Biochemistry 46*, 10713-10721.

69. Chroni,A., Kan,H.Y., Kypreos,K.E., Gorshkova,I.N., Shkodrani,A., and Zannis,V.I. (2004) Substitutions of glutamate 110 and 111 in the middle helix 4 of human apolipoprotein A-I (apoA-I) by alanine affect the structure and in vitro functions of apoA-I and induce severe hypertriglyceridemia in apoA-I-deficient mice, *Biochemistry 43*, 10442-10457.

70. Rowczenio,D., Dogan,A., Theis,J.D., Vrana,J.A., Lachmann,H.J., Wechalekar,A.D., Gilbertson,J.A., Hunt,T., Gibbs,S.D., Sattianayagam,P.T., Pinney,J.H., Hawkins,P.N., and

Gillmore,J.D. (2011) Amyloidogenicity and clinical phenotype associated with five novel mutations in apolipoprotein A-I, *Am. J. Pathol. 179*, 1978-1987.

71. Gomaraschi,M., Obici,L., Simonelli,S., Gregorini,G., Negrinelli,A., Merlini,G., Franceschini,G., and Calabresi,L. (2011) Effect of the amyloidogenic L75P apolipoprotein A-I variant on HDL subpopulations, *Clin. Chim. Acta 412*, 1262-1265.

72. Sorci-Thomas,M.G., Zabalawi,M., Bharadwaj,M.S., Wilhelm,A.J., Owen,J.S., Asztalos,B.F., Bhat,S., and Thomas,M.J. (2012) Dysfunctional HDL containing L159R ApoA-I leads to exacerbation of atherosclerosis in hyperlipidemic mice, *Biochim. Biophys. Acta 1821*, 502-512.

73. Recalde,D., Velez-Carrasco,W., Civeira,F., Cenarro,A., Gomez-Coronado,D., Ordovas,J.M., and Pocovi,M. (2001) Enhanced fractional catabolic rate of apo A-I and apo A-II in heterozygous subjects for apo A-I(Zaragoza) (L144R), *Atherosclerosis 154*, 613-623.

74. Fiddyment,S., Barcelo-Batllori,S., Pocovi,M., and Garcia-Otin,A.L. (2011) Expression and purification of recombinant apolipoprotein A-I Zaragoza (L144R) and formation of reconstituted HDL particles, *Protein Expr. Purif. 80*, 110-116.

75. Franceschini,G., Sirtori,C.R., Capurso,A., Weisgraber,K.H., and Mahley,R.W. (1980) A-IMilano apoprotein. Decreased high density lipoprotein cholesterol levels with significant lipoprotein modifications and without clinical atherosclerosis in an Italian family, *J. Clin. Invest 66*, 892-900.

76. Shah,P.K., Nilsson,J., Kaul,S., Fishbein,M.C., Ageland,H., Hamsten,A., Johansson,J., Karpe,F., and Cercek,B. (1998) Effects of recombinant apolipoprotein A-I(Milano) on aortic atherosclerosis in apolipoprotein E-deficient mice, *Circulation 97*, 780-785.

77. Nicholls,S.J., Tuzcu,E.M., Sipahi,I., Schoenhagen,P., Crowe,T., Kapadia,S., and Nissen,S.E. (2006) Relationship between atheroma regression and change in lumen size after infusion of apolipoprotein A-I Milano, *J. Am. Coll. Cardiol. 47*, 992-997.

78. Lagerstedt,J.O., Cavigiolio,G., Roberts,L.M., Hong,H.S., Jin,L.W., Fitzgerald,P.G., Oda,M.N., and Voss,J.C. (2007) Mapping the structural transition in an amyloidogenic apolipoprotein A-I, *Biochemistry 46*, 9693-9699.

79. Petrlova,J., Duong,T., Cochran,M.C., Axelsson,A., Morgelin,M., Roberts,L.M., and Lagerstedt,J.O. (2012) The fibrillogenic L178H variant of apolipoprotein A-I forms helical fibrils, *J. Lipid Res. 53*, 390-398.

80. Haase,C.L., Frikke-Schmidt,R., Nordestgaard,B.G., Kateifides,A.K., Kardassis,D., Nielsen,L.B., Andersen,C.B., Kober,L., Johnsen,A.H., Grande,P., Zannis,V.I., and Tybjaerg-Hansen,A. (2011) Mutation in APOA1 predicts increased risk of ischaemic heart disease and total mortality without low HDL cholesterol levels, *J. Intern. Med. 270*, 136-146.

81. Dodani,S., Grice,D.G., and Joshi,S. (2009) Is HDL function as important as HDL quantity in the coronary artery disease risk assessment?, *J. Clin. Lipidol. 3*, 70-77.

82. Saemann,M.D., Poglitsch,M., Kopecky,C., Haidinger,M., Horl,W.H., and Weichhart,T. (2010) The versatility of HDL: a crucial anti-inflammatory regulator, *Eur. J. Clin. Invest 40*, 1131-1143.

83. Jones,M.K., Catte,A., Li,L., and Segrest,J.P. (2009) Dynamics of activation of lecithin:cholesterol acyltransferase by apolipoprotein A-I, *Biochemistry 48*, 11196-11210.

84. Rothblat,G.H. and Phillips,M.C. (2010) High-density lipoprotein heterogeneity and function in reverse cholesterol transport, *Curr. Opin. Lipidol. 21*, 229-238.

85. Luo,D.X., Cao,D.L., Xiong,Y., Peng,X.H., and Liao,D.F. (2010) A novel model of cholesterol efflux from lipid-loaded cells, *Acta Pharmacol. Sin. 31*, 1243-1257.

86. Yvan-Charvet,L., Wang,N., and Tall,A.R. (2010) Role of HDL, ABCA1, and ABCG1 transporters in cholesterol efflux and immune responses, *Arterioscler. Thromb. Vasc. Biol. 30*, 139-143.

87. van,M.G., Halter,D., Sprong,H., Somerharju,P., and Egmond,M.R. (2006) ABC lipid transporters: extruders, flippases, or flopless activators?, *FEBS Lett. 580*, 1171-1177.

88. Zannis,V.I., Kypreos,K.E., Chroni,A., Kardassis,D., and Zanni,E.E. Chapter 8: Lipoproteins and atherogenesis. Molecular Mechanisms of Atherosclerosis. 2004.

Ref Type: Generic

89. Hamon,Y., Broccardo,C., Chambenoit,O., Luciani,M.F., Toti,F., Chaslin,S., Freyssinet,J.M., Devaux,P.F., McNeish,J., Marguet,D., and Chimini,G. (2000) ABC1 promotes engulfment

of apoptotic cells and transbilayer redistribution of phosphatidylserine, *Nat. Cell Biol. 2*, 399-406.

90. Chambenoit,O., Hamon,Y., Marguet,D., Rigneault,H., Rosseneu,M., and Chimini,G. (2001) Specific docking of apolipoprotein A-I at the cell surface requires a functional ABCA1 transporter, *J. Biol. Chem. 276*, 9955-9960.

91. Liu,L., Bortnick,A.E., Nickel,M., Dhanasekaran,P., Subbaiah,P.V., Lund-Katz,S., Rothblat,G.H., and Phillips,M.C. (2003) Effects of apolipoprotein A-I on ATP-binding cassette transporter A1-mediated efflux of macrophage phospholipid and cholesterol: formation of nascent high density lipoprotein particles, *J. Biol. Chem. 278*, 42976-42984.

92. Oram,J.F. and Heinecke,J.W. (2005) ATP-binding cassette transporter A1: a cell cholesterol exporter that protects against cardiovascular disease, *Physiol Rev. 85*, 1343-1372.

93. Choi,H.Y., Karten,B., Chan,T., Vance,J.E., Greer,W.L., Heidenreich,R.A., Garver,W.S., and Francis,G.A. (2003) Impaired ABCA1-dependent lipid efflux and hypoalphalipoproteinemia in human Niemann-Pick type C disease, *J. Biol. Chem. 278*, 32569-32577.

94. Bowden,K.L., Bilbey,N.J., Bilawchuk,L.M., Boadu,E., Sidhu,R., Ory,D.S., Du,H., Chan,T., and Francis,G.A. (2011) Lysosomal acid lipase deficiency impairs regulation of ABCA1 gene and formation of high density lipoproteins in cholesteryl ester storage disease, *J. Biol. Chem. 286*, 30624-30635.

95. Fielding,P.E., Nagao,K., Hakamata,H., Chimini,G., and Fielding,C.J. (2000) A two-step mechanism for free cholesterol and phospholipid efflux from human vascular cells to apolipoprotein A-1, *Biochemistry 39*, 14113-14120.

96. Gillotte,K.L., Zaiou,M., Lund-Katz,S., Anantharamaiah,G.M., Holvoet,P., Dhoest,A., Palgunachari,M.N., Segrest,J.P., Weisgraber,K.H., Rothblat,G.H., and Phillips,M.C. (1999) Apolipoprotein-mediated plasma membrane microsolubilization. Role of lipid affinity and membrane penetration in the efflux of cellular cholesterol and phospholipid, *J. Biol. Chem. 274*, 2021-2028.

97. Denis,M., Landry,Y.D., and Zha,X. (2008) ATP-binding cassette A1-mediated lipidation of apolipoprotein A-I occurs at the plasma membrane and not in the endocytic compartments, *J. Biol. Chem. 283*, 16178-16186.

98. Neufeld,E.B., Remaley,A.T., Demosky,S.J., Stonik,J.A., Cooney,A.M., Comly,M., Dwyer,N.K., Zhang,M., Blanchette-Mackie,J., Santamarina-Fojo,S., and Brewer,H.B., Jr. (2001) Cellular localization and trafficking of the human ABCA1 transporter, *J. Biol. Chem. 276*, 27584-27590.

99. Neufeld,E.B., Stonik,J.A., Demosky,S.J., Jr., Knapper,C.L., Combs,C.A., Cooney,A., Comly,M., Dwyer,N., Blanchette-Mackie,J., Remaley,A.T., Santamarina-Fojo,S., and Brewer,H.B., Jr. (2004) The ABCA1 transporter modulates late endocytic trafficking: insights from the correction of the genetic defect in Tangier disease, *J. Biol. Chem. 279*, 15571-15578.

100. Remaley,A.T., Stonik,J.A., Demosky,S.J., Neufeld,E.B., Bocharov,A.V., Vishnyakova,T.G., Eggerman,T.L., Patterson,A.P., Duverger,N.J., Santamarina-Fojo,S., and Brewer,H.B., Jr. (2001) Apolipoprotein specificity for lipid efflux by the human ABCAI transporter, *Biochem. Biophys. Res. Commun. 280*, 818-823.

101. Denis,M., Haidar,B., Marcil,M., Bouvier,M., Krimbou,L., and Genest,J. (2004) Characterization of oligomeric human ATP binding cassette transporter A1. Potential implications for determining the structure of nascent high density lipoprotein particles, *J. Biol. Chem. 279*, 41529-41536.

102. Lee,J.Y., Karwatsky,J., Ma,L., and Zha,X. (2011) ABCA1 increases extracellular ATP to mediate cholesterol efflux to ApoA-I, *Am. J. Physiol Cell Physiol 301*, C886-C894.

103. Zarubica,A., Trompier,D., and Chimini,G. (2007) ABCA1, from pathology to membrane function, *Pflugers Arch. 453*, 569-579.

104. Costet,P., Luo,Y., Wang,N., and Tall,A.R. (2000) Sterol-dependent transactivation of the ABC1 promoter by the liver X receptor/retinoid X receptor, *J. Biol. Chem. 275*, 28240-28245.

105. Schmitz,G. and Langmann,T. (2005) Transcriptional regulatory networks in lipid metabolism control ABCA1 expression, *Biochim. Biophys. Acta 1735*, 1-19.

106. Venkateswaran,A., Laffitte,B.A., Joseph,S.B., Mak,P.A., Wilpitz,D.C., Edwards,P.A., and Tontonoz,P. (2000) Control of cellular cholesterol efflux by the nuclear oxysterol receptor LXR alpha, *Proc. Natl. Acad. Sci. U. S. A 97*, 12097-12102.

107. Repa,J.J., Turley,S.D., Lobaccaro,J.A., Medina,J., Li,L., Lustig,K., Shan,B., Heyman,R.A., Dietschy,J.M., and Mangelsdorf,D.J. (2000) Regulation of absorption and ABC1-mediated efflux of cholesterol by RXR heterodimers, *Science 289*, 1524-1529.

108. Ogata,M., Tsujita,M., Hossain,M.A., Akita,N., Gonzalez,F.J., Staels,B., Suzuki,S., Fukutomi,T., Kimura,G., and Yokoyama,S. (2009) On the mechanism for PPAR agonists to enhance ABCA1 gene expression, *Atherosclerosis 205*, 413-419.

109. Hao,X.R., Cao,D.L., Hu,Y.W., Li,X.X., Liu,X.H., Xiao,J., Liao,D.F., Xiang,J., and Tang,C.K. (2009) IFN-gamma down-regulates ABCA1 expression by inhibiting LXRalpha in a JAK/STAT signaling pathway-dependent manner, *Atherosclerosis 203*, 417-428.

110. Yancey,P.G., Kawashiri,M.A., Moore,R., Glick,J.M., Williams,D.L., Connelly,M.A., Rader,D.J., and Rothblat,G.H. (2004) In vivo modulation of HDL phospholipid has opposing effects on SR-BI- and ABCA1-mediated cholesterol efflux, *J. Lipid Res. 45*, 337-346.

111. Uehara,Y., Miura,S., von,E.A., Abe,S., Fujii,A., Matsuo,Y., Rust,S., Lorkowski,S., Assmann,G., Yamada,T., and Saku,K. (2007) Unsaturated fatty acids suppress the expression of the ATP-binding cassette transporter G1 (ABCG1) and ABCA1 genes via an LXR/RXR responsive element, *Atherosclerosis 191*, 11-21.

112. Wang,Y.H., Chen,Y.F., Chen,S.R., Chen,X., Chen,J.W., Shen,X.Y., Mou,Y.G., and Liu,P.Q. (2010) Aspirin increases apolipoprotein-A-I-mediated cholesterol efflux via enhancing expression of ATP-binding cassette transporter A1, *Pharmacology 86*, 320-326.

113. Brooks-Wilson,A., Marcil,M., Clee,S.M., Zhang,L.H., Roomp,K., van,D.M., Yu,L., Brewer,C., Collins,J.A., Molhuizen,H.O., Loubser,O., Ouelette,B.F., Fichter,K., Ashbourne-Excoffon,K.J., Sensen,C.W., Scherer,S., Mott,S., Denis,M., Martindale,D., Frohlich,J., Morgan,K., Koop,B., Pimstone,S., Kastelein,J.J., Genest,J., Jr., and Hayden,M.R. (1999)

Mutations in ABC1 in Tangier disease and familial high-density lipoprotein deficiency, *Nat. Genet. 22*, 336-345.

114. Lawn,R.M., Wade,D.P., Garvin,M.R., Wang,X., Schwartz,K., Porter,J.G., Seilhamer,J.J., Vaughan,A.M., and Oram,J.F. (1999) The Tangier disease gene product ABC1 controls the cellular apolipoprotein-mediated lipid removal pathway, *J. Clin. Invest 104*, R25-R31.

115. Fitzgerald,M.L., Morris,A.L., Rhee,J.S., Andersson,L.P., Mendez,A.J., and Freeman,M.W. (2002) Naturally occurring mutations in the largest extracellular loops of ABCA1 can disrupt its direct interaction with apolipoprotein A-I, *J. Biol. Chem. 277*, 33178-33187.

116. Schou,J., Frikke-Schmidt,R., Kardassis,D., Thymiakou,E., Nordestgaard,B.G., Jensen,G., Grande,P., and Tybjaerg-Hansen,A. (2012) Genetic variation in ABCG1 and risk of myocardial infarction and ischemic heart disease, *Arterioscler. Thromb. Vasc. Biol. 32*, 506-515.

117. Gao,X., Gu,H., Li,G., Rye,K.A., and Zhang,D.W. (2012) Identification of an amino acid residue in ATP-binding cassette transport G1 critical for mediating cholesterol efflux, *Biochim. Biophys. Acta 1821*, 552-559.

118. Zhu,X., Lee,J.Y., Timmins,J.M., Brown,J.M., Boudyguina,E., Mulya,A., Gebre,A.K., Willingham,M.C., Hiltbold,E.M., Mishra,N., Maeda,N., and Parks,J.S. (2008) Increased cellular free cholesterol in macrophage-specific Abca1 knock-out mice enhances pro-inflammatory response of macrophages, *J. Biol. Chem. 283*, 22930-22941.

119. Koseki,M., Hirano,K., Masuda,D., Ikegami,C., Tanaka,M., Ota,A., Sandoval,J.C., Nakagawa-Toyama,Y., Sato,S.B., Kobayashi,T., Shimada,Y., Ohno-Iwashita,Y.,

Matsuura,F., Shimomura,I., and Yamashita,S. (2007) Increased lipid rafts and accelerated lipopolysaccharide-induced tumor necrosis factor-alpha secretion in Abca1-deficient macrophages, *J. Lipid Res. 48*, 299-306.

120. Yvan-Charvet,L., Welch,C., Pagler,T.A., Ranalletta,M., Lamkanfi,M., Han,S., Ishibashi,M., Li,R., Wang,N., and Tall,A.R. (2008) Increased inflammatory gene expression in ABC transporter-deficient macrophages: free cholesterol accumulation, increased signaling via toll-like receptors, and neutrophil infiltration of atherosclerotic lesions, *Circulation 118*, 1837-1847.

121. Pagler,T.A., Wang,M., Mondal,M., Murphy,A.J., Westerterp,M., Moore,K.J., Maxfield,F.R., and Tall,A.R. (2011) Deletion of ABCA1 and ABCG1 impairs macrophage migration because of increased Rac1 signaling, *Circ. Res. 108*, 194-200.

122. Meurs,I., Lammers,B., Zhao,Y., Out,R., Hildebrand,R.B., Hoekstra,M., Van Berkel,T.J., and Van,E.M. (2012) The effect of ABCG1 deficiency on atherosclerotic lesion development in LDL receptor knockout mice depends on the stage of atherogenesis, *Atherosclerosis 221*, 41-47.

123. Vaisman,B.L., Demosky,S.J., Stonik,J.A., Ghias,M., Knapper,C.L., Sampson,M.L., Dai,C., Levine,S.J., and Remaley,A.T. (2012) Endothelial expression of human ABCA1 in mice increases plasma HDL cholesterol and reduces diet-induced atherosclerosis, *J. Lipid Res. 53*, 158-167.

124. Warden,C.H., Langner,C.A., Gordon,J.I., Taylor,B.A., McLean,J.W., and Lusis,A.J. (1989) Tissue-specific expression, developmental regulation, and chromosomal mapping of the

lecithin: cholesterol acyltransferase gene. Evidence for expression in brain and testes as well as liver, *J. Biol. Chem. 264*, 21573-21581.

125. Kunnen,S. and Van,E.M. (2012) Lecithin-cholesterol acyltransferase: old friend or foe in atherosclerosis?, *J. Lipid Res.*

126. Jonas,A. (2000) Lecithin cholesterol acyltransferase, *Biochim. Biophys. Acta 1529*, 245-256.

127. Laccotripe,M., Makrides,S.C., Jonas,A., and Zannis,V.I. (1997) The carboxyl-terminal hydrophobic residues of apolipoprotein A-I affect its rate of phospholipid binding and its association with high density lipoprotein, *J. Biol. Chem. 272*, 17511-17522.

128. Dobiasova,M. and Frohlich,J.J. (1999) Advances in understanding of the role of lecithin cholesterol acyltransferase (LCAT) in cholesterol transport, *Clin. Chim. Acta 286*, 257-271.

129. Dergunov,A.D. (2012) A mechanistic model of lecithin:cholesterol acyltransferase activity exploits discoidal HDL composition and structure, *Arch. Biochem. Biophys. 520*, 81-87.

130. Carlucci,A., Cigliano,L., Maresca,B., Spagnuolo,M.S., Di,S.G., Calabro,R., and Abrescia,P. (2012) LCAT cholesterol esterification is associated with the increase of ApoE/ApoA-I ratio during atherosclerosis progression in rabbit, *J. Physiol Biochem.*

131. Kuivenhoven,J.A., Pritchard,H., Hill,J., Frohlich,J., Assmann,G., and Kastelein,J. (1997) The molecular pathology of lecithin:cholesterol acyltransferase (LCAT) deficiency syndromes, *J. Lipid Res. 38*, 191-205.

132. Glomset,J.A. (1968) The plasma lecithins:cholesterol acyltransferase reaction, *J. Lipid Res. 9*, 155-167.

133. Czarnecka,H. and Yokoyama,S. (1996) Regulation of cellular cholesterol efflux by lecithin:cholesterol acyltransferase reaction through nonspecific lipid exchange, *J. Biol. Chem. 271*, 2023-2028.

134. Navab,M., Berliner,J.A., Subbanagounder,G., Hama,S., Lusis,A.J., Castellani,L.W., Reddy,S., Shih,D., Shi,W., Watson,A.D., Van Lenten,B.J., Vora,D., and Fogelman,A.M. (2001) HDL and the inflammatory response induced by LDL-derived oxidized phospholipids, *Arterioscler. Thromb. Vasc. Biol. 21*, 481-488.

135. Daniil,G., Phedonos,A.A., Holleboom,A.G., Motazacker,M.M., Argyri,L., Kuivenhoven,J.A., and Chroni,A. (2011) Characterization of antioxidant/anti-inflammatory properties and apoA-I-containing subpopulations of HDL from family subjects with monogenic low HDL disorders, *Clin. Chim. Acta 412*, 1213-1220.

136. Hine,D., Mackness,B., and Mackness,M. (2012) Coincubation of PON1, APO A1, and LCAT increases the time HDL is able to prevent LDL oxidation, *IUBMB. Life 64*, 157-161.

137. Kappelle,P.J., de Boer,J.F., Perton,F.G., Annema,W., de,V.R., Dullaart,R.P., and Tietge,U.J. (2012) Increased LCAT activity and hyperglycaemia decrease the antioxidative functionality of HDL, *Eur. J. Clin. Invest 42*, 487-495.

138. Vaisman,B.L., Klein,H.G., Rouis,M., Berard,A.M., Kindt,M.R., Talley,G.D., Meyn,S.M., Hoyt,R.F., Jr., Marcovina,S.M., Albers,J.J., and . (1995) Overexpression of human lecithin cholesterol acyltransferase leads to hyperalphalipoproteinemia in transgenic mice, *J. Biol. Chem. 270*, 12269-12275.

139. Francone,O.L., Gong,E.L., Ng,D.S., Fielding,C.J., and Rubin,E.M. (1995) Expression of human lecithin-cholesterol acyltransferase in transgenic mice. Effect of human apolipoprotein AI and human apolipoprotein all on plasma lipoprotein cholesterol metabolism, *J. Clin. Invest 96*, 1440-1448.

140. Mehlum,A., Staels,B., Duverger,N., Tailleux,A., Castro,G., Fievet,C., Luc,G., Fruchart,J.C., Olivecrona,G., Skretting,G., and . (1995) Tissue-specific expression of the human gene for lecithin: cholesterol acyltransferase in transgenic mice alters blood lipids, lipoproteins and lipases towards a less atherogenic profile, *Eur. J. Biochem. 230*, 567-575.

141. Berard,A.M., Foger,B., Remaley,A., Shamburek,R., Vaisman,B.L., Talley,G., Paigen,B., Hoyt,R.F., Jr., Marcovina,S., Brewer,H.B., Jr., and Santamarina-Fojo,S. (1997) High plasma HDL concentrations associated with enhanced atherosclerosis in transgenic mice overexpressing lecithin-cholesteryl acyltransferase, *Nat. Med. 3*, 744-749.

142. Berti,J.A., de Faria,E.C., and Oliveira,H.C. (2005) Atherosclerosis in aged mice over-expressing the reverse cholesterol transport genes, *Braz. J. Med. Biol. Res. 38*, 391-398.

143. Furbee,J.W., Jr. and Parks,J.S. (2002) Transgenic overexpression of human lecithin: cholesterol acyltransferase (LCAT) in mice does not increase aortic cholesterol deposition, *Atherosclerosis 165*, 89-100.

144. Mehlum,A., Muri,M., Hagve,T.A., Solberg,L.A., and Prydz,H. (1997) Mice overexpressing human lecithin: cholesterol acyltransferase are not protected against diet-induced atherosclerosis, *APMIS 105*, 861-868.

145. Mehlum,A., Gjernes,E., Solberg,L.A., Hagve,T.A., and Prydz,H. (2000) Overexpression of human lecithin:cholesterol acyltransferase in mice offers no protection against diet-induced atherosclerosis, *APMIS 108*, 336-342.

146. Sakai,N., Vaisman,B.L., Koch,C.A., Hoyt,R.F., Jr., Meyn,S.M., Talley,G.D., Paiz,J.A., Brewer,H.B., Jr., and Santamarina-Fojo,S. (1997) Targeted disruption of the mouse lecithin:cholesterol acyltransferase (LCAT) gene. Generation of a new animal model for human LCAT deficiency, *J. Biol. Chem. 272*, 7506-7510.

147. Ng,D.S., Francone,O.L., Forte,T.M., Zhang,J., Haghpassand,M., and Rubin,E.M. (1997) Disruption of the murine lecithin:cholesterol acyltransferase gene causes impairment of adrenal lipid delivery and up-regulation of scavenger receptor class B type I, *J. Biol. Chem. 272*, 15777-15781.

148. Lambert,G., Sakai,N., Vaisman,B.L., Neufeld,E.B., Marteyn,B., Chan,C.C., Paigen,B., Lupia,E., Thomas,A., Striker,L.J., Blanchette-Mackie,J., Csako,G., Brady,J.N., Costello,R., Striker,G.E., Remaley,A.T., Brewer,H.B., Jr., and Santamarina-Fojo,S. (2001) Analysis of glomerulosclerosis and atherosclerosis in lecithin cholesterol acyltransferase-deficient mice, *J. Biol. Chem. 276*, 15090-15098.

149. Chang,P.Y., Lu,S.C., Su,T.C., Chou,S.F., Huang,W.H., Morrisett,J.D., Chen,C.H., Liau,C.S., and Lee,Y.T. (2004) Lipoprotein-X reduces LDL atherogenicity in primary biliary cirrhosis by preventing LDL oxidation, *J. Lipid Res. 45*, 2116-2122.

150. Li,L., Hossain,M.A., Sadat,S., Hager,L., Liu,L., Tam,L., Schroer,S., Huogen,L., Fantus,I.G., Connelly,P.W., Woo,M., and Ng,D.S. (2011) Lecithin cholesterol acyltransferase null mice

are protected from diet-induced obesity and insulin resistance in a gender-specific manner through multiple pathways, *J. Biol. Chem. 286*, 17809-17820.

151. Hager,L., Li,L., Pun,H., Liu,L., Hossain,M.A., Maguire,G.F., Naples,M., Baker,C., Magomedova,L., Tam,J., Adeli,K., Cummins,C.L., Connelly,P.W., and Ng,D.S. (2012) Lecithin:Cholesterol acyltransferase deficiency protects against cholesterol-induced hepatic endoplasmic reticulum stress in mice, *J. Biol. Chem.*

152. Chen,Z., Wang,S.P., Krsmanovic,M.L., Castro-Perez,J., Gagen,K., Mendoza,V., Rosa,R., Shah,V., He,T., Stout,S.J., Geoghagen,N.S., Lee,S.H., McLaren,D.G., Wang,L., Roddy,T.P., Plump,A.S., Hubbard,B.K., Sinz,C.J., and Johns,D.G. (2012) Small molecule activation of lecithin cholesterol acyltransferase modulates lipoprotein metabolism in mice and hamsters, *Metabolism 61*, 470-481.

153. Sashidhara,K.V., Kumar,M., Sonkar,R., Singh,B.S., Khanna,A.K., and Bhatia,G. (2012) Indole-based fibrates as potential hypolipidemic and antiobesity agents, *J. Med. Chem. 55*, 2769-2779.

154. Acton,S., Rigotti,A., Landschulz,K.T., Xu,S., Hobbs,H.H., and Krieger,M. (1996) Identification of scavenger receptor SR-BI as a high density lipoprotein receptor, *Science 271*, 518-520.

155. Krieger,M. (1999) Charting the fate of the "good cholesterol": identification and characterization of the high-density lipoprotein receptor SR-BI, *Annu. Rev. Biochem. 68*, 523-558.

156. Wiersma,H., Gatti,A., Nijstad,N., Oude Elferink,R.P., Kuipers,F., and Tietge,U.J. (2009) Scavenger receptor class B type I mediates biliary cholesterol secretion independent of ATP-binding cassette transporter g5/g8 in mice, *Hepatology 50*, 1263-1272.

157. Krieger,M. (2001) Scavenger receptor class B type I is a multiligand HDL receptor that influences diverse physiologic systems, *J. Clin. Invest 108*, 793-797.

158. Acton,S.L., Scherer,P.E., Lodish,H.F., and Krieger,M. (1994) Expression cloning of SR-BI, a CD36-related class B scavenger receptor, *J. Biol. Chem. 269*, 21003-21009.

159. Murao,K., Terpstra,V., Green,S.R., Kondratenko,N., Steinberg,D., and Quehenberger,O. (1997) Characterization of CLA-1, a human homologue of rodent scavenger receptor BI, as a receptor for high density lipoprotein and apoptotic thymocytes, *J. Biol. Chem. 272*, 17551-17557.

160. Urban,S., Zieseniss,S., Werder,M., Hauser,H., Budzinski,R., and Engelmann,B. (2000) Scavenger receptor BI transfers major lipoprotein-associated phospholipids into the cells, *J. Biol. Chem. 275*, 33409-33415.

161. Greene,D.J., Skeggs,J.W., and Morton,R.E. (2001) Elevated triglyceride content diminishes the capacity of high density lipoprotein to deliver cholesteryl esters via the scavenger receptor class B type I (SR-BI), *J. Biol. Chem. 276*, 4804-4811.

162. Thuahnai,S.T., Lund-Katz,S., Williams,D.L., and Phillips,M.C. (2001) Scavenger receptor class B, type I-mediated uptake of various lipids into cells. Influence of the nature of the donor particle interaction with the receptor, *J. Biol. Chem. 276*, 43801-43808.

163. Stangl,H., Hyatt,M., and Hobbs,H.H. (1999) Transport of lipids from high and low density lipoproteins via scavenger receptor-BI, *J. Biol. Chem. 274*, 32692-32698.

164. Gu,X., Lawrence,R., and Krieger,M. (2000) Dissociation of the high density lipoprotein and low density lipoprotein binding activities of murine scavenger receptor class B type I (mSR-BI) using retrovirus library-based activity dissection, *J. Biol. Chem. 275*, 9120-9130.

165. Gu,X., Trigatti,B., Xu,S., Acton,S., Babitt,J., and Krieger,M. (1998) The efficient cellular uptake of high density lipoprotein lipids via scavenger receptor class B type I requires not only receptor-mediated surface binding but also receptor-specific lipid transfer mediated by its extracellular domain, *J. Biol. Chem. 273*, 26338-26348.

166. Liadaki,K.N., Liu,T., Xu,S., Ishida,B.Y., Duchateaux,P.N., Krieger,J.P., Kane,J., Krieger,M., and Zannis,V.I. (2000) Binding of high density lipoprotein (HDL) and discoidal reconstituted HDL to the HDL receptor scavenger receptor class B type I. Effect of lipid association and APOA-I mutations on receptor binding, *J. Biol. Chem. 275*, 21262-21271.

167. Rodrigueza,W.V., Thuahnai,S.T., Temel,R.E., Lund-Katz,S., Phillips,M.C., and Williams,D.L. (1999) Mechanism of scavenger receptor class B type I-mediated selective uptake of cholesteryl esters from high density lipoprotein to adrenal cells, *J. Biol. Chem. 274*, 20344-20350.

168. Thuahnai,S.T., Lund-Katz,S., Dhanasekaran,P., Llera-Moya,M., Connelly,M.A., Williams,D.L., Rothblat,G.H., and Phillips,M.C. (2004) Scavenger receptor class B type I-mediated cholesteryl ester-selective uptake and efflux of unesterified cholesterol. Influence of high density lipoprotein size and structure, *J. Biol. Chem. 279*, 12448-12455.

169. Wang,N., Arai,T., Ji,Y., Rinninger,F., and Tall,A.R. (1998) Liver-specific overexpression of scavenger receptor BI decreases levels of very low density lipoprotein ApoB, low density lipoprotein ApoB, and high density lipoprotein in transgenic mice, *J. Biol. Chem. 273*, 32920-32926.

170. Ueda,Y., Royer,L., Gong,E., Zhang,J., Cooper,P.N., Francone,O., and Rubin,E.M. (1999) Lower plasma levels and accelerated clearance of high density lipoprotein (HDL) and non-HDL cholesterol in scavenger receptor class B type I transgenic mice, *J. Biol. Chem. 274*, 7165-7171.

171. Arai,T., Wang,N., Bezouevski,M., Welch,C., and Tall,A.R. (1999) Decreased atherosclerosis in heterozygous low density lipoprotein receptor-deficient mice expressing the scavenger receptor BI transgene, *J. Biol. Chem. 274*, 2366-2371.

172. Ueda,Y., Gong,E., Royer,L., Cooper,P.N., Francone,O.L., and Rubin,E.M. (2000) Relationship between expression levels and atherogenesis in scavenger receptor class B, type I transgenics, *J. Biol. Chem. 275*, 20368-20373.

173. Kozarsky,K.F., Donahee,M.H., Glick,J.M., Krieger,M., and Rader,D.J. (2000) Gene transfer and hepatic overexpression of the HDL receptor SR-BI reduces atherosclerosis in the cholesterol-fed LDL receptor-deficient mouse, *Arterioscler. Thromb. Vasc. Biol. 20*, 721-727.

174. Rigotti,A., Trigatti,B.L., Penman,M., Rayburn,H., Herz,J., and Krieger,M. (1997) A targeted mutation in the murine gene encoding the high density lipoprotein (HDL) receptor

scavenger receptor class B type I reveals its key role in HDL metabolism, *Proc. Natl. Acad. Sci. U. S. A 94*, 12610-12615.

175. Out,R., Hoekstra,M., Spijkers,J.A., Kruijt,J.K., Van,E.M., Bos,I.S., Twisk,J., and Van Berkel,T.J. (2004) Scavenger receptor class B type I is solely responsible for the selective uptake of cholesteryl esters from HDL by the liver and the adrenals in mice, *J. Lipid Res. 45*, 2088-2095.

176. Zhao,Y., Pennings,M., Vrins,C.L., Calpe-Berdiel,L., Hoekstra,M., Kruijt,J.K., Ottenhoff,R., Hildebrand,R.B., van der Sluis,R., Jessup,W., Le,G.W., Chapman,M.J., Huby,T., Groen,A.K., Van Berkel,T.J., and Van,E.M. (2011) Hypocholesterolemia, foam cell accumulation, but no atherosclerosis in mice lacking ABC-transporter A1 and scavenger receptor BI, *Atherosclerosis 218*, 314-322.

177. Zhao,Y., Pennings,M., Hildebrand,R.B., Ye,D., Calpe-Berdiel,L., Out,R., Kjerrulf,M., Hurt-Camejo,E., Groen,A.K., Hoekstra,M., Jessup,W., Chimini,G., Van Berkel,T.J., and Van,E.M. (2010) Enhanced foam cell formation, atherosclerotic lesion development, and inflammation by combined deletion of ABCA1 and SR-BI in Bone marrow-derived cells in LDL receptor knockout mice on western-type diet, *Circ. Res. 107*, e20-e31.

178. Korporaal,S.J., Meurs,I., Hauer,A.D., Hildebrand,R.B., Hoekstra,M., Cate,H.T., Pratico,D., Akkerman,J.W., Van Berkel,T.J., Kuiper,J., and Van,E.M. (2011) Deletion of the high-density lipoprotein receptor scavenger receptor BI in mice modulates thrombosis susceptibility and indirectly affects platelet function by elevation of plasma free cholesterol, *Arterioscler. Thromb. Vasc. Biol. 31*, 34-42.

179. Ma,Y., Ashraf,M.Z., and Podrez,E.A. (2010) Scavenger receptor BI modulates platelet reactivity and thrombosis in dyslipidemia, *Blood 116*, 1932-1941.

180. Yuhanna,I.S., Zhu,Y., Cox,B.E., Hahner,L.D., Osborne-Lawrence,S., Lu,P., Marcel,Y.L., Anderson,R.G., Mendelsohn,M.E., Hobbs,H.H., and Shaul,P.W. (2001) High-density lipoprotein binding to scavenger receptor-BI activates endothelial nitric oxide synthase, *Nat. Med. 7*, 853-857.

181. Mineo,C. and Shaul,P.W. (2006) Circulating cardiovascular disease risk factors and signaling in endothelial cell caveolae, *Cardiovasc. Res. 70*, 31-41.

182. Vergeer,M., Korporaal,S.J., Franssen,R., Meurs,I., Out,R., Hovingh,G.K., Hoekstra,M., Sierts,J.A., Dallinga-Thie,G.M., Motazacker,M.M., Holleboom,A.G., Van Berkel,T.J., Kastelein,J.J., Van,E.M., and Kuivenhoven,J.A. (2011) Genetic variant of the scavenger receptor BI in humans, *N. Engl. J. Med. 364*, 136-145.

183. Hoekstra,M., Van,E.M., and Korporaal,S.J. (2012) Genetic studies in mice and humans reveal new physiological roles for the high-density lipoprotein receptor scavenger receptor class B type I, *Curr. Opin. Lipidol. 23*, 127-132.

184. Brunham,L.R., Tietjen,I., Bochem,A.E., Singaraja,R.R., Franchini,P.L., Radomski,C., Mattice,M., Legendre,A., Hovingh,G.K., Kastelein,J.J., and Hayden,M.R. (2011) Novel mutations in scavenger receptor BI associated with high HDL cholesterol in humans, *Clin. Genet. 79*, 575-581.

185. Burgess,J.W., Frank,P.G., Franklin,V., Liang,P., McManus,D.C., Desforges,M., Rassart,E., and Marcel,Y.L. (1999) Deletion of the C-terminal domain of apolipoprotein A-I impairs cell surface binding and lipid efflux in macrophage, *Biochemistry 38*, 14524-14533.

186. Scott,B.R., McManus,D.C., Franklin,V., McKenzie,A.G., Neville,T., Sparks,D.L., and Marcel,Y.L. (2001) The N-terminal globular domain and the first class A amphipathic helix of apolipoprotein A-I are important for lecithin:cholesterol acyltransferase activation and the maturation of high density lipoprotein in vivo, *J. Biol. Chem. 276*, 48716-48724.

187. Reardon,C.A., Kan,H.Y., Cabana,V., Blachowicz,L., Lukens,J.R., Wu,Q., Liadaki,K., Getz,G.S., and Zannis,V.I. (2001) In vivo studies of HDL assembly and metabolism using adenovirus-mediated transfer of ApoA-I mutants in ApoA-I-deficient mice, *Biochemistry 40*, 13670-13680.

188. von,E.A., Funke,H., Walter,M., Altland,K., Benninghoven,A., and Assmann,G. (1990) Structural analysis of human apolipoprotein A-I variants. Amino acid substitutions are nonrandomly distributed throughout the apolipoprotein A-I primary structure, *J. Biol. Chem. 265*, 8610-8617.

189. Chroni,A., Liu,T., Fitzgerald,M.L., Freeman,M.W., and Zannis,V.I. (2004) Cross-linking and lipid efflux properties of apoA-I mutants suggest direct association between apoA-I helices and ABCA1, *Biochemistry 43*, 2126-2139.

190. Chroni,A., Koukos,G., Duka,A., and Zannis,V.I. (2007) The carboxy-terminal region of apoA-I is required for the ABCA1-dependent formation of alpha-HDL but not prebeta-HDL particles in vivo, *Biochemistry 46*, 5697-5708.

191. Wang,N., Silver,D.L., Costet,P., and Tall,A.R. (2000) Specific binding of ApoA-I, enhanced cholesterol efflux, and altered plasma membrane morphology in cells expressing ABC1, *J. Biol. Chem. 275*, 33053-33058.

192. Assmann,G. Familial analphalipoproteineima: Tangier disease. von, Eckardstein A. and Brewer, H. B. The Metabolic and Molecular Basis of Inherited Disease , 2937-2960. 2001. McGraw-Hill, New York.

Ref Type: Generic

193. Matsunaga,T., Hiasa,Y., Yanagi,H., Maeda,T., Hattori,N., Yamakawa,K., Yamanouchi,Y., Tanaka,I., Obara,T., and Hamaguchi,H. (1991) Apolipoprotein A-I deficiency due to a codon 84 nonsense mutation of the apolipoprotein A-I gene, *Proc. Natl. Acad. Sci. U. S. A 88*, 2793-2797.

194. Timmins,J.M., Lee,J.Y., Boudyguina,E., Kluckman,K.D., Brunham,L.R., Mulya,A., Gebre,A.K., Coutinho,J.M., Colvin,P.L., Smith,T.L., Hayden,M.R., Maeda,N., and Parks,J.S. (2005) Targeted inactivation of hepatic Abca1 causes profound hypoalphalipoproteinemia and kidney hypercatabolism of apoA-I, *J. Clin. Invest 115*, 1333-1342.

195. Singaraja,R.R., Stahmer,B., Brundert,M., Merkel,M., Heeren,J., Bissada,N., Kang,M., Timmins,J.M., Ramakrishnan,R., Parks,J.S., Hayden,M.R., and Rinninger,F. (2006) Hepatic ATP-binding cassette transporter A1 is a key molecule in high-density lipoprotein cholesteryl ester metabolism in mice, *Arterioscler. Thromb. Vasc. Biol. 26*, 1821-1827.

196. Hassan,H.H., Denis,M., Lee,D.Y., Iatan,I., Nyholt,D., Ruel,I., Krimbou,L., and Genest,J. (2007) Identification of an ABCA1-dependent phospholipid-rich plasma membrane apolipoprotein A-I binding site for nascent HDL formation: implications for current models of HDL biogenesis, *J. Lipid Res. 48*, 2428-2442.

197. Arakawa,R. and Yokoyama,S. (2002) Helical apolipoproteins stabilize ATP-binding cassette transporter A1 by protecting it from thiol protease-mediated degradation, *J. Biol. Chem. 277*, 22426-22429.

198. Kozyraki,R., Fyfe,J., Kristiansen,M., Gerdes,C., Jacobsen,C., Cui,S., Christensen,E.I., Aminoff,M., de la Chapelle,A., Krahe,R., Verroust,P.J., and Moestrup,S.K. (1999) The intrinsic factor-vitamin B12 receptor, cubilin, is a high-affinity apolipoprotein A-I receptor facilitating endocytosis of high-density lipoprotein, *Nat. Med. 5*, 656-661.

199. Hammad,S.M., Stefansson,S., Twal,W.O., Drake,C.J., Fleming,P., Remaley,A., Brewer,H.B., Jr., and Argraves,W.S. (1999) Cubilin, the endocytic receptor for intrinsic factor-vitamin B(12) complex, mediates high-density lipoprotein holoparticle endocytosis, *Proc. Natl. Acad. Sci. U. S. A 96*, 10158-10163.

200. Singaraja,R.R., Van,E.M., Bissada,N., Zimetti,F., Collins,H.L., Hildebrand,R.B., Hayden,A., Brunham,L.R., Kang,M.H., Fruchart,J.C., Van Berkel,T.J., Parks,J.S., Staels,B., Rothblat,G.H., Fievet,C., and Hayden,M.R. (2006) Both hepatic and extrahepatic ABCA1 have discrete and essential functions in the maintenance of plasma high-density lipoprotein cholesterol levels in vivo, *Circulation 114*, 1301-1309.